JOURNAL OF THE AERONAUTICAL SCIENCES

VOLUME 24 NOVEMBER, 1957 NUMBER 11

ST. LOUIS NOV 7 1957 PUBLIC LIBRARY

CONTENTS

Characteristics and Sound Speed in Nonisentropic Gas Flows With Nonequilibrium Thermodynamic States ..... E. L. RESLER, JR. 785

Favorable Interference in Lifting Systems in Supersonic Flow ..... ANTONIO FERRI, JOSEPH H. CLARKE, AND LU TING 791

Rotating Stall in Axial Flow Compressors ..... JEAN FABRI AND RAYMOND SIESTRUNCK 805

A Simple Method of Matric Structural Analysis: Part II—Effects of Taper and Consideration of Curvature ..... BERTRAM KLEIN 813

Diffraction of Disturbances Around a Convex Right Corner With Applications in Acoustics and Wing-Body Interference ..... LU TING 821

Transonic Flow With a Detached Bow Wave Past a Wedge Between Two Parallel Plane Walls ..... SHIGEKI MORIOKA 831

Experiments on Interaction Between a Traveling Shock Wave and a Turbulent Jet ..... DARSHAN S. DOSANJH 838

Readers' Forum 845

Published by

INSTITUTE OF THE AERONAUTICAL SCIENCES, INC.

JOURNAL OF THE AERONAUTICAL SCIENCES

Editor: W. R. Sears
Director, Graduate School of Aeronautical Engineering, Cornell University

Associate Editor: Robert R. Dexter *Managing Editor:* Rita J. Turino
Editorial Assistant: Caroline Taylor

Editorial Committee

Aerodynamics and Fluid Mechanics

Holt Ashley
H. Julian Allen
Dean R. Chapman
Francis H. Clauser
Hugh L. Dryden
John C. Evvard
Antonio Ferri
Alexander Flax
Wallace D. Hayes
R. T. Jones
Carl Kaplan
H. W. Liepmann
C. C. Lin
H. F. Ludloff
Harold Luskin
Clark B. Millikan
Henry T. Nagamatsu
H. J. E. Reid
George S. Schairer
G. B. Schubauer
John Stack
Theodore Theodorsen
Arthur N. Tifford
Th. von Kármán

Flight Testing

R. R. Gilruth
Melvin N. Gough
W. L. Howland
W. F. Milliken, Jr.

Rotating Wing Aircraft

F. B. Gustafson
K. H. Hohenemser
Bartram Kelley
R. B. Maloy
Ralph McClarren
R. H. Miller
R. H. Prewitt
Igor I. Sikorsky

Structures

John E. Duberg
R. R. Heldenfels
N. J. Hoff
Samuel Levy
J. F. McBrearty
W. Ramberg
E. E. Sechler
F. R. Shanley
C. R. Strang
S. Timoshenko

Meteorology

C. F. Brooks
D. M. Little
F. W. Reichelderfer
K. C. Spengler

Vibration and Flutter

Lee Arnold
M. A. Biot
R. L. Bisplinghoff
Harold A. Cheilek
I. E. Garrick
Martin Goland

Aircraft Design

W. E. Beall
E. H. Heinemann
Hall L. Hibbard
Richard Hutton
C. L. Johnson
A. A. Kartveli
F. K. Teichmann

Electronics

K. C. Black
M. V. Kiebert, Jr.
David S. Little
Paul Rosenberg
Giles J. Strickroth

Physiologic Problems

H. G. Armstrong
Louis H. Bauer
Robert J. Benford
W. Randolph Lovelace, II
Ross A. MacFarland

Flight Propulsion

William Bollay
George W. Brady
R. P. Kroon
Frank E. Marble
Abe Silverstein
E. S. Taylor

Instruments

Alan G. Binnie
Charles H. Colvin
Frank R. Cook
C. S. Draper
S. G. Eskin
C. F. Savage
R. C. Sylvander

SUBSCRIPTION RATES

Journal of the Aeronautical Sciences, Published Monthly. United States and Possessions: 1 Year, $15.00; Single Copies, $1.50. Foreign Countries Including Canada (American Currency Rates): 1 Year, $16.00; Single Copies, $1.50.

Aeronautical Engineering Review, Published Monthly. United States and Possessions: 1 Year, $3.00; Single Copies, $0.50. Foreign Countries Including Canada (American Currency Rates): 1 Year, $3.50; Single Copies, $0.50.

Notices of change of address should be sent to the Institute at least 30 days prior to actual change of address.

Manuscripts for publication, proofs, and all correspondence should be addressed to the Editorial Office of the Journal.

Publication Office, 20th and Northampton Sts., Easton, Pa. Correspondence regarding subscriptions may be addressed to the Editorial Office of the Journal of the Aeronautical Sciences, 2 East 64th Street, New York 21, N.Y.

© *Copyright, 1957, by the Institute of the Aeronautical Sciences, Inc.*

Entered as Second-Class Matter at the Post Office, Easton, Pa., May 1, 1937. Acceptance for mailing at a special rate of Postage provided for in the Act of August 24, 1912. Authorized April 29, 1937.

JOURNAL OF THE AERONAUTICAL SCIENCES

VOLUME 24 NOVEMBER, 1957 NUMBER 11

Characteristics and Sound Speed in Nonisentropic Gas Flows With Nonequilibrium Thermodynamic States†

E. L. RESLER, JR.*
Cornell University

SUMMARY

A theory is developed extending the method of characteristics to flow problems involving lagging heat capacities and/or finite chemical reaction rates. Special cases appropriate to present high-speed flow problems are considered in more detail—namely, heat-capacity lag and dissociation of a gas made up of diatomic molecules. The theory is easily adaptable to the usual finite-wave approximation used for computations.

INTRODUCTION

WITH MUCH ATTENTION being focused on problems relating to both chemical and gas-dynamic phenomena simultaneously, it is appropriate to examine how chemical processes affect flow parameters or, similarly, how flow phenomena can be utilized in chemical-kinetic studies. For example, the mechanism of excitation of the vibrational degrees of freedom of air molecules is of importance in studies of the internal aerodynamics of air-breathing jet engines; similar problems face the rocket engine designer. The lag times of heat capacities, including processes of dissociation and ionization, affect the flow about high-speed missiles. Also, aerodynamic phenomena have been utilized to study basic chemical kinetics of some reactions—e.g., the impact-tube method of measuring relaxation times[1, 2] or the shock tube used for various studies.[3–5] This paper develops a theory which treats flows that are not isentropic due to phenomena occurring in the gas itself, such as a net energy flow between various degrees of freedom of molecules due to heat-capacity lag or chemical reactions. Emphasis is placed on a formulation free of particular assumptions concerning the chemical reaction rates. Previous theories, of course, occur as special cases. The theory is developed for one-dimensional unsteady and two-dimensional steady flows with special attention paid to processes of dissociation and ionization.

Received January 31, 1957. Revised and received July 23, 1957.

† This research was partially supported by the United States Air Force through the AF Office of Scientific Research, Air Research and Development Command under Contract AF 18 (600)-993 at the University of Maryland.

* Associate Professor of Aeronautical Engineering.

ONE-DIMENSIONAL UNSTEADY FLOWS

Let ξ be the single space coordinate on which the velocity u (in the ξ direction) and the thermodynamic variables depend, and let t be the time. Then if ρ is the density, p the pressure, and A the area of cross-sections normal to the coordinate ξ, the fluid flow equations, neglecting friction and other transport phenomena, are

Equation of Motion:

$$(\partial u/\partial t) + u(\partial u/\partial \xi) = -(1/\rho)(\partial p/\partial \xi) \qquad (1)$$

Conservation of Mass:

$$A(\partial \rho/\partial t) + (\partial \rho u A/\partial \xi) = 0 \qquad (2)$$

Although we have only two equations and three unknowns, we will proceed as far as possible without specifying what our third equation is. If we can combine Eqs. (1) and (2) so as to define the derivative of our unknowns along a particular direction, then that direction will be a "characteristic direction"[6] if it is a function of ξ, t, and the unknowns. Define the operator $\delta/\delta t$ as

$$\delta/\delta t = (\partial/\partial t) + (u \pm a)(\partial/\partial \xi)$$

that is, the derivative in the ξ, t plane in the direction $d\xi/dt = u \pm a$. The velocity a is as yet undefined but will turn out to be the speed of sound. Choose u as the

unknown to operate on; then we have

$$\delta u/\delta t = (\partial u/\partial t) + (u \pm a)(\partial u/\partial \xi) = (\partial u/\partial t) + u(\partial u/\partial \xi) \pm a(\partial u/\partial \xi)$$

Using Eq. (1) and (2) to eliminate the u derivatives, one finds

$$\delta u/\delta t = -(1/\rho)(\partial p/\partial \xi) \pm a[-(1/\rho)(\partial \rho/\partial t) - (u/\rho)(\partial \rho/\partial \xi) - (u/A)(\partial A/\partial \xi)]$$

but since $A = A(\xi)$ only,

$$\partial A/\partial \xi = [1/(u \pm a)](\delta A/\delta t)$$

and defining the substantial derivative D/Dt as

$$D/Dt = (\partial/\partial t) + u(\partial/\partial \xi)$$

we find

$$a(\partial/\partial \xi) = \pm(\delta/\delta t) \mp (D/Dt)$$

therefore,

$$\delta u/\delta t = \mp(1/\rho a)(\delta p/\delta t) \mp [ua/A(u \pm a)](\delta A/\delta t) \pm [(1/\rho a)(Dp/Dt) - (a/\rho)(D\rho/Dt)]$$

Now if we set the last bracket of this expression equal to zero, we have defined a and have a differential expression for our unknowns in a particular direction; so for

$$a^2 = (Dp/Dt)/(D\rho/Dt) \tag{3}$$

$$\delta u = \mp(1/\rho a)\delta p \mp [ua/A(u \pm a)]\delta A \tag{4}$$

The quantity a so defined can now definitely be identified as the speed of small disturbances. For a small disturbance theory with $\delta A = 0$, and replacing the δ by differences, we have from Eq. (4), $\Delta p = \mp \rho_0 a_0 \Delta u$ along directions $d\xi/dt = \pm a_0$, where

$$a_0 = [(\partial p/\partial t)/(\partial \rho/\partial t)]_0^{1/2}$$

and the subscript 0 denotes that the quantities are to take on the values appropriate to the undisturbed state. Then in the direction $d\xi/dt = a_0$ the quantity $P = p + \rho_0 a_0 u$ is propagated unchanged and, in the direction $d\xi/dt = -a_0$, $Q = p - \rho_0 a_0 u$ is constant. Notice that

$$p = (P + Q)/2 \quad \text{and} \quad u = (P - Q)/2\rho_0 a_0$$

Consider a disturbance moving into a region where Q = constant; then as P is propagated unchanged with velocity a_0, so are u and p and, therefore, the disturbance. Eq. (3) which has now been identified as the speed of sound was given by M. Munk.[7] As Munk points out, the speed of sound depends upon the rate of change of p with ρ along a particle path. This definition is more general than the usual more specialized relation $a^2 = dp/d\rho]_{\text{isentropic}}$.

Also note that for $\delta A = 0$ we have $\delta p = \mp \rho a \delta u$. That we actually have defined the velocity of wave propagation can also be recognized from this expression. Across the wave we have a change in pressure δp, which is the force changing the velocity by amount δu of an amount of fluid per unit time given by ρa, the amount of fluid affected by the wave per unit time.

Suppose we now introduce the gas law into our system of equations in the form

$$p = \rho RT \tag{5}$$

Here T is the temperature appropriate to the translational degrees of freedom of the gas atoms or molecules. This temperature may or may not be the same as the temperature appropriate to describe any of the other degrees of freedom the molecule may possess. We will no longer concern ourselves with the area term in Eq. (4), as we may take it into account at any time; so for $\delta A = 0$,

$$\delta u = \mp(\delta \rho RT/\rho a) = \mp(\delta RT/a) \mp (RT/a)\delta \ln \rho \tag{6}$$

When chemical reactions occur in the flow field they affect the velocity u only insofar as they change the pressure p. This is done by changing either the translational temperature T or the gas constant R by means of the reaction. To keep account of energy exchange between the translational degrees of freedom and other degrees, it is convenient to define the entropy η of that part of the system that is always in equilibrium with the translational temperature T. The degrees of freedom not in equilibrium with T we will call the lagging degrees of freedom; these are to be considered as a heat reservoir carried along with each unit mass of the flow, which can change the entropy of the unit mass by energy exchange with that part of the internal energy in equilibrium with the temperature T. How much heat is exchanged between the lagging and following degrees of freedom is governed by the laws of chemical kinetics and depends on the thermodynamic state of the unit mass as it proceeds through the flow field. Of course, if the chemical composition of the unit mass changes, this must also be taken into account. In defining η in this way we have assumed that there always exists a translational temperature T which is defined by means of the gas law $p = \rho RT$.

If E is the internal energy that is in equilibrium at all times with the translational temperature T, we can write, with

$$E = E(T) \tag{7}$$

$$d \ln \rho = (dE/RT) - (1/R)d\eta \tag{8}$$

To compute η we must follow the particles in their motion, in which case if U is the lagging internal energy, we can write

$$D\eta/Dt = -(1/T)/(DU/Dt) \tag{9}$$

The specification of DU/Dt amounts to specifying the needed chemical relations. *So*, given DU/Dt, the specification of our problem is complete. Unfortunately, in most cases of aerodynamic interest the form of the function specifying DU/Dt has not been determined.

Summarizing then, we have, in the most general case, the following set of equations to solve:

$$
\begin{aligned}
\delta u &= \mp[\delta(E + RT)/a] \pm (T/a)\delta\eta \mp [ua/\Delta(u \pm a)]\delta\Delta \\
a^2 &= (Dp/Dt)/(D\rho/Dt) \\
p &= \rho RT \\
E &= E(T) \\
d\ln\rho &= (1/RT)dE - (1/R)d\eta \\
D\eta/Dt &= -(1/T)(DU/Dt) \\
DU/Dt &= \text{sum total of appropriate chemical rates of components with lagging internal energy} \\
R &= \text{function of the concentrations of the components making up the fluid}
\end{aligned}
\qquad (10)
$$

Perfect Gas, Constant Composition, Lagging Heat Capacity

Consider the general case where $U = \sum_i U_i$, where U_i is the energy in lagging part i of the internal energy. Then

$$D\eta/Dt = -(1/T)\sum_i (DU_i/Dt)$$

and if $E = E(T)$,

$$D\ln\rho/Dt = (1/RT)(dE/dT)(DT/Dt) + (1/RT)\sum_i (DU_i/Dt)$$

To find a^2, we use the gas law; viz.,

$$a^2 = (Dp/Dt)/(D\rho/Dt) = (p/\rho)[(D\ln p/Dt)/(D\ln\rho/Dt)]$$

$$= \frac{p}{\rho}\frac{(D\ln\rho/Dt) + (D\ln T/Dt)}{(D\ln\rho/Dt)}$$

$$= RT \times \frac{(1/R)(dE/dT)(DT/Dt) + (DT/Dt) + (1/R)\sum_i (DU_i/Dt)}{(1/R)(dE/dT)(DT/Dt) + (1/R)\sum_i (DU_i/Dt)}$$

Now let C_{v_T} denote dE/dT; then if $U_i = U_i(\Theta_i)$ where Θ_i is a temperature typifying U_i, and if C_{v_i} denotes $dU_i/d\Theta_i$, the formula for a^2 becomes

$$a^2 = RT\frac{(C_{v_T} + R)(DT/Dt) + \sum_i C_{v_i}(D\Theta_i/Dt)}{C_{v_T}(DT/Dt) + \sum_i (D\Theta_i/Dt)} \qquad (11)$$

Also,

$$\delta u = \mp[(C_{v_T} + R)/a]\delta T \pm (T/a)\delta\eta \quad \text{if} \quad \delta\Delta = 0 \qquad (12)$$

Θ_i here defined need not be interpreted as a temperature in the usual thermodynamic sense, but merely as a means of accounting for the energy in the "reservoir" associated with the lagging internal energy U_i. It is convenient, however, in many cases to identify it in such a way that when Θ_i becomes equal to T, U_i takes on its equilibrium value. Such a procedure is followed below.

Lagging Rotational Heat Capacity of a Diatomic Molecule

In this case $C_{v_T} = (3/2)R$ and $C_{v_i} = R$, at least at temperatures such that the rotational heat capacity is fully excited. Let Θ_R be the rotational temperature. Then expression (11) for the speed of sound becomes

$$a^2 = RT\frac{5(DT/Dt) + 2(D\Theta_R/Dt)}{3(DT/Dt) + 2(D\Theta_R/Dt)} = \beta_R RT \qquad (13)$$

Note that if $D\Theta_R/Dt = 0$ we get the monatomic gas result—i.e., $a^2 = (5/3)RT$—and if $\Theta_R \equiv T$ so that $DT/Dt = D\Theta_R/Dt$, we get the diatomic gas result—i.e., $a^2 = (7/5)RT$. For Θ_R lagging T by various amounts we get appropriate intermediate sound speeds.

Working with expression (12), we find

$$\delta u = \mp(5/2)(R/a)\delta T \pm (T/a)\delta\eta$$

$$\pm\,\delta u = -(5/2)(R/a)\delta(a^2/\beta_R R) + (T/a)\delta\eta$$

$$\delta[(5a/\beta_R) \pm u] = (5/\beta_R)\delta a + (5a/2\beta_R{}^2)\delta\beta_R - (5/\beta_R)\delta a - (5a/\beta_R{}^2)\,\delta\beta_R + (a/R\beta_R)\rho\eta$$

$$\delta[(5a/\beta_R) \pm u] = (a/\beta_R)[-(5/2)\delta\ln\beta_R + (\partial\eta/R)] \qquad (14)$$

Using Eqs. (13) and (14), and given that $D\Theta_R/Dt = f(\rho, T, \Theta_R)$, one can proceed as in the usual case to construct solutions. Notice that if $D\Theta_R/Dt = 0$, then $\beta_R = 5/3 =$ constant and $\delta\eta = 0$, so that $\delta(3a \pm u) = 0$, in agreement with the Riemann invariants for the case of a perfect monatomic gas with constant heat capacities. If $\Theta_R = T$ everywhere, then $D\eta = -(R/T)DT$ or $\eta = -R\ln T + \eta_0$ along particle paths, where η_0 is the entropy, say at $t = 0$, of the particles. If all the particles were initially in the same thermodynamic state, then η_0 is the same for all particles, and we can use the relation $\eta = -R\ln T + \eta_0$ anywhere in the field. Thus, for $\Theta_R = T$, $\beta_R = 7/5$, $\delta\beta_R = 0$, and

$$(a/R\beta_R)\delta\eta = [a/R(7/5)][-R(\delta T/T)] = -(5a/7a^2)2a\delta a = -(10/7)\delta a$$

so that Eq. (14) becomes

$$\delta\{[5a/(7/5)] \pm u\} = -(10/7)\delta a$$

or

$$\delta(5a \pm u) = 0$$

in accordance with well known theory for a perfect diatomic gas with constant heat capacities.

Lagging Vibrational Heat Capacity of a Diatomic Molecule

This is similar to the previous case. Suppose the rotational degrees of freedom are assumed to be in equilibrium with the translational degrees; then if $U_{v_i} =$ (vibrational energy in degrees of freedom i), one finds, since $E = (5/2)RT$,

$$a^2 = RT\frac{7(DT/Dt) + (2/R)\sum_i (DU_{v_i}/Dt)}{5(DT/Dt) + (2/R)\sum_i (DU_{v_i}/Dt)} = \beta_v RT \qquad (15)$$

$$\delta[(7a/\beta_v) \pm u] = (a/\beta_v)[-(7/2)\delta\ln\beta_v + (\delta\eta/R)] \qquad (16)$$

It is appropriate for some applications to neglect the lag of rotation and not that of vibration, even though one knows that in reality all the degrees of freedom lag behind the translational degrees of freedom. One must

decide first what mass of fluid he is willing to regard as the smallest mass of interest to him in any particular circumstance, then find the typical volume and thus length, from the chosen mass and a typical density. Finding the time, given by this length divided by the speed of sound, one can neglect the adjustment times of degrees of freedom which adjust faster than this time.

Of course, if the particular circumstances in question are such that the phenomena cover a large range of density, the criteria as to when times are negligible or not will change with the density and temperature. For example, in ordinary acoustics we are quite content to assume that air is a diatomic gas with no lagging rotational heat capacity, which we know is not true. This is quite a good approximation, since the human ear does not respond to frequencies above 20,000 cycles per sec., or to a time scale of about 50 μsec. The rotational degrees of freedom come to equilibrium with the translational degrees of freedom in at most 100 collisions. Under atmospheric conditions the time between collisions is about 10^{-9} sec., so that the time scale for the adjustment for rotational degrees of freedom is 10^{-7} sec. Thus the human ear has a frequency response 500 times too low to be able to detect any rotational heat capacity lag effects in acoustic waves.

Dissociating Diatomic Gas With Vibrational Heat-Capacity Lag

In this case we must allow for a chemical change in species, due to the dissociation as the particles move about. If α is the fraction of the original diatomic molecules that have become dissociated, we have for the gas constant $R = (1 + \alpha)R_0$, where R_0 is the gas constant appropriate to the undissociated particles. We shall assume that the rotational degrees of freedom of the diatomic molecules are always in equilibrium with the translational degrees of freedom. Then, per unit mass, we can write the energy

$$E = (5/2)(1 - \alpha)R_0T + (3/2)(2\alpha)R_0T = [(5 + \alpha)/2]R_0T$$

and

$$U = \alpha q_0 + E_r(\Theta_r)$$

where q_0 is the dissociation energy, E_r the energy in the vibrational heat capacity (only one mode for a diatomic gas), and Θ_r is the vibrational temperature. Thus,

$$DU/Dt = q_0(D\alpha/Dt) + (D/Dt)(E_r) = q_0(D\alpha/Dt) + (dE_r/d\Theta_r)(D\Theta_r/Dt) = q_0(D\alpha/Dt) + C_{rib}(D\Theta_r/Dt)$$

where C_{rib} denotes the vibrational heat capacity, which may be a function of Θ_r. Proceeding as before,

$$\left.\begin{aligned} a^2 &= (1 + \alpha)R_0T\,\frac{(7 + 3\alpha)(DT/Dt) + T(D\alpha/Dt)\{1 + (2q_0/R_0T)\} + (2C_{rib}/R_0)(D\Theta_r/Dt)}{(5 + \alpha)(DT/Dt) + T(D\alpha/Dt)\{(2q_0/R_0T) - 1\} + (2C_{rib}/R_0)(D\Theta_r/Dt)} \\ &= \beta RT \end{aligned}\right\} \tag{17}$$

$$\left.\begin{aligned} \delta\{[(7 + 3\alpha)/\beta]a \pm u\} &= (3a/2\beta)\delta\alpha - [(7 + 3\alpha)/\beta^2]a\delta\beta + (a/\beta R)\delta\eta \\ &= (a/\beta)\{(3/2)\delta\alpha - [(7 + 3\alpha)/\beta]\delta\beta + [\delta\eta/(1 + \alpha)R_0]\} \end{aligned}\right\} \tag{18}$$

Equations similar to Eqs. (17) and (18) can be derived in like fashion for the case of ionization of a monatomic gas.

Steady Two-Dimensional Flow

To discuss steady two-dimensional flow, we will choose as coordinates the distance along a streamline, s, and the normal to the streamline, n. Then our hydrodynamic equations are

Continuity:

$$\partial\vartheta/\partial n = -(1/\rho)(\partial\rho/\partial s) - (1/w)(\partial w/\partial s) \tag{19}$$

Motion:

$$\partial\vartheta/\partial s = -(1/\rho w^2)(\partial p/\partial n), \qquad w(\partial w/\partial s) = -(1/\rho)(\partial p/\partial s) \tag{20}$$

where w is the velocity of the fluid and ϕ the angle that the velocity vector makes with some reference direction. Define the directional derivative $\delta/\delta l$ as $\delta/\delta l = (\partial/\partial s) \pm (1/\sqrt{M^2 - 1})(\partial/\partial n)$, where $M = w/a$. The direction is not yet determined, as a is not yet defined. Operating on the variable ϕ, we have

$$\delta\vartheta/\delta l = (\partial\vartheta/\partial s) \mp (1/\sqrt{M^2 - 1})(\partial\vartheta/\partial n)$$

Using Eqs. (19) and (20),

$$\delta\vartheta/\delta l = -(1/\rho w^2)(\partial p/\partial n) \pm (1/\sqrt{M^2 - 1})(1/\rho) \times (\partial\rho/\partial s) \mp (1/\sqrt{M^2 - 1}\,\rho w^2)(\partial p/\partial s)$$

and using the identity

$$\partial/\partial n = \sqrt{M^2 - 1}\,[\mp(\delta/\delta l) \pm (\partial/\partial s)]$$

we have

$$\delta\vartheta/\delta l = \pm(\sqrt{M^2 - 1}/\rho w^2)(\delta p/\delta l) \mp (\sqrt{M^2 - 1}/\rho w^2)(\partial p/\partial s) \pm (1/\sqrt{M^2 - 1}) \times (1/\rho)(\partial\rho/\partial s) \mp (1/\sqrt{M^2 - 1}\,\rho w^2)(\partial p/\partial s) \tag{21}$$

Setting the terms with the streamline derivatives equal to zero, we find

$$a^2 = (\partial p/\partial s)/(\partial\rho/\partial s) \tag{22}$$

in agreement with Eq. (3), since derivatives along the streamline direction are now derivatives along the particle path. Again, as in the unsteady case, it is easy to show that a so defined is the speed of propagation of small disturbances—i.e., the speed of sound. Also,

$$\delta\vartheta/\delta l = \pm(\sqrt{M^2-1}/\rho w^2)(\delta p/\delta l) \tag{23}$$

Using the gas law, Eq. (23) becomes

$$\delta\vartheta/\delta l = \pm(\sqrt{M^2-1}/\rho w^2)(\delta\rho RT/\delta l) = \pm(\sqrt{M^2-1}/w^2) \times (\delta RT/\delta l) \pm (\sqrt{M^2-1}\, RT/w^2)[(\delta \ln \rho)/\delta l]$$

and using Eq. (8),

$$\delta\vartheta/\delta l = \pm (\sqrt{M^2-1}/w^2)[\delta(E+RT)/\delta l] \mp (\sqrt{M^2-1}/w^2)T(\delta\eta/\delta l) \tag{24}$$

In this case,

$$\partial\eta/\partial s = -(1/T)(\partial U/\partial s) \tag{25}$$

where a specification of $\partial U/\partial s$ amounts to a description of the chemical kinetics.

Summarizing the two-dimensional relations, we have the following set of equations to work with:

$$\left.\begin{aligned}
\delta\vartheta &= \pm(\sqrt{M^2-1}/w^2)\delta(E+RT) \mp (\sqrt{M^2-1}/w^2)T\,\delta\eta \\
a^2 &= (\partial p/\partial s)/(\partial\rho/\partial s) \\
p &= \rho RT \\
E &= E(T) \\
d\ln\rho &= (1/RT)dE - (1/R)\,d\eta \\
\partial\eta/\partial s &= -(1/T)(\partial U/\partial s) \\
\partial U/\partial s &= \text{sum total of appropriate chemical rates of components with lagging internal energy} \\
M &= w/a \\
R &= \text{function of the concentrations of the components making up the fluid}
\end{aligned}\right\} \tag{26}$$

In this case we require another equation, which involves an assumption about the flow field. We assume here that there is no heat transfer across streamlines, so that

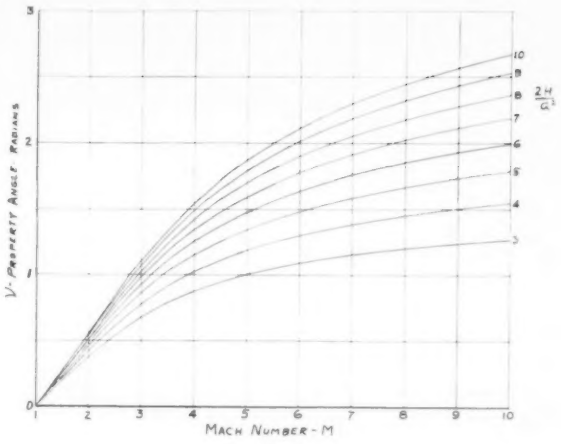

Fig. 1.

at any point along a stream tube the stagnation enthalpy will be constant. Then to the set (26) we can add the equation

$$H_0 = E + RT + (1/2)w^2 + U \tag{27}$$

where H_0, the stagnation enthalpy, is constant along a streamline.

Nonisentropic Steady Two-Dimensional Flow Starting From Uniform Conditions

For a flow starting from uniform conditions, such as a body flying through the atmosphere, as all stream tubes originate in a region of constant stagnation enthalpy H_0, H_0 will be a constant everywhere in the flow field. In this case we can differentiate Eq. (27) in any arbitrary direction; so

$$0 = d(E+RT) + w\,dw + dU$$

and

$$\delta\vartheta = \pm(\sqrt{M^2-1}/w^2)[-w\delta w - \delta U] \mp (\sqrt{M^2-1}/w^2)T\delta\eta$$
$$= \mp(\sqrt{M^2-1}/2)\delta\ln[w^2/(2H_0-2U)] \pm \sqrt{M^2-1}[\delta U/(2H_0-2U)] \mp (\sqrt{M^2-1}/w^2)\delta U \mp (\sqrt{M^2-1}/w^2)T\delta\eta$$

But

$$w^2/(2H_0-2U) = M^2/\{M^2 + [2(E+RT)/a^2]\}$$

so that

$$\delta\vartheta = \mp\frac{1}{2\sqrt{M^2-1}}\left\{\frac{1}{1+\left((M^2-1)/\{1+[2(E+RT)/a^2]\}\right)} - \frac{1}{1+(M^2-1)}\right\}\delta M^2 \mp \frac{\sqrt{M^2-1}}{M^2+[2(E+RT)/a^2]}\,\delta\frac{(E+RT)}{a^2} \mp \frac{\sqrt{M^2-1}}{w^2}\left\{\frac{[2(E+RT)/a^2]}{M^2+[2(E+RT)/a^2]}\right\}\delta U \mp \frac{\sqrt{M^2-1}}{w^2}T\delta\eta$$

and finally, if we let $E + RT = H$, we find

$$\pm\delta\vartheta = -(\partial/\partial M^2)\{\sqrt{1+(2H/a^2)}\tan^{-1}\sqrt{[1+(2H/a^2)]^{-1}(M^2-1)} - \tan^{-1}\sqrt{M^2-1}\}\delta M^2 - \{\sqrt{M^2-1}/[M^2+(2H/a^2)]\}\delta(H/a^2) - (\sqrt{M^2-1}/w^2)\{(2H/a^2)/[M^2+(2H/a^2)]\}\delta U - (\sqrt{M^2-1}/w^2)T\delta\eta$$

Now suppose we define a property angle ν as

$$\nu = \sqrt{1+(2H/a^2)}\tan^{-1}\sqrt{[1+(2H/a^2)]^{-1}(M^2-1)} - \tan^{-1}\sqrt{M^2-1} \tag{28}$$

so that $\nu = \nu(M^2, 2H/a^2)$; then,

$$\delta(\nu \pm \vartheta) = \left(2[\partial\nu/\partial(2H/a^2)]_{M^2} - \left\{\sqrt{M^2-1}/[M^2 + (2H/a^2)]\right\}\right)\delta(H/a^2) - (\sqrt{M^2-1}/w^2)\left\{(2H/a^2)/[M^2 + (2H/a^2)]\right\}\delta U - (\sqrt{M^2-1}/w^2)T\delta\eta \quad (29)$$

Dissociating Diatomic Gas With Vibrational Heat-Capacity Lag

Here, as before, $R = R_0(1+\alpha)$, $E = [(5+\alpha)/2]R_0T$, and $U = \alpha q_0 + E_v(\Theta_v)$, so that

$$\left.\begin{aligned} a^2 &= (1+\alpha)R_0T\,\frac{(7+3\alpha)(\partial T/\partial s) + T(\partial\alpha/\partial s)\left\{1 + (2q_0/R_0T)\right\} + 2(C_{vib}/R_0)(\partial\Theta_v/\partial s)}{(5+\alpha)(\partial T/\partial s) + T(\partial\alpha/\partial s)\left\{(2q_0/R_0T) - 1\right\} + 2(C_{vib}/R_0)(\partial\Theta_v/\partial s)} \\ &= \beta RT \end{aligned}\right\} \quad (30)$$

Also,

$$\frac{H}{a^2} = \frac{\left\{[(5+\alpha)/2] + (1+\alpha)\right\}R_0T}{\beta R_0(1+\alpha)T} = \frac{7+3\alpha}{2\beta(1+\alpha)}$$

and

$$\delta U = q_0\delta\alpha + C_{vib}\delta\Theta_v$$

Although we could eliminate H/a^2 from Eq. (29), it is more convenient to leave it and prepare a graph of ν for various values of $2H/a^2$, which varies from 3 to possibly 10 depending on the circumstances. Fig. 1 gives a chart of ν versus M for various values of $2H/a^2$. Eq. (29) for this case is

$$\delta(\nu \pm \vartheta) = \left[\frac{\partial\nu}{\partial(2H/a^2)}\right]_{M^2}\delta\left(\frac{2H}{a^2}\right) - \frac{\sqrt{M^2-1}}{M^2 + (2H/a^2)}\left\{\delta\left(\frac{H}{a^2}\right) + \frac{2H}{a^2}\,\frac{(q_0\delta\alpha + C_{vib}\,\delta\Theta_v)}{w^2}\right\} - \sqrt{M^2-1}\,\frac{T\delta\eta}{w^2} \quad (31)$$

Note that for $\alpha = 0$, $\Theta_v = 0$, $\beta = 7/5$ and $H/a^2 = 5/2$; then for $\eta =$ constant we have the well known result for a diatomic gas—namely, $\delta(\nu \pm \phi) = 0$ along the directions $dn/ds = \mp 1/\sqrt{M^2-1}$, where $\nu = \sqrt{6}\tan^{-1}\sqrt{(1/6)(M^2-1)} - \tan^{-1}\sqrt{M^2-1}$. The case of ionization can be treated in similar fashion. The extension to flows with axial symmetry can also be made easily.

Conclusions

To calculate flow fields about bodies flying at speeds high enough that relaxation phenomena and chemical reaction rates are important, one must introduce chemical-rate data into the fluid-flow equations. Fortunately, a general theory may be developed, appropriate to such cases, which does not require a knowledge of the detailed chemical-kinetic mechanisms, although the actual flow field resulting from the application of the theory certainly does depend on the rate equations. In cases where the rate equations are not known, observations of flow phenomena can lead, via the theory, to conclusions concerning the chemical kinetics.

References

[1] Kantrowitz, A. R., *Heat Capacity Lag in Gas Dynamics*, J. Chem. Phys., Vol. 14, pp. 150–164, 1946.

[2] Bauer, S. H., and Gustavson, M. R., *Relaxation Techniques for Fast Reactions, A Study of the Dissociation of Nitrogen Tetroxide*, Faraday Society Discussion, No. 17, pp. 69–90, 1954.

[3] Resler, E. L., Jr., and Cary, B. B., *Dissociation of Air Behind Strong Shock Waves*, Proc. Chemical Aeronomy Conference, Cambridge, Mass., 1956 (to be published).

[4] Carrington, T., and Davidson, N., *Shock Waves in Chemical Kinetics: The Rate of Dissociation of* N_2O_4, J. of Physical Chem., Vol. 57, pp. 418–427, 1953.

[5] Blackman, V., *Vibrational Relaxation in Oxygen and Nitrogen*, J. Fluid Mech., Vol. 1, Part 1, pp. 61–85, May, 1956.

[6] Courant, R., and Friedrichs, K. O., *Supersonic Flow and Shock Waves*, p. 40, Interscience Publishers, Inc., New York, 1948.

[7] Munk, M. M., *Remarks on the Velocity of Sound*, Readers' Forum, Journal of the Aeronautical Sciences, Vol. 22, No. 11, p. 795, November, 1955.

Change of Address

Since the Post Office Department does not as a rule forward magazines to forwarding addresses, it is important that the Institute be notified of changes in address 30 days in advance of publishing date to ensure receipt of every issue of the JOURNAL and REVIEW.

Notices should be printed legibly and sent directly to:

Subscription Department
Institute of the Aeronautical Sciences, Inc.
2 East 64th Street, New York 21, N.Y.

Favorable Interference in Lifting Systems in Supersonic Flow†

ANTONIO FERRI,* JOSEPH H. CLARKE,** AND LU TING***

Polytechnic Institute of Brooklyn

Summary

Certain simple integral relations are applied to the qualitative assessment and calculation of the favorable interference effects arising in various spatial arrangements of wings and bodies in a supersonic stream. The arrangements include slender bodies in proximity to wings, wings with underslung pylons or other vertical surfaces, and wing-fuselage combinations. The elementary considerations used in these examples serve to demonstrate to the designer how the pressure drag due to volume and lift can be reduced by arranging the several components comprising the configuration so that they exhibit mutually advantageous shapes and orientations. Vertically antisymmetric modifications of the fuselage shape in the neighborhood of the midwing are suggested which reduce the drag due to lift of midwing-body systems. The considerations are different from those giving rise to the supersonic area rule, according to which vertically symmetric fuselage indentations are made in order to reduce the drag due to thickness or volume, and might have comparable significance.

Symbols

A = area
A = reduced aspect ratio
B = $\sqrt{M^2 - 1}$
b = span
C_D = drag coefficient, based on exposed wing area
C_L = lift coefficient, based on exposed wing area
c, c_0 = chord
c_p = $-2u/V$, pressure coefficient
D = drag
F = lineal source intensity
f = surface source intensity
$\bar{f}$ = image source intensity
h = semiheight of fuselage
L = lift
M = Mach Number of undisturbed stream
q = dynamic pressure of undisturbed stream
R = dimensionless height of wedge; see Fig. 5
S = cross-sectional area
u = x-component of perturbation velocity
V = velocity of undisturbed stream
v = y-component of perturbation velocity
w = z-component of perturbation velocity
x = streamwise Cartesian coordinate
y = lateral Cartesian coordinate
z = normal Cartesian coordinate
α = angle of attack of wing
δ_i, $\bar{\delta}_i$ = inclination of bottom and top of body, respectively; positive when opening body; ($i = 1, 2, 3 \ldots$)
ζ = normal Cartesian coordinate
η = lateral Cartesian coordinate
λ = $\partial z/\partial x$; streamwise inclination
λ_i, $\bar{\lambda}_i$ = inclination of lower and of upper sides of body, respectively; positive when opening body; ($i = 1, 2, 3 \ldots$)
μ = Mach angle of undisturbed stream
ξ = streamwise Cartesian coordinate
σ = thickness ratio of slender body
τ = thickness ratio of wing
ϕ = velocity potential
$\delta\omega$ = elemental width
$(\ )_b$ refers to isolated body
$(\ )_I$ refers to inverted system
$(\ )_m$ refers to minimum value
$(\ )_s$ refers to isolated system
$(\ )_T$ denotes two-dimensional value
$(\ )_w$ refers to wing
$(\ )_0$ denotes incident disturbance
$(\ )_1$ denotes additional disturbance
$(\ )_2$ denotes additional disturbance

Presented at the Aerodynamics—III Session, Twenty-Fifth Annual Meeting, IAS, New York, January 28–31, 1957.

† This research was supported by the United States Air Force through the Air Force Office of Scientific Research, Air Research and Development Command, under Contract No. AF 18(600)-694, Project No. R-352-30-11.

* Professor of Aerodynamics and Director of Aerodynamics Laboratory.

** Assistant Professor of Aeronautical Engineering.

*** Research Associate.

Introduction

A CONSIDERABLE LITERATURE exists concerning the favorable interference in arrangements of wings and bodies in a supersonic stream. In reference 1 it is shown that it is possible to establish a wave system between two infinite rectangular wings in biplane arrangement such that the internal wave drag is zero. A number of authors have subsequently considered the three-dimensional interfering biplane. An axially symmetric counterpart of the biplane, consisting of a body of revolution enveloped by a cowling, is proposed in reference 2 and analyzed by other writers. In reference 3 it is shown that the wave drag of an array of slender bodies can be reduced through use of orientations wherein each body is in the buoyant field of another. Additional examples of such favorable interference have been given by others.

Recent developments make it possible to study spatial distributions of sources, horseshoe vortices, and multipoles which simulate, in principle, any array or combination of wings and bodies to the linear approximation. Hayes' theorem, permitting the construction of equivalent lineal distributions of singularities by moving disturbances along certain oblique planes, is the fundamental device employed. It has become possible, for example, to construct a complementary line of multipoles corresponding to a given body which eliminates the wave drag of the combination, and to consider distributions of singularities which provide minimum wave drag for a given total lift and volume in

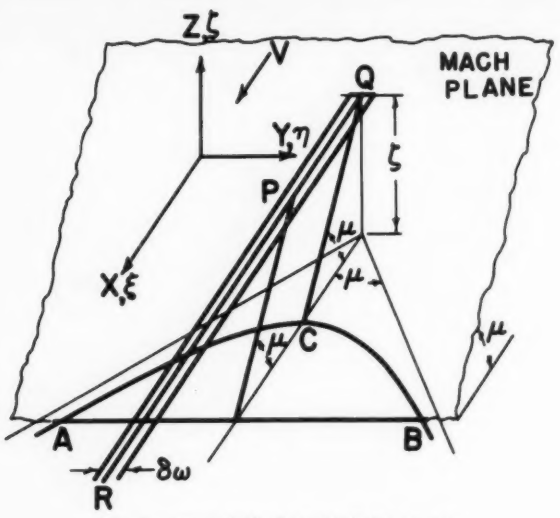

FIG. 1. Flow field of semi-infinite source.

a prescribed region. References 4, 5, and 6 (and the further research cited therein) offer accounts of these methods. It is now clear that unconventional arrangements of suitably shaped wings and bodies make possible significant reductions in pressure drag. In the case of symmetric combinations of wings and slender bodies at zero lift, it is possible to relate the singularities studied to the geometry of the system and there results the supersonic area rule. When the bodies are nonslender or the system develops lift, the geometry simulated by the singularities is not usually known or considered in detail. Whereas the geometry can, in principle, be determined in the last step, no assurance usually exists that it conforms to engineering exigencies or even is real; there is encountered the fiction of negative volume, for example. This factor constitutes a difficulty in a significant body of research.

In the present paper, certain simple integral relations for the flow field of an elemental supersonic source are stated in the first section and then applied in subsequent sections in the design and analysis of a number of lifting systems exhibiting favorable interference. These are (1) a slender body under a lifting wing, (2) a wedge or wedges in the vertical plane of symmetry of a lifting wing, and (3) a pylon under a lifting wing. From the integral relations, certain properties of the chordwise distribution of pressure in wing-fuselage combinations are then deduced. These are used in the design and analysis of (4) a lifting wing-fuselage combination, the fuselage of which is antisymmetrically contoured about the plane of the midwing. The proposed advantageous contouring for lifting combinations is related to the familiar symmetric contouring for nonlifting combinations. All configurations analyzed exhibit a single method for the reduction of the pressure drag of lifting systems, the concept being developed synthetically in the several examples. Whereas the drag of each of the arrangements considered is certainly not a minimum in the sense discussed above, significant reductions in drag relative to the chosen standards of comparison are found in all cases, the physical processes are reasonably clear, the geometric boundaries are explicit, and some new avenues of study are perhaps suggested.

Integral Relations for Source Flow Field

Consider a semi-infinite horizontal elemental surface QR, with width $\delta\omega$, which is aligned in the streamwise direction at a distance ζ from the x-y plane as shown in Fig. 1. Let there be distributed over this surface a source sheet with surface intensity $f(\xi)$. The trace of the Mach cone from Q in the x-y plane is denoted by ACB. At an arbitrary distance downstream of C construct in the x-y plane a lateral line segment AB which runs between the two branches of the hyperbola. It may be verified by direct calculation that the line integral along AB of either the x or the z component of the perturbation velocity, induced by the line of disturbances, is given by the product of the elemental width $\delta\omega$ and the two-dimensional value of the corresponding component which is associated with the source intensity at the point P. That is

$$\int_A^B \delta u \, dy = -[\pi f(P)/B]\delta\omega \equiv u_T(P)\,\delta\omega \tag{1}$$

$$\int_A^B \delta w \, dy = -\pi f(P)\delta\omega \equiv w_T(P)\,\delta\omega, \quad \zeta \neq 0 \tag{2}$$

The point P is defined by the intersection of the elemental surface QR with the forward-leaning Mach plane containing the line AB (see Fig. 1). The reason for the appearance here of the two-dimensional value is suggested by the following observation: the integral of the potential due to a point source at $Q(\xi, \eta, \zeta)$,

$$\phi(x, y, z) = -\frac{1}{\sqrt{(x-\xi)^2 - B^2[(y-\eta)^2 + (z-\zeta)^2]}} \tag{3}$$

with respect to y over the limits defined by the vanishing of the radicand is the same as the integral of the potential with respect to η over similarly defined limits; since the roles of y and η are interchangeable, the two-dimensional value appears in each case. Eqs. (1) and (2) give some insight into how disturbances spread laterally in three-dimensional flow.

Provided that the distance ζ is nonzero, results (1) and (2) are unchanged if the surface element QR is rotated about its streamwise axis to an arbitrary position, or if the distribution of disturbances is regarded as a line distribution instead of an elemental surface distribution. In the latter case, one lets

$$f(\xi)\delta\omega \rightarrow F(\xi) \tag{4}$$

where $F(\xi)$ is the lineal intensity of the source distribution.

If the source intensity is independent of ξ, the integrals of induction, along the line segments defined by successive Mach planes and the hyperbola in the x-y plane associated with Q, are the same. A rectangular

element with area $\delta\xi\delta\omega$ (See Fig. 2) may be formed from two such uniform distributions by subtraction. From Eqs. (1) and (2), there follows immediately that the induction due to the disturbances distributed over this rectangular element is such that

$$\int_A \delta u \, dA = -(\pi f/B)\delta\xi\delta\omega \tag{5}$$

$$\int_A \delta w \, dA = \mp \pi f \, \delta\xi\delta\omega \tag{6}$$

$$\int_L^N \delta u \, dy = 0, \, x > B\zeta \tag{7}$$

$$\int_L^N \delta w \, dy = 0, \, x > B\zeta \tag{8}$$

In the above, A is the area defined by the two hyperbolas and the lateral tangent shown in Fig. 2. The lateral line segment LN is any line downstream of A which extends from one branch of the upstream hyperbola to the other branch. The plus sign in Eq. (6) is taken when ζ is negative. This subtraction process is used to avoid singularities connected with the induction between the two hyperbolas when, in the limit, the two merge into one.[7] As mentioned above, the element may be rotated about its streamwise axis to an arbitrary position or reduced to a line supporting an elemental lineal source distribution; as will be shown later, the integral relations can be used to study diffraction around a corner in connection with wing-body interference problems.

The relations (5)–(8) provide a simple, physical means to assess and calculate representative examples in a number of classes of interference problems. When the geometry is appropriate, they make possible the computation of the lift force, and sometimes the drag force, from a knowledge of the source distribution satisfying the boundary conditions without computing the induced flow field. A number of such applications is presented in the following sections of this paper. In the procedure used, the induction of each elemental source is integrated before consideration is extended to all elements of the distribution. This reversal of the order of integration may be interpreted in terms of a finite-step approximation to the actual source distribution, the limiting process being reserved for the final operation.[7] It is possible to generalize the integral relations to the case where the line segments, such as AB in Fig. 1, are swept. Various features and applications of these relations are discussed in references 7, 8, 9, and 10.

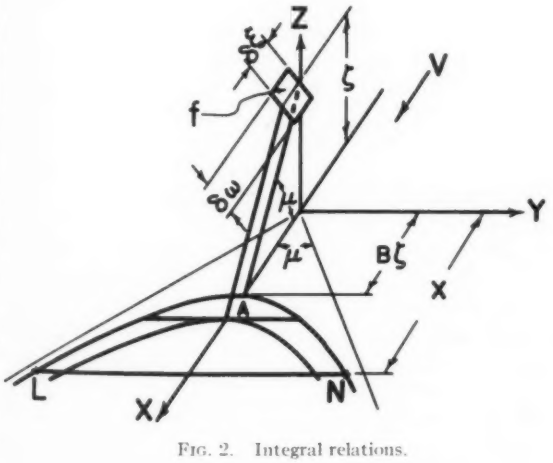

FIG. 2. Integral relations.

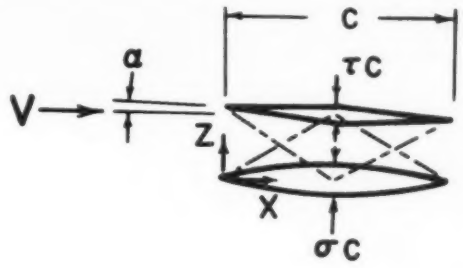

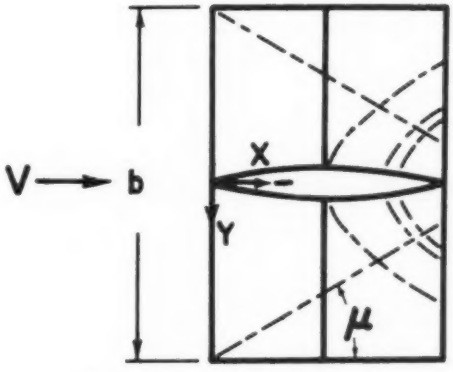

FIG. 3. Slender body under wing.

FAVORABLE INTERFERENCE BETWEEN SLENDER BODY AND LIFTING WING

Consider a rectangular wing having a chord c, a span b, a symmetric diamond profile with thickness ratio τ, and an angle of attack α which is sufficient to generate a prescribed lift. Assume that the reduced aspect ratio A is greater than two, so that the tip effects do not overlap. Suppose that a given symmetric body of revolution, with thickness ratio σ, is to be positioned under the wing such that the attendant rise in pressure drag is as small as possible. For simplicity of discussion, assume that the length of the body is equal to the chord of the wing (see Fig. 3).

Consider the chordwise load distribution induced on the wing by the body, as the body is moved beneath the wing in a streamwise direction. This loading in any position is given immediately by Eqs. (5) and (7) [or Eq. (1)] in terms of the known source distribution representing the body (in this application, the rec-

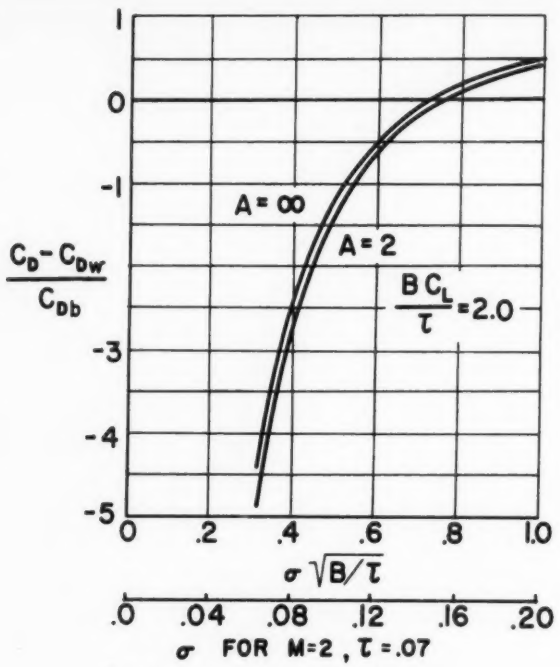

FIG. 4. Drag rise for body under wing.

tangular element in Fig. 2 is reduced to a line element); it is seen that each elemental source of the forebody makes a positive contribution to the load, whereas each elemental sink representing the afterbody makes a negative contribution. (Away from the surface of the body it is sufficient to use the linear form of the pressure coefficient.) Evidently, the value of the normal force is a maximum when the body is positioned so that the nose Mach cone strikes the shoulder of the wing profile and the midbody Mach cone strikes the trailing edge of the wing. Furthermore, the interference force for this position corresponds to a lift and, when $\tau > \alpha$, to a thrust on the afterwing. Since the boundary shape of the wing is to be preserved in the presence of the body upwash, the integral of which is given by Eqs. (6) and (8), the load distribution must be doubled in order to account for the reflections. Using Eq. (4) in Eq. (5), noting Eq. (7), and integrating from zero to $c/2$, one obtains

$$\int_w u\, dA = -(\pi/B)\int_0^{c/2} F(\xi)d\xi \tag{9}$$

After use is made of the relations

$$F(x) = (V/2\pi)S'(x) \tag{10}$$

$$c_p = -(2u/V) \tag{11}$$

and account is taken of reflections, there results

$$\int_w c_p\, dA = (2/B)S_{max} \tag{12}$$

for the integral of the pressure induced by the slender body over the lower afterwing. The force components associated with Eq. (12) are

$$L_{bw}/q = (2/B)S_{max} \tag{13}$$

$$D_{bw}/q = -(2/B)(\tau - \alpha)S_{max} \tag{14}$$

The orientation of the body with respect to the wing is not completely fixed by the above considerations. It is seen from Fig. 3 that the body may still be translated along the Mach waves until the Mach wave from the wing leading edge strikes the midpoint of the body, and the wave from the wing shoulder strikes the tail of the body. The two-dimensional positive pressure field induced by the forewing thus imparts a thrust to the body which is given by the relation

$$D_{wb}/q = -(2/B)(\tau + \alpha)S_{ma} \tag{15}$$

For simplicity, the uniform downwash from the wing is permitted to camber or kink the body at its midpoint. This does not alter the transverse cross sections of the body. The self-induced drag of the body in the presence of the wing is the same as the drag of the uncambered isolated body (the source distribution retains the requisite "smoothness" in the presence of the discontinuous downwash). In the case of a Sears-Haack body, this drag is

$$D_b/q = (9\pi/2)(S^2_{max}/c^2) \tag{16}$$

The lift of the wing is given by the sum of its self-induced lift, corresponding to the angle of attack α, and the lift imparted to the wing by the body, given by Eq. (13). Because the lift of the system is prescribed, the introduction of the body permits a diminution of the wing angle of attack, with a corresponding decrease in its drag due to lift. The drag of the system is given by the sum of the isolated drag of the wing, corresponding to an angle of attack α and thickness ratio τ, and the components given by Eqs. (14), (15), and (16). If the angle of attack is eliminated between these two expressions, the drag coefficient in polar form results. Subtraction from this expression of the drag of the isolated wing, for the same value of the lift coefficient, gives the following expression for the drag rise, relative to the isolated drag of the body:

$$(C_D - C_{Dw})/C_{Db} = 1 - (32/9\pi^2)(\tau/B\sigma^2) - (8/9\pi^2)\times \left\{\frac{[(\tau/B\sigma^2)(BC_L/\tau) - (\pi/4A)]}{[1 - (1/2A)]}\right\} \tag{17}$$

In the above, the lift coefficient is based upon the wing area; A denotes the reduced aspect ratio of the wing.

For the case

$$B\,C_L/\tau = 2.0 \tag{18}$$

the variation of the relative drag rise with the parameter $\sqrt{B/\tau}\,\sigma$ is given in Fig. 4 for values of the reduced aspect ratio of both two and infinity. In order to facilitate interpretation, a second scale for the abscissa, which reads directly in terms of σ for the case $M = 2.0$ and $\tau = 0.07$, is also provided. In the latter case, it is noted that the pressure drag rise is zero for a body thickness ratio of about 15 per cent. For thickness ratios less than this value, a great deal of thrust appears

Even for a thickness ratio of 20 per cent, well outside the range of the theory, the drag rise appears to be only half of the isolated value. It is noted from Fig. 4 that the influence of aspect ratio on the relative drag rise is slight. The numerical calculations indicate that the contribution by the body to the wing lift is responsible for about 35 per cent of the reduction in drag, for the value of the lift coefficient considered.

A body under an elliptic wing with zero thickness and constant loading is studied in reference 4, using Hayes' theorem, in connection with the use of multipole distributions to reduce the wave drag. Vortex drag is not considered. Because the loading of the wing in such analyses is specified, rather than the geometry, the body flow field deforms the wing instead of loading it.

Three-Dimensional Biplane

A number of three-dimensional biplanes of the Busemann type are analyzed in reference 8. The configurations considered involve wings with swept leading edges and straight, unswept trailing edges. The high and intermediate ranges of aspect ratios are treated. Positioned over each wing is a small, flat reflecting plate which intercepts forewing disturbances and reflects them to the afterwing, providing a thrust contribution. For the thickness distributions considered, it is found possible to compute the interference effects, without determining the flow field, by means of Eqs. (5)–(8). In these applications, the rectangular element of Fig. 2 is used in the horizontal position—i.e., parallel to the plane of the wing. Results indicate that the thickness drag of the wing can be greatly reduced, or that the thickness of the root section of the wing can be considerably increased without penalty in drag. The details may be found in reference 8.

Vertical Surfaces Used to Induce Lift on a Wing

In the case of the slender body under the wing, some of the reduction in drag resulted from the lifting pressures induced over the wing surface by the forebody. It appears to be of interest to study further the possibility of offsetting the drag rise due to adding a given body to a lifting system by using an arrangement wherein the body induces lifting pressures on the wing. This approach would be of particular interest in cases where the components of the system do not exhibit inclinations which offer the possibility of obtaining direct thrust contributions from remotely induced disturbances. More generally, it might be conjectured that the drag of a lifting system can be reduced if primarily nonlifting components, such as the fuselage, are designed to produce lift indirectly in this way.

A simple system which is suitable for such a study is shown in Fig. 5. It consists of a wedge, with a semi-included angle λ_1, mounted beneath a sweptback flat wing, with angle of attack α, in its vertical plane of symmetry. The wedge is truncated at the tip as shown, in order to study the effect of its height, and along a Mach wave forming its trailing edge, so that every part of its surface will influence the wing. The leading edge of the wing is swept at the Mach angle so that every portion of the wing will be influenced by the wedge. The wing trailing edge is formed by the hyperbolic trace of the Mach cone from the point of intersection of the lines defining the leading and trailing edges of the wedge, and by an arbitrary lateral line.

The flow field induced by this configuration, and by similar ones, can be determined by superposing the flow fields due to (1) the wing alone at angle of attack α, and (2) the wedge in the presence of the wing when at zero angle of attack. Because no communication between the top and bottom of the wing exists, both subproblems are readily handled with wing theory. For the case $c/c_0 = 1$, the integral over the lower surface of the wing of the pressure coefficient induced in the plane of the wing by the wedge (second subproblem) can be written down immediately by use of Eqs. (5) and (7); the integral is equal to twice the two-dimensional pressure coefficient, corresponding to the inclination λ_1, times the elevation area of the wedge. The factor two accounts for the image of the wedge in the plane of the wing. The rectangular element of Fig. 2 is used vertically in this application (see Fig. 5). Thus the lift, as well as the drag, induced on the wing by the wedge is readily determined and is evidently appreciable. As pointed out in reference 7, the self-induced lift and drag of the flat triangular wing can also be written at once in

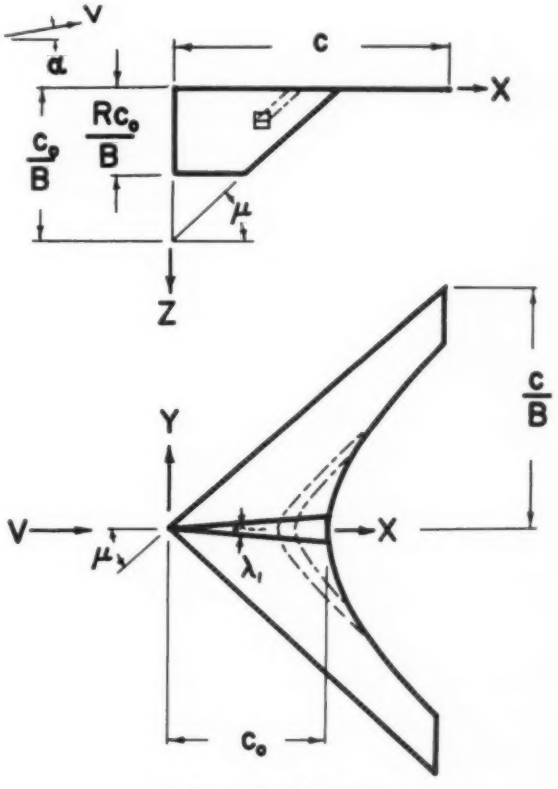

Fig. 5. Wedge under wing.

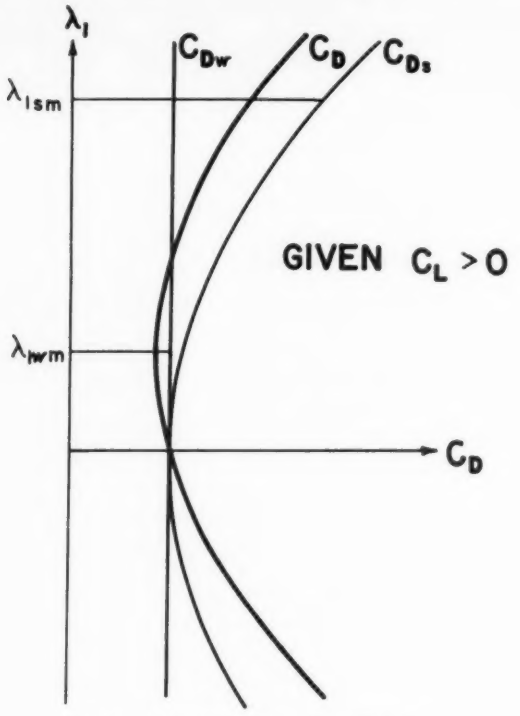

FIG. 6. Variation of drag with inclination.

the same way. When $R = 1$, the flow field induced by the wedge is evidently two-dimensional; from a consideration of this field, it may be seen that a greater amount of lift can be obtained from a given wedge if the trailing edge of the wing is extended rearward to the hyperbolic boundary of the two-dimensional region (see Fig. 5). The trailing edge of the wing was designed as specified above in order to provide this feature.

The computed drag C_D of the configuration may be compared to the drag C_{Ds} of the isolated system—i.e., the sum of the isolated drag of the same wedge and the isolated drag of the wing when generating the same lift. The drag of the configuration can also be compared to the drag C_{Dw} of the wing alone when producing the same lift. The latter provides a standard for comparison when the wedge is regarded to exist primarily to produce the lift.

The force coefficients for interfering configurations of the type discussed evidently assume the forms

$$C_D = a_{\alpha\alpha}\alpha^2 + a_{\alpha\lambda}\alpha\lambda_1 + a_{\lambda\alpha}\alpha\lambda_1 + a_{\lambda\lambda}\lambda_1^2 \qquad (19)$$

$$C_L = a_{\alpha\alpha}\alpha + a_{\lambda\alpha}\lambda_1 \qquad (20)$$

where the a's are all positive (here functions of c/c_0 and/or R) and where

$$a_{\alpha\lambda} \neq a_{\lambda\alpha}$$

in general. Evidently the two $\alpha\lambda_1$ drag components, as well as the λ_1^2 component, tend to offset the favorable lift contribution of the wedge to a certain extent in the present simple design. From Eqs. (19) and (20), the expression for the drag in polar form is

$$C_D = (C_L^2/a_{\alpha\alpha}) + [(a_{\alpha\lambda} - a_{\lambda\alpha})/a_{\alpha\alpha}]\lambda_1 C_L + [(a_{\alpha\alpha}a_{\lambda\lambda} - a_{\alpha\lambda}a_{\lambda\alpha})/a_{\alpha\alpha}]\lambda_1^2 \qquad (21)$$

As long as

$$a_{\lambda\alpha} > a_{\alpha\lambda} \qquad (22)$$

so that the coefficient of $\lambda_1 C_L$ is negative, some advantage due to the interference will always appear. (This means that the life due to the wedge can outweigh the $\alpha\lambda_1$ interference drag terms. If the reverse of Eq. (22) were true, then a corresponding advantage would appear when the wedge is placed above the wing.) The design of the interfering configuration of Fig. 5 is adequate to fulfill Eq. (22). Eq. (21) has the form of the expression for the polar drag of a warped planar wing without thickness. The drag coefficient C_{Ds} of the isolated system assumes the polar form

$$C_{Ds} = (C_L^2/a_{\alpha\alpha}) + a'_{\lambda\lambda}\lambda_1^2 \qquad (23)$$

where, in the present example,

$$a'_{\lambda\lambda} < a_{\lambda\lambda}$$

The drag coefficient C_{Dw} of the wing alone is given by Eq. (21) with $\lambda_1 \equiv 0$.

The properties of the three configurations are conveniently exhibited in terms of two diagrams. Fig. 6 shows, for a given value of C_L, the variation of the drag coefficient with the wedge inclination λ_1 for the three cases. In the case of the specific configuration discussed, R and c/c_0 are regarded as fixed. Evidently the drag of the interfering configuration is less than that of the isolated wing over a range of positive inclinations. Its drag is less than that of the isolated system over the entire range of positive inclinations of interest, and greater than that of the isolated system for all negative inclinations. This diagram provides the basis for selecting a wedge angle at some design value of C_L. Fig. 7 shows, for a given positive value of λ_1, the variation of the drag with C_L for the three cases. Also shown is the drag coefficient C_{DI} of the configuration formed from the one in Fig. 5 by removing the positive wedge from the bottom and placing it on top of the wing. The curve for C_{DI} is evidently the reflection of the C_D curve about the abscissa. All of these parabolas are congruent, being merely displaced relative to one another. The interfering configuration exhibits less drag than its inverted counterpart for all positive values of C_L. As C_L increases from zero the configuration successively overtakes and excels first the isolated system, and then the isolated wing. Two quantities are suggested by these diagrams which are of special interest. The first is the minimum value of C_D/C_{Ds} corresponding to an optimum value of the ratio λ_1/C_L; these two quantities are denoted by the subscripts m and sm, respectively. The second is the minimum value of C_D/C_{Dw} corresponding to an optimum value of the ratio λ_1/C_L; these two quantities are denoted by subscripts m and wm, respectively. The optimum values of λ_1 and C_L are indicated in the sketches of Figs. 6 and 7. Fig. 8 shows, for the specific configuration discussed, the variation of $(C_D/C_{Ds})_m$

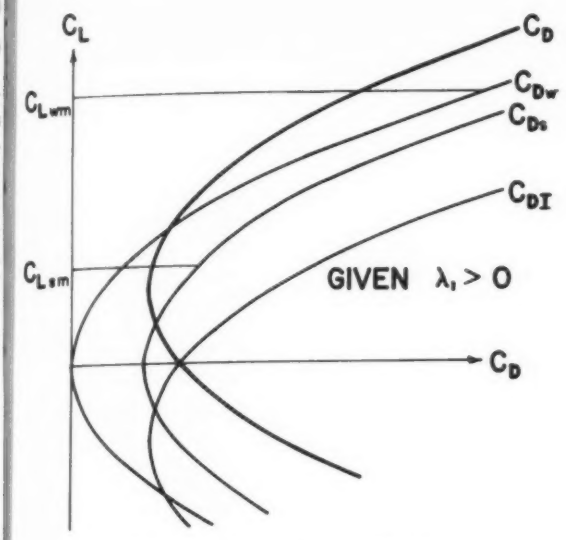

FIG. 7. Variation of drag with lift.

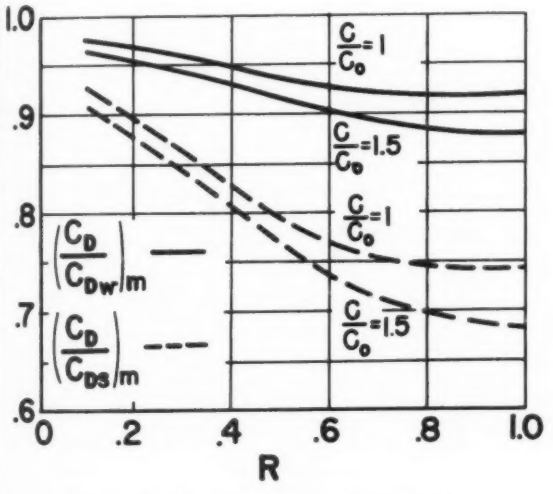

FIG. 8. Drag reductions for wedge under wing.

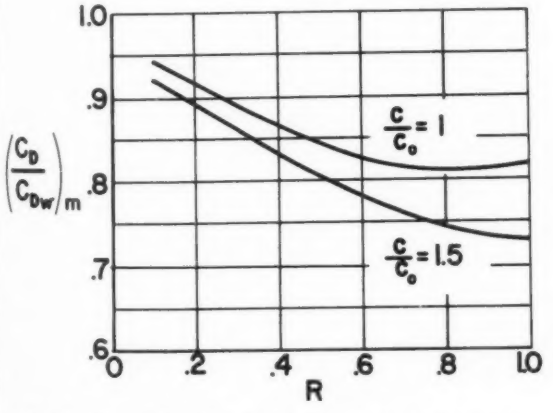

FIG. 9. Drag reductions for wedge on both sides of wing

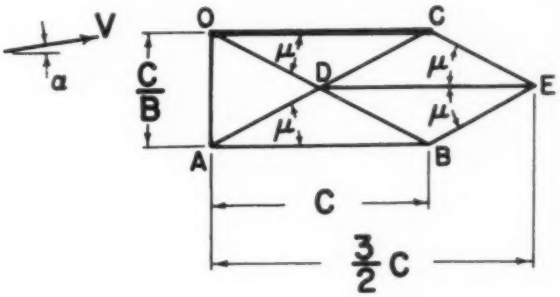

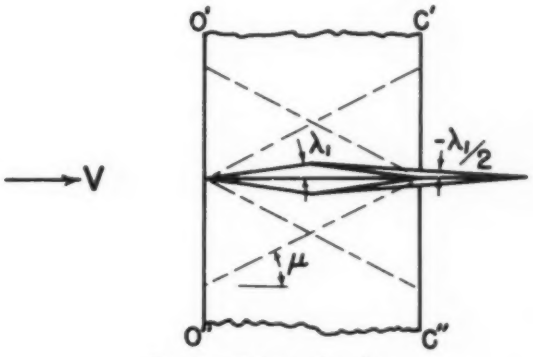

FIG. 10. Pylon under wing.

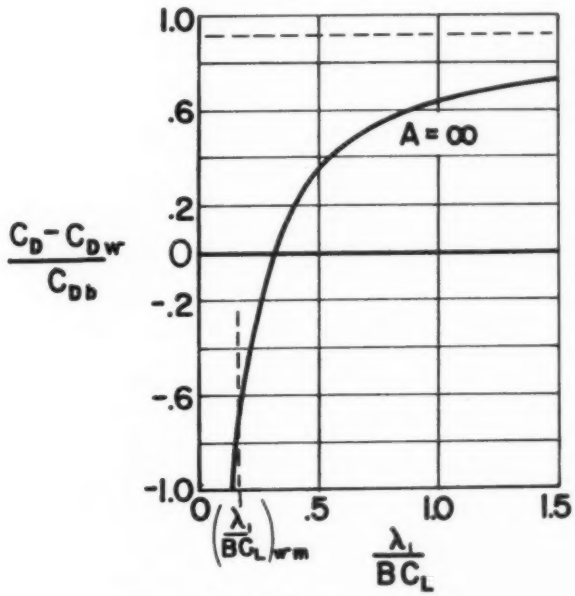

FIG. 11. Drag rise for pylon under wing.

and $(C_D/C_{Dw})_m$ with R for values of c/c_0 of 1.0 and 1.5. Both ratios decrease with increasing R. Evidently the effect of sweeping the trailing edge is beneficial. It is noted that the value of $(C_D/C_{Ds})_m$ falls as low as 0.68 and $(C_D/C_{Dw})_m$ drops to 0.88.

It appears that the drag rise due to adding a vertical surface such as a pylon can be considerably reduced by establishing interference of the type discussed. Furthermore, one might interpret the wedge as representing the sides and bottom of the neighboring fuselage surface of a high wing-body configuration. It would appear then that drag reductions can be obtained by bulging the fuselage section beneath the wing of a high wing-body configuration or by converting a low wing configuration into a high wing configuration.

An obvious modification of the interfering configuration shown in Fig. 5 is to add a negative wedge to the top of the wing in order to double the lifting force induced on the wing by the vertical surfaces. The configuration then becomes vertically antisymmetric, and the coefficients $a_{\lambda\lambda}$, $a_{\lambda\alpha}$ and $a_{\alpha\lambda}$ in Eq. (19) and (20) become twice their former values. Its characteristics are qualitatively the same as previously discussed. The only standard of reference which appears to be of interest is the isolated wing producing the same lift, since the total change of volume due to the addition of the wedges is zero. In Fig. 9 the variation of $(C_D/C_{Dw})_m$ with R for values of c/c_0 of 1.0 and 1.5 is plotted. In the latter case, $(C_D/C_{Dw})_m$ falls to 0.73 when $R = 1.0$. The wedges in this configuration might be interpreted as the antisymmetric contouring of the sides, top, and bottom of the fuselage near the wing in a midwing-body combination. These results suggest the possibility of important reductions in the drag of such lifting systems and will receive further attention in a later section.

Configurations of the type discussed herein were first proposed in references 11 and 12 and are also studied in reference 13. A configuration composed of a circular half cone mounted on the lower side of an arrowhead wing with sonic edges is considered in reference 14. The cone induces lifting pressures on the lower wing and supports some lift over its own surface as well. The drag of the configuration C_D, is compared to that of its inverted counterpart C_{DI}, to the drag C_{Ds} of a configuration employing a symmetrically disposed cone of equal volume, and to the drag C_{Dw} of the wing alone. The polar diagrams of these four configurations are as shown in Fig. 7. For given values of the Mach number, cone angle, and wing form parameter, the values of C_L for which the ratios C_D/C_{DI}, C_D/C_{Ds}, and C_D/C_{Dw} are a minimum may be computed. The best values found in reference 14 for these ratios are 0.64, 0.89, and 0.95, respectively. It is again found that the effect of sweeping the wing trailing edge is favorable.

Favorable Interference Between Pylon and Wing

By use of the ideas developed in the previous Section, it is possible to design a closed pylon positioned below a flat plate wing at incidence in such a way that considerable favorable interference is established at the design Mach Number. Such a pylon might be used for the support of an engine or other installation. It can also be interpreted as any other vertical underslung surface. In Fig. 10 is shown a rectangular wing in combination with a simple pylon, each side of which is formed by five planes. The four swept edges are sonic. A constant positive streamwise inclination λ_1 appears on either side over the region OAD (in this paper a body inclination is counted positive when it tends to open the body, and is counted negative when it tends to close the body). This region induces lifting pressures on the wing which are readily computed by the integral relations. This lift is produced in a relatively efficient manner because the region does not support wing-induced interference drag. The pylon is gradually closed over the region $CDBE$ by means of two planes on either side, the inclinations of which are $-\lambda_1/2$. The region $CDBE$ induces no negative lift on the wing and receives a thrust contribution from the two-dimensional pressure field induced by the lower wing surface. The streamwise inclination of regions OCD and ABD is zero.

The configuration may be analyzed by the method discussed in the last section. The calculations are very simple; they are given in reference 12. The expressions for the lift and drag assume the forms given in Eqs. (19), (20), and (21). The configuration considered is of special interest for the following reason: the drag of the body in the presence of the uninclined wing is virtually the same as that of the isolated body, as is indicated by the asymptote in Fig. 11; also, the two interference drags cancel. When the isolated pylon and wing are brought together, the increment in lift therefore appears without sensible concomitant extraneous effects. When the aspect ratio of the wing is regarded to be large, the performance of the configuration may be evaluated according to the relative drag rise criterion used previously in the case of the interfering wing and slender body. (This parameter plays the role of the parameter C_D/C_{Ds} but is more suited to interfering systems with disparate dimensions and loads; the latter parameter must tend to one as the aspect ratio tends to infinity.)

Fig. 11 presents the variation of $(C_D - C_{Dw})/C_{Ds}$ with the characteristic parameter λ_1/BC_L for the case where the reduced aspect ratio is infinite. As previously remarked, the influence of aspect ratio on this variation is small. Shown on the curve is the value of $(\lambda_1/BC_L)_{wm}$, corresponding to which the ratio C_D/C_{Ds} is a minimum. It appears from the curve that, when the thickness ratio of the pylon is on the order of typical wing thickness ratios, then the relative drag rise can be significantly less than one. When the thickness of the wing is taken into consideration, it may be expected that pylons which exhibit even more favorable interference can be designed. This point is illustrated by the wing-slender body configuration previously discussed.

It is of interest to present here results for the case where the pylon is mounted beneath a triangular wing

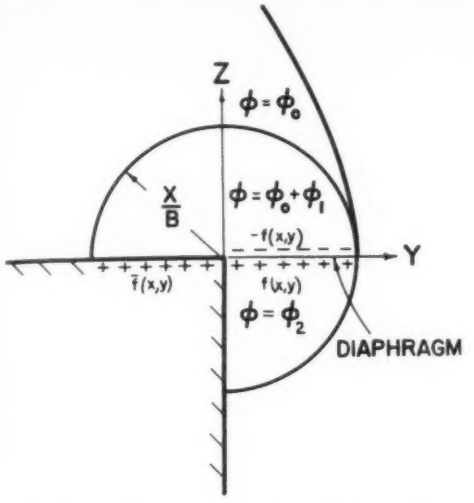

FIG. 12. Diffraction of ϕ_0 around right corner.

with sonic edges. It is found that

$$(C_D/C_{Dw})_m = 0.919 \tag{24}$$

$$(C_D/C_{Ds})_m = 0.713 \tag{25}$$

When a negative pylon is placed above this wing in addition, we pass to the case of antisymmetric contouring in the vertical plane. In this case,

$$(C_D/C_{Dw})_m = 0.849 \tag{26}$$

These results may be compared to those given for the configuration illustrated in Fig. 5 for $R = 1$ and $c/c_0 = 1$. The comparison gives an indication of the effect of closing the wedge(s) in the presence of favorable interference.

ANTISYMMETRIC CONTOURING OF LIFTING WING-FUSELAGE COMBINATIONS

It has been established that appreciable reductions in the pressure drag of lifting cruciform systems are possible through use of appropriate antisymmetric contouring in the vertical plane. The contouring serves either to induce lifting pressures on the wing or to receive thrust contributions from the wing-induced flow field. We now turn to lifting configurations composed of wings midmounted on semi-infinite quasi-prismatic bodies of essentially rectangular cross section—i.e., the body surfaces differ so slightly from the surface of the basic rectangular prism that the boundary conditions may be imposed on the latter surface. Only the case where the prism is at zero angle of attack will be considered. By extending the method discussed, the bodies will be antisymmetrically contoured about the plane of the wing in order to reduce the pressure drag at given lift.

Determination of Flow Field

The flow field of this system may be determined by superposition, once the solution to the problem of the diffraction of disturbances around a semi-infinite right convex corner is available. The solution of this problem is obtained in reference 15 by an extension of the familiar diaphragm method of reference 16. The procedure may be briefly indicated with the aid of Fig. 12. The disturbance field incident to the right corner is given by the velocity potential ϕ_0, which crosses the corner at $x = 0$. The Figure suggests the wave pattern in a plane x = constant > 0. The potential ϕ_0 is defined for $z \geq 0$ and satisfies the boundary conditions

$$(\partial\phi_0/\partial z)(x,\ y < 0,\ 0) = V\lambda(x,\ y) \tag{27}$$

$$(\partial\phi_0/\partial z)(x,\ y > 0,\ 0) = 0 \tag{28}$$

The resulting discontinuity in pressure in the x-y plane for $y > 0$ is relieved by the back-to-back source distributions $-f(x,\ y)$ and $f(x,\ y)$, and by the distribution $\bar{f}(x,\ y)$; these are indicated in the Figure. The satisfaction of the boundary condition

$$(\partial\phi/\partial y)(x,\ 0,\ z < 0) = 0 \tag{29}$$

is assured by the distribution $\bar{f}(x,\ y)$, which is the image of $f(x,\ y)$ and therefore satisfies the relation

$$\bar{f}(x,\ y < 0) = f(x,\ -y) \tag{30}$$

Appearing inside the Mach cone springing from the corner are the additional potentials ϕ_1, defined for $z > 0$ and induced by $-f(x,\ y)$, and ϕ_2, defined for $z < 0$ and induced by $f(x,\ y)$ and $\bar{f}(x,\ y)$. The additional potentials are determined from the integral condition that the aforesaid pressure discontinuity vanish.

It is convenient here to regard the solution to the wing-body problem to be given by the superposition of the solutions to the following three subproblems: (1) the wing panels supporting deflections in combination with the body when free of deflections, (2) the wing when free of deflections in combination with the body when supporting only side deflections, and (3) the wing when free of deflections in combination with the body when supporting deflections only on the top and bottom. Each subproblem is subject to further decomposition. The solution of each subproblem is begun with the solution to the planar problem associated with the deflections considered, these incident disturbances

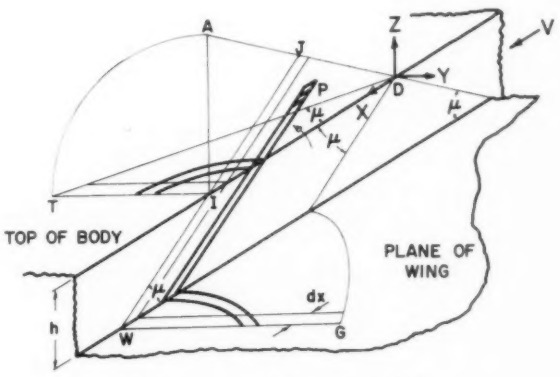

FIG. 13. Vertical diaphragm *DIA*.

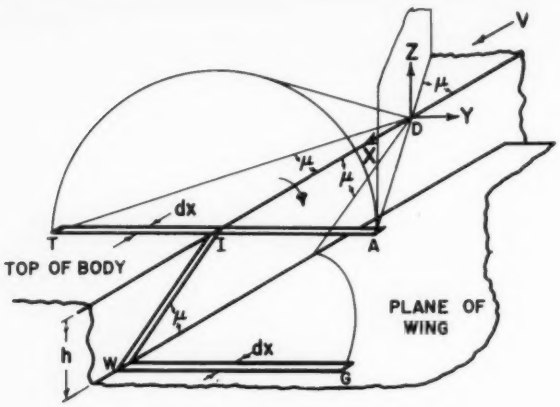

FIG. 14. Horizontal diaphragm *DIA*.

giving rise to systems of horizontal and vertical diaphragms at the four corners of the body. When, in the problems considered, no interference exists between the flow field above the wing plane and the flow field below the wing plane, the wing may be regarded as a plane of symmetry in each half space and the image artifice employed.

Integral Relations

The integral pressure relations for an elemental source [Eqs. (5) and (7)] yield considerable information about the chordwise distribution of pressure in the system without determining the interference flow field. Consider, for example, the diffraction phenomenon shown in Fig. 13. Assume that all faces of the body are free of inclination and that the flow field of the planar wing panel has been determined for the case where the side of the body shown extends vertically to infinity, behaving like the vertical plane of symmetry of the wing (first subproblem). This field corresponds to the incident disturbance at the corner D of the body and gives rise to the vertical diaphragm DIA inside the Mach cone from the point D. An oblique elemental source on either side of the diaphragm is shown at point P. It gives rise to the two illustrated hyperbolic traces on the top of the body and on the plane of the wing. Let TI be a lateral line segment on the top of the body which extends from the Mach wave from D to the corner. Let WG be a lateral line segment extending from the wing-body junction to the hyperbolic trace from D in the plane of the wing. Let the line WG be displaced downstream from the line TI a distance Bh. It follows immediately from the integral relations that

$$\int_T^I u_2 dy = -\int_W^G 2u_1 dy = -(\pi/B)\int_I^J f\, dz \quad (31)$$

The subscripts correspond to the additional potentials shown in Fig. 12. If the plane of the wing may be regarded as a plane of symmetry, the additional induction thereon is $2u_1$. Other incident disturbances which generate vertical diaphragms arise from subsequent reflections and refractions; the associated additional disturbances bear the identical relationship.

An incident disturbance propagating across the top of the fuselage and giving rise to a horizontal diaphragm indicated by DIA, is shown in Fig. 14. This flow field might be due to the far wing panel or to inclinations appearing on the top of the fuselage. Assume that the plane of the wing is free of other disturbances, serving only as a plane of symmetry. Let TIA be a horizontal, lateral, elemental strip extending from one Mach wave from D in this plane to the other. Let WG be a similar strip, displaced downstream from the first by a distance Bh, which extends from the wing-body junction to the hyperbolic trace from D in the plane of the wing. Then the integral pressure relations, applied to the three diffraction source distributions, indicate that the load induced over strip IA by the incident disturbance reappears over strips TI and WG when the additional disturbances are introduced to relieve this loading. This fact may be demonstrated with the aid of Figs. 12 and 14. By definition, the additional disturbances must be such as to fulfill the condition

$$dx\int_I^A u_0 dy + dx\int_I^A u(-f)dy = dx\int_I^A u(\bar{f})dy + dx\int_I^A u(f)dy \quad (32)$$

where the notation $u(-f)$ denotes the value of the x-component of the perturbation velocity induced by the distribution $-f(x, y)$ over the strip, etc. Use is now made of Eqs. (5) and (7) for the case where ζ in Fig. 2 is zero. The induction in the plane of the diaphragm due to the distributions $-f$ and f is such that

$$dx\int_T^I u(-f)dy + dx\int_I^A u(-f)dy = -(\pi/B)dx\int_I^A (-f)dy \quad (33)$$

$$dx\int_T^I u(f)dy + dx\int_I^A u(f)dy = -(\pi/B)dx\int_I^A f\, dy \quad (34)$$

Also, by symmetry,

$$dx\int_I^A u(\bar{f})dy = dx\int_T^I u(f)dy \quad (35)$$

Substitution of Eqs. (33)–(35) into Eq. (32) yields

$$dx\int_I^A u_0 dy = dx\int_T^I u(-f)dy - (\pi/B)dx\int_T^I \bar{f}\, dy - (\pi/B)dx\int_I^A f\, dy \quad (36)$$

Use is now made of Eqs. (5) and (7) for the case $\zeta = h$. With application of vertical symmetry and a change to the subscript notation of Fig. 12, there results

$$dx\int_I^A u_0\, dy = dx\int_T^I u_1 dy + dx\int_W^G 2u_2\, dy \quad (37)$$

Because the plane of the wing is a plane of symmetry, the reflection of the additional disturbances therefrom has the effect of doubling the pressure induced over the strip WG by the diffraction distributions $\bar{f}$ and f. The pressure is then proportional to $2u_s$. Therefore, Eq. (37) is the desired result.

When the geometry is appropriate, the chordwise distribution of pressure in each of the three subproblems enumerated above follows immediately from Eqs. (31) and (37), repeatedly applied. Consider the laterally symmetric configuration shown in Fig. 15. The basic rectangular prismatic body is at zero angle of attack. The wing leading edge LE is everywhere forward of the hyperbola HY from the point D. The shape of the trailing edge is at first arbitrary. Consider a forward-leaning Mach plane which intersects the wing-body juncture at right angles and which is everywhere upstream of the trailing edge.

(1) Let the wing panel planes support an arbitrary distribution of thickness and angle of attack and let the body surfaces be undeflected. Then

$$\int_M^S u\,dy + \int_C^I u\,dy = \int_C^I u_s\,dy \qquad (38a)$$

That is, the integral of induced pressure along the horizontal lines of intersection of the Mach plane with the combination is equal to the integral of induced pressure ($\sim u_s$) along the lines of intersection with the wing panels in the case where the body sidewalls are extended vertically to infinity. The latter integral is determined from the planar wing problem; if the leading edges of the wing panels are supersonic, this line integral can be written at once with use of Eqs. (5) and (7), applied in a plane. Eq. (38a) may then be written

$$\int_M^S u\,dy + \int_C^I u\,dy = -(\pi/B)\int_C^I f\,dy \qquad (38b)$$

where f is the source intensity appropriate to the planar wing problem. If the trailing edges of the wing are straight and unswept, it follows from the above (considering both upper and lower half spaces) that the lift supported by the system, forward of the two Mach planes which contain the trailing edge, is the same as that supported by the wing panels in the case where the body sidewalls are extended vertically to infinity. When the leading edges are supersonic, this is the two-dimensional value. These results appear to carry forward some of the ideas presented in reference 7.

(2) Let the sides of the body support deflections. Let the wing panels and the top and bottom of the body be free of deflection. If the additional disturbances do not extend forward to the wing leading edges, Eq. (38a) again applies. If no disturbances extend forward to the wing leading edges, then

$$\int_M^S u\,dy + \int_C^I u\,dy = \int_C^I u_s\,dy = -(\pi/B)\int_C^S dz \qquad (39)$$

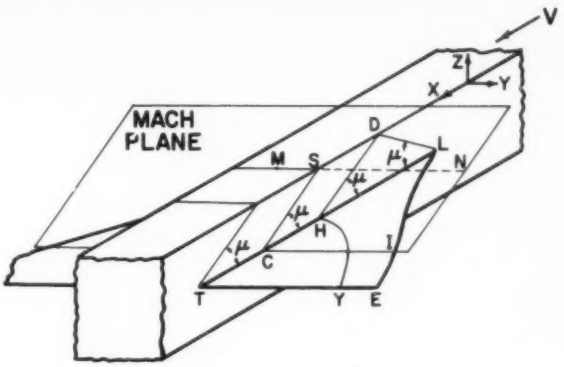

FIG. 15 Flow field of wing-body combination.

where u_s and f are, respectively, the value of u and the source intensity which are associated with the side deflections for the problem where the sidewalls extend vertically without further deflections to infinity. The statement with respect to the lift is also similar to case (1) above.

(3) Let the top of the body support deflections which induce additional disturbances not extending to the leading edges. Let the wing panels and the body sides be free of deflection. Then

$$\int_M^S u\,dy + \int_C^I u\,dy = \int_M^N u_t\,dy = -(\pi/B)\int_M^S f\,dy \qquad (40)$$

where u_t and f are, respectively, the value of u and the source intensity associated with the top deflections for the planar problem where the top of the body extends laterally without further deflections to infinity.

When no disturbances extend forward of the wing leading edges, these results for the chordwise distribution of pressure can be summarized for the complete wing-body system by the statement that the integral of the pressure along the lines of intersection of the three horizontal surfaces with any Mach plane forward of the trailing edges assumes the two-dimensional value based on the integral of the source intensity along the lines of intersection of all of the surfaces with this Mach plane. The source intensity is to be related to the local surface deflections by the planar wing relation.

Role of Antisymmetric Fuselage Contours

The results for the chordwise distribution of pressure supply information on the lifting action of deflected portions of the wing-body surfaces and provide some basis for the antisymmetric contouring of the fuselage in order to reduce the pressure drag of the combination for a given lift. The information is, however, incomplete because it does not extend sufficiently far downstream. In order to determine the drag, the surface pressure distribution must still be computed, in general, but the labor involved when the method of reference 15

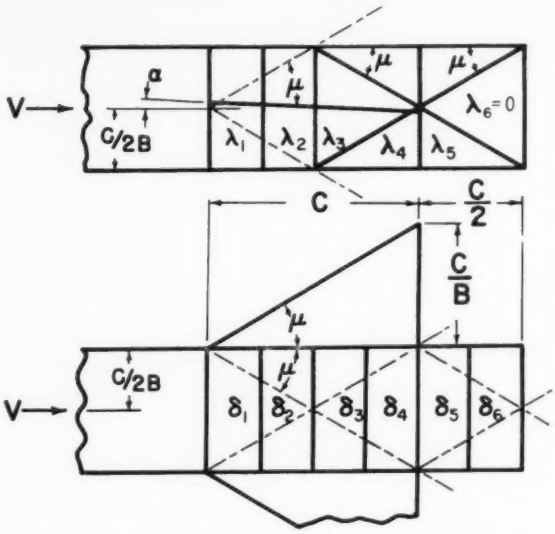

FIG. 16. Wing in combination with antisymmetrically contoured fuselage.

is applied to this end is substantially reduced by use of these results.

Consider the lifting problem where the wing has zero thickness and, for simplicity, supersonic leading edges. Then the sides of the body may be antisymmetrically deflected about the plane of the wing in order to induce lift indirectly on the horizontal surfaces or to receive thrust therefrom. The lifting action is evidently the same as for the cruciform systems previously considered. Similarly, the top and bottom of the body near the wing would be deflected downward in the direction of the wing chord, so that the body is kinked near the leading edge and again near the trailing edge. In the sign convention employed, the lower deflection is positive and the upper negative. These deflected surfaces then induce lifting pressures over the wing in accordance with the mechanism just discussed in terms of oblique Mach planes. But these surfaces are distinguished from the sides by their ability to support direct lift. In fact, forward of Mach planes defining straight trailing edges, they behave like high aspect ratio wing surfaces. It is then evident that the drag of the system considered, at given lift, may be reduced by providing antisymmetric deflections of the top and bottom of the body near the wing which are equal in magnitude to the wing angle of attack. This simply increases the effective wing area and therefore amounts to passing the wing through the body in some way. A second method for the further reduction of the drag of lifting systems, which is possibly coordinate with the first method utilizing indirect lift, now appears. This involves providing a deflection distribution to the top and bottom of the body and to the wing which achieves between the three horizontal planes the same favorable interference effects which are derived from the cambering and twisting of a planar wing with unchanged lift. Because each deflected element supports only part of the lift it induces, the second method also exhibits the indirect lift feature.

A fuselage with an essentially rectangular cross section is used in the present study in order to divide the body into regions which support direct lift and regions which do not support direct lift. Fortunately, the rectangular cross section is also analytically simpler. A fuselage which is deflected on the top and bottom near the wing perhaps suggests an uncontoured fuselage which is at an angle of attack. The upwash field of the fuselage at angle of attack is known to impart an apparent angle of attack to the wing; the resulting lift can be estimated by passing the wing through the body in some way and considering the so-called blanketed area. Whereas the wing is effectively passed through the body in both cases, the two mechanisms are considerably different.

Example

Fig. 16 illustrates a particular wing-body combination which has been subjected to analysis. Each wing panel has zero thickness, an angle of attack α, a chord c, a sonic leading edge, and a straight, unswept trailing edge. The body has an essentially square cross section with sides c/B. It has been terminated at a distance $c/2$ from the trailing edge of the panels so that the domain of influence of the trailing edge does not extend to the top and bottom of the body. Base effects are not considered. Body contouring is provided which is considered to strike a balance between effects desired and analytic complexities. Beginning directly below the apexes of the triangular panels, six plane rectangular surface elements, with deflections δ_1 to δ_6, appear on the bottom of the body, as shown. The top of the body (not shown) is antisymmetric with deflections $-\delta_1$ to $-\delta_6$. Below the wing on either side of the

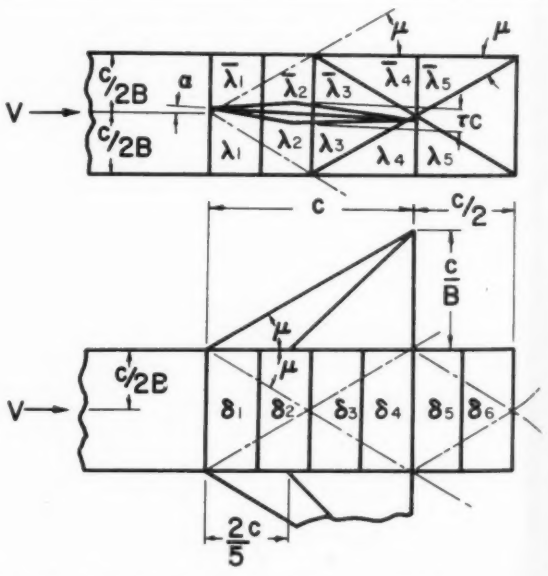

FIG. 17. Wing in combination with asymmetrically contoured fuselage.

body are two rectangular elements and three triangular elements, the dimensions and orientation of these appearing in the Figure. The inclination of the sides of the body in the domain of influence of the wing wake is zero. The upper sides of the body are contoured antisymmetrically. The plan-form area of the wing panels is c^2/B. The plan-form area of the deflected horizontal portions of the fuselage is $3c^2/2B$.

The flow field is given by the superposition of the flow fields of the three subproblems. Each subproblem is divided into equivalent symmetric problems, these then being further decomposed. Each problem is solved by the method of reference 15 with the aid of the integral relations. For a given lift coefficient, the minimum drag of the combination, corresponding to optimum deflections of the planar contour elements, may be computed. There results for the minimum drag

$$C_D/B\ C_L{}^2 = 0.1083 \tag{41}$$

corresponding to the optimum deflections,

$$\left.\begin{array}{llll} \alpha/B\ C_L = & 0.0573 & \delta_1/B\ C_L = & 0.0579 \\ \lambda_1/B\ C_L = & 0.1253 & \delta_2/B\ C_L = & 0.0596 \\ \lambda_2/B\ C_L = & 0.1179 & \delta_3/B\ C_L = & 0.0724 \\ \lambda_3/B\ C_L = & 0.1034 & \delta_4/B\ C_L = & 0.0895 \\ \lambda_4/B\ C_L = & 0.0159 & \delta_5/B\ C_L = & 0.1068 \\ \lambda_5/B\ C_L = & -0.0047 & \delta_6/B\ C_L = & 0.1248 \end{array}\right\} \tag{42}$$

The deflections above the wing are the negative of these values. For the case

$$\left.\begin{array}{l} \delta_i = \alpha, \quad (i = 1\text{–}6) \\ \lambda_i = 0, \quad (i = 1\text{–}5) \end{array}\right\} \tag{43}$$

the drag is found to be

$$C_D/B\ C_L{}^2 = 0.1291 \tag{44}$$

for which

$$\alpha/B\ C_L = 0.1276 \tag{45}$$

When the body is entirely free of deflection, the drag of the combination is

$$C_D/B\ C_L{}^2 = 0.1830 \tag{46}$$

for which

$$\alpha/B\ C_L = 0.2139 \tag{47}$$

The drag of the optimum design is 16.1 per cent less than the drag of the configuration in which all horizontal elements are equally deflected and all vertical elements are undeflected. Further, the drag of the optimum design is 40.8 per cent less than the drag of the wing in combination with the undistorted body. If the horizontal surfaces assume optimum inclinations, the vertical inclinations being suppressed, there results a value for the drag which is only slightly less than the value given by Eq. (44). The inclinations are, however, quite different from the value given by Eq. (45). It is believed that Eq. (44), and not Eq. (46), provides a reasonable standard to which the drag of the optimum design can be compared. The modification of the body according to Eq. (43) is an obvious improvement of the configuration considered which merely increases the effective wing area. The 16.1 per cent additional improvement in the drag, through use of antisymmetric distortions, is evidently significant.

Relationship With Symmetric Contouring

It is of interest to indicate for the midwing configuration the relationship between antisymmetric contouring to reduce the drag due to lift and symmetric contouring to reduce the drag due to volume or thickness. The now familiar body distortions of the latter type are given by the supersonic area rule (see reference 17) in the case of wings in combination with slender fuselages, and by more elaborate considerations when the fuselages are not slender (see, for example, references 18 and 19). Fig. 17 shows the same basic configuration just considered. However, the wing has been provided with a thickness distribution corresponding to symmetric diamond sections, the shoulder falling at the 2/5 chord point. The thickness ratio of the section is τ. The deflection of each planar contour element above the wing is now distinguished from its image below the wing by a bar (see Fig. 17). The flow field and drag for the symmetric, zero-lift problem where $\alpha = 0$ may be calculated within the framework already established. For a given value of the thickness ratio τ, the minimum drag for optimum deflections of the planar contour elements may be computed. There results for the minimum drag

$$C_D B/\tau^2 = 3.891 \tag{48}$$

corresponding to the optimum deflections

$$\left.\begin{array}{llll} \lambda_1/\tau = & -1.2028 & \delta_1/\tau = & 0.1720 \\ \lambda_2/\tau = & -0.0988 & \delta_2/\tau = & 0.0828 \\ \lambda_3/\tau = & 0.3391 & \delta_3/\tau = & 0.0323 \\ \lambda_4/\tau = & 0.1452 & \delta_4/\tau = & -0.0199 \\ \lambda_5/\tau = & 0.2888 & \delta_5/\tau = & -0.0253 \\ & & \delta_6/\tau = & -0.0052 \end{array}\right\} \tag{49}$$

and

$$\left.\begin{array}{l} \bar{\lambda}_i = \lambda_i, \quad (i = 1\text{–}5) \\ \bar{\delta}_i = \delta_i, \quad (i = 1\text{–}6) \end{array}\right\} \tag{50}$$

by symmetry. When all body deflections are suppressed, the drag is given by

$$C_D B/\tau^2 = 5.583 \tag{51}$$

The results for the deflections given by Eq. (49) as well as Hayes' theorem, show the importance of the four leading planar elements for the plan form considered and suggest that a subdivision into smaller elements is in order. In spite of the fact that the coarse contouring is not especially appropriate upstream for the thickness problem, Eq. (48) indicates a 30.3 per cent reduction with respect to Eq. (51).

Consider, finally, the combined problem where the asymmetrically contoured configuration in Fig. 17 is to generate a prescribed lift and the wing has a prescribed

thickness. When the plane of the wing is the horizontal plane of symmetry of the surfaces which support the boundary conditions, as is the case here, an important simplification appears. It is clear that the optimum deflections for minimum pressure drag in the combined problem are linear functions of the prescribed C_L and τ, and that α is a linear function of C_L alone; these deflections are then given by the sum of the corresponding optima already calculated for the separate lift and thickness problems. The optimum flow field is, therefore, the sum of the two optima. As has already been noted, the optimum body deflections for the lifting problem, corresponding to an arbitrary distribution of wing deflections, are antisymmetric (odd potential), and the optimum deflections for the thickness problem are symmetric (even potential). When an odd and even potential are superposed, the pressure corresponding to the first produces no drag on the boundaries corresponding to the second, and vice versa; the drag corresponding to the combined potential is then the sum of the drags corresponding to each taken separately, as in the planar wing problem. In particular, we find that the minimum drag for the combined problem is the sum of the two minima given by Eqs. (41) and (48). More generally, if either Eq. (48) or (51) is added to Eq. (41), (44), or (46), there results the drag of the system corresponding to the two superposed boundaries. We then see at a glance the effect on the drag, for given lift and thickness, of the several contour combinations.

Conclusions

The integral relations for the flow field of an elemental supersonic source provide a useful means for the assessment and calculation of the interference effects arising in various spatial arrangements of wings and bodies, and in wing-body combinations. The relations implemented the analysis of a number of special problems. It appears that slender bodies and pylons can be located under lifting wings with small, or even negative rise in pressure drag. Antisymmetric modifications of the fuselage near the midwing can provide significant drag reductions in lifting wing-body combinations. In the example given, the pressure drag for given lift was reduced 16.1 per cent below the drag of the combination with the wing, in effect, passed through the body, and 40.8 per cent below the drag of the combination with an undistorted body. In these antisymmetric modifications, vertical surfaces of the body are distorted either to induce lift on the wing or to receive thrust from the flow field induced by the wing. Since horizontal surfaces of the body near the wing can be deflected to support self-induced lift, they can be provided with a distribution of angle of attack related to the wing distribution of angle of attack in such a way as to provide mutual favorable interference analogous to that obtained by warping planar lifting systems. The antisymmetric contouring bears the same relation to the drag due to lift that symmetric contouring bears to the zero-lift drag, and appears to have comparable significance.

References

[1] Busemann, A., *Atti del V. Convego "Volta"*, Rome, Reale Accademia d'Italia, 1935.

[2] Ferrari, C., *Campi di corrente ipersonora attorno a solidi di rivoluzione*, L'Aerotecnica, Vol. XVII, Fasc. 6, pp. 507–518, 1937.

[3] Friedman, M. D., and Cohen, D., *Arrangement of Fusiform Bodies to Reduce the Wave Drag at Supersonic Speeds*, NACA TN 3345, November, 1954.

[4] Lomax, H., and Heaslet, M. A., *Recent Developments in the Theory of Wing-Body Wave Drag*, Journal of the Aeronautical Sciences, Vol. 23, No. 12, pp. 1061–1074, December, 1956.

[5] Graham, E. W., Lagerstrom, P. A., Licher, R. M., and Beane, B. J., *A Theoretical Investigation of the Drag of Generalized Aircraft Configurations in Supersonic Flow*, NACA TM 1421, January, 1957.

[6] Jones, R. T., *Minimum Wave Drag for Arbitrary Arrangements of Wings and Bodies*, NACA TN 3530, February, 1956.

[7] Lagerstrom, P. A., and Van Dyke, M. D., *General Considerations About Planar and Non-planar Lifting Systems*, Rep. No. SM-13432, Douglas Aircraft Co., Inc., June, 1949.

[8] Ferri, A., and Clarke, J. H., *On the Use of Interfering Flow Fields for the Reduction of Drag at Supersonic Speeds*, Journal of the Aeronautical Sciences, Vol. 24, No. 1, pp. 1–18, January, 1957.

[9] Bleviss, Z. O., *Some Integrated Properties of Pressure Fields About Supersonic Wings*, Journal of the Aeronautical Sciences, Readers' Forum, Vol. 20, No. 12, pp. 849–851, December, 1953.

[10] Sears, W. R. (Ed.), *General Theory of High Speed Aerodynamics*, Vol. VI of "High Speed Aerodynamics and Jet Propulsion," Princeton University Press, Princeton, N.J., 1954.

[11] Ferri, A., *Recent Theoretical Work in Supersonic Aerodynamics at the Polytechnic Institute of Brooklyn*, pp. 341–362 of "Proceedings of the Conference on High-Speed Aerodynamics, Jan. 20–22, 1955," Polytechnic Institute of Brooklyn, Brooklyn, N.Y., 1955.

[12] Ferri, A., Clarke, J. H., and Casaccio, A., *Drag Reduction in Lifting Systems by Advantageous Use of Interference*, PIBAL Rep. No. 272, Polytechnic Institute of Brooklyn, May, 1955. **Classified Confidential.**

[13] Rossow, V. J., *A Theoretical Study of the Lifting Efficiency at Supersonic Speeds of Wings Utilizing Indirect Lift Induced by Vertical Surfaces*, NACA RM A55L08, March, 1956.

[14] Reyn, J. W., and Clarke, J. H., *An Assessment of Body Lift Contributions and of Linearized Theory for Some Particular Wing-Body Configurations*, PIBAL Rep. No. 305, Polytechnic Institute of Brooklyn, June, 1956.

[15] Ting, L., *Diffraction of Disturbances Around a Convex Right Corner with Applications in Acoustics and Wing-Body Interference*, PIBAL Rep. No. 307, Polytechnic Institute of Brooklyn, August, 1956.

[16] Evvard, J. C., *Distribution of Wave Drag and Lift in the Vicinity of Wing Tips at Supersonic Speeds*, NACA TN 1382, July, 1947.

[17] Jones, R. T., *Theory of Wing-Body Drag at Supersonic Speeds*, NACA RM A53H18a, September, 1953.

[18] Lomax, H., and Heaslet, M. A., *A Special Method for Finding Body Distortions that Reduce the Wave Drag of Wing-Body Combinations at Supersonic Speeds*, NACA RM A55B16, May, 1955.

[19] Nielson, J. N., *General Theory of Wave-Drag Reduction for Combinations Employing Quasi-Cylindrical Bodies with an Application to Swept-Wing and Body Combinations*, NACA RM A55807, June, 1955.

Rotating Stall in Axial Flow Compressors

JEAN FABRI* AND RAYMOND SIESTRUNCK**

Office National d'Etudes et de Recherches Aéronautiques

SUMMARY

The classical theories of linearized aerodynamics yields a complete description of the flow field due to the rotating stall in a two-dimensional cascade of airfoils, when the extension of the stalled region is small. The corresponding physical scheme can be used for larger stalled regions, without the limitations of the linearizing assumptions, if no through flow is assumed through the stall zones. Experimental researches on a single rotor confirm the results of the theoretical calculations, where the mean radius section of the rotor is described by means of a two-dimensional model.

SYMBOLS

p	= static pressure
P	= total pressure in the absolute motion
R-	= motion relative to the rotor
S-	= motion relative to the stall
U	= tangential velocity of the rotor
V	= tangential velocity of the stall
W	= axial velocity of the flow
(u, v)	= local upstream S-perturbation velocity for linearized theory and actual upstream S-velocity for nonlinearized theory
(u', v')	= local harmonic parts of the downstream S-perturbation velocity of linearized theory
$(\bar{u}, \bar{v})$	= asymptotic downstream rotational S-perturbation velocity for linearized theory
x	= direction normal to the cascade (itself defined by $x = 0$)
y	= direction parallel to the cascade
α	= R-angle of the uniform motion
$\hat{\alpha}$	= critical R-angle
α_*	= R-exit angle from the cascade
ζ	= stagger angle of blades
θ	= downstream S-streamline angle at infinity
Θ	= angular distance between two hot-wire anemometers
ν	= stalled fraction of a period
ρ	= density
φ	= flow coefficient
ψ	= total pressure coefficient
ψ_s	= static pressure coefficient

the sign $\hat{}$ designates all quantities corresponding to the ideal point of rotating stall onset

(1) INTRODUCTION

(1.1) *Occurrence of Rotating Stall*

WHEN THE FLOW RATE in an axial-flow turbomachine decreases, due, for instance, to the throttling of the engine, the angles of attack of the blade rows increase and eventually the machine stalls. Very often this stall appears as a periodic disturbance of the general flow and is characterized by the uniform propagation, from pressure faces toward suction faces of the blades, of symmetrically disposed stalled zones made up of one or several groups of stalled blades.

The flow and pressure fields observed during such a rotating stall undergo periodic variations, the steep fronts and high intensities of which show the nonlinear character of the process. However, as long as the extent of the stalled zones is not too large—i.e., at an operation close to the point where rotating stall appears—linearized theories may apply and yield a mathematical scheme for the physical aspects of the phenomenon.

Such a linearized theory was given by W. R. Sears,[1] who thoroughly examined all the basic assumptions and the results they can yield. The very important part played by the assumed behavior of the stalled airfoils was clearly emphasized, as well as the eigenvalue character of the speed of stall propagation, which experimentally seems to be a perfectly determined parameter of the phenomenon. This character appears in the theory only if the pressure versus the angle of attack performance curve is not linear. Neither the introduction of a time lag between the angle of attack and the lift of the airfoil, in order to take into account the unsteadiness of the phenomenon, nor, as suggested by H. W. Emmons et al.[2] and later by A. H. Stenning,[3] the replacement of the airfoil theory by a blade-channel theory, would avoid these difficulties.

On the other hand, F. E. Marble[4] succeeded in describing by means of an aerodynamic theory the main properties of the rotating stall, by assuming that the pressure versus angle of attack performance curve is discontinuous for the critical angle of attack.

A result which seems new to us and which constitutes the main point of interest of the linearized approach[5] given briefly hereafter, is that all the main kinematic properties of rotating stall may be obtained, qualitatively as well as quantitatively, without using any definite performance curve for the operation of the stalled airfoil cascade, as long as it can be assumed that both the stalled and unstalled performance curves can be linearized and that there is an actual discontinuity between these two operating conditions.

Then the conclusions of our linearized theory are the following: when rotating stall appears in an axial flow compressor, the angle of attack of the unstalled blades remains constant and equal to its maximum value, compatible with a nonseparated flow, whereas practically no flow goes through the stalled zones.

These results are further generalized to a one-dimensional representation of the flow—where the

Presented at the Aerodynamics—I Session, Twenty-Fifth Annual Meeting, IAS, New York, January 28–31, 1957. Revised and received March 14, 1957.

* Chief of Research Group, ONERA, Paris.

** Chief of Research Division, ONERA, Paris.

linearizing assumptions are no longer necessary—which gives the corresponding results for stalled operations with large stall cells.

Both representations are described in the case of two-dimensional cascade flow only.

(1.2) *Mathematical Representation of the Flow*

Let us consider a two-dimensional cascade of infinitely close airfoils placed along the y-axis of the xy-plane. This cascade moves along the y-axis with the velocity $-U(U > 0)$. A uniform incompressible flow (density ρ, velocity $W > 0$ directed along the x-axis) attacks the profiles. In the R-motion, relative to the blades, the ratio U/W defines the angle of attack α ($\tan \alpha = U/W$) and as long as α does not exceed its critical value $\hat{\alpha}$, the whole motion is uniform and permanent.

However, when $\alpha > \hat{\alpha}$, equidistant stalled regions propagate along the cascade with the absolute velocity $-V(V > 0)$. (See Fig. 1.) Then both the absolute motion and the R-motion are unstationary. On the contrary, the S-motion, the motion relative to the stall, is stationary if an infinitely close blade spacing is assumed.

For the sake of simplicity, the distance separating two stalled zones is measured by 2π, each stalled zone extending over a fraction ν of the whole period. It is further assumed that the R-exit angle α_* may be considered in first approximation as constant and independent of the angle of attack.[6]

(2) Linearized Flow Field Corresponding to the Onset of Rotating Stall

(2.1) *Description of the Flow Field*

The upstream S-motion is obtained by superimposing on the uniform (W, V) flow an *irrotational* perturbation field (w, v) periodic with respect to y and vanishing at the upstream infinity.

A similar description of the downstream field can be obtained only in the case when the extent $2\nu\pi$ of each stalled zone is small in comparison with the period of the phenomenon ($\nu \ll 1$). Then the *rotational* downstream S-flow is made up of the main flow $(W, W \tan \theta)$ which assures the mass flow rate and gives asymptotic streamlines with a slope $\tan \theta$, of a harmonic perturbation field (w', v') which vanishes at the downstream infinity, and of a rotational perturbation flow the local value of which can be derived from the asymptotic perturbation velocity $(\bar{w}, \bar{v})$, where $\bar{v} = \bar{w} \tan \theta$, by calculating $(\bar{w}, \bar{v})$ for the local value of $y - x \tan \theta$, since in the case of the linearized theory the downstream S-streamlines coincide nearly with the straight lines

$$y - x \tan \theta = \text{const}$$

(2.2) *Correspondence Between the Perturbation Velocities on the Two Faces of the Cascade*

As all perturbations are periodic in y it follows that

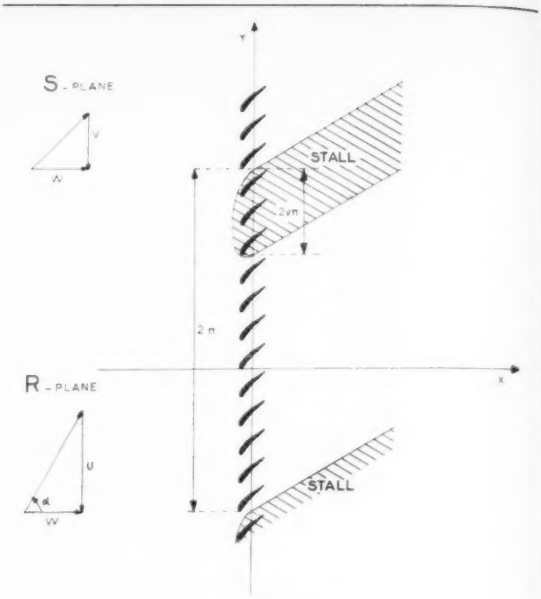

FIG. 1. Stalled cascade.

$$W(\tan \alpha_* - \tan \theta) = U - V \tag{1}$$

With the subscript 0 designating the values of the perturbations at $x = 0$, the following relations are obtained:

$$w_0 = w_0' + \bar{w}_0, \quad v_0' + \bar{v}_0 = w_0 \tan \alpha^* \tag{2}$$

which express the conservation of the mass flow rate across the cascade and the constancy of the R-exit angle.

By eliminating the rotational perturbation ($\bar{w}_0$, $\bar{v}_0 = \bar{w}_0 \tan \theta$) there follows the relation of correspondence

$$w_0(\tan \alpha_* - \tan \theta) = v_0' - w_0' \tan \theta \tag{3}$$

between the two harmonic fields (w, v) and (w', v') along their common boundary ($x = 0$), from which there results the conjugate relation (see Appendix A):

$$v_0 (\tan \alpha_* - \tan \theta) = w_0' + v_0' \tan \theta \tag{4}$$

(2.3) *Energy Equations*

Now, in the unstalled regions, the energy equations can be written in their usual form, providing that only steady motions be considered and also that the same streamline be followed.

In the upstream field, the S-motion is steady and, if P designates the *absolute* upstream stagnation pressure and p_0 the pressure at a point of the upstream front of the unstalled region, the Bernoulli equation follows in the form

$$(P/\rho) + (V^2/2) = (p_0/\rho) + [(W + w_0)^2/2] + [(V + v_0)^2/2] \tag{5}$$

As the flow passes through the rotor, a steady R-motion can be assumed; thus, p' being the pressure at the corresponding point of the downstream face of the

cascade, one obtains

$$(p_0/\rho) + [(W + w_0)^2/2] + [(V + v_0)^2/2] = (p_0'/\rho) + [(W + w_0)^2/2](1 + \tan^2 \alpha_*) \quad (5')$$

Finally, in the downstream S-field, the asymptotic pressure $\bar{p}$ is related to the conditions at the cascade exit by the equation

$$(p_0'/\rho) + [(W + w_0)^2/2] + [(W \tan \theta + w_0 \tan \alpha_*)^2/2] = (\bar{p}/\rho) + [(W + \bar{w}_0)^2/2](1 + \tan^2 \theta) \quad (5'')$$

By linearizing Eqs. (5), (5′), and (5″)—that is, by cancelling all squares of the perturbation terms—there follows

$$\frac{P - \bar{p}}{\rho} + \frac{V^2}{2} - \frac{W^2}{2}(1 + \tan^2 \alpha_*) = Ww_0 \tan \alpha_* (\tan \alpha_* - \tan \theta) - v_0(U - V) + W\bar{w}_0(1 + \tan^2 \theta) \quad (6)$$

Then by Eqs. (1), (2), (3), and (4), the pressure increase through the cascade is:

$$[(P - \bar{p})/\rho] + (U^2/2) - (W^2/2)(1 + \tan^2 \alpha_*) = W[w_0(1 + \tan^2 \alpha_*) - 2v_0(\tan \alpha_* - \tan \theta)] \quad (7)$$

(2.4) *Determination of the Flow Field*

For the sake of simplification, Eq. (7) will be written as

$$w_0 - v_0 \cot \beta = b \quad (8)$$

valid in the unstalled fraction of the cascade front; there is of course a very similar relation

$$w_0 - v_0 \cot \gamma = c \quad (9)$$

valid in the stalled fraction, the exact values of the constants c and γ depending upon the assumption made concerning the energy transfer through the stalled blade channels.

The analytical function $w - iv$ defined in the $x < 0$ half of the $x + iy$ plane by means of Eqs. (8) and (9) is given by (see Appendix B)

$$w - iv = \frac{b \tan \beta - c \tan \gamma + i(c - b) \tan \beta \tan \gamma}{\tan \beta - \tan \gamma} + \lambda e^{-i\beta}\left[\frac{e^{-i\nu\pi - z} - 1}{e^{-z} - e^{-i\nu\pi}}\right]^{(\gamma - \beta)/\pi} \quad (10)$$

if the stalled zones are assumed to occupy the fractions

$$[(2k - \nu)\pi \leq y \leq (2k + \nu)\pi;\ k = \pm 1, \pm 2, \ldots]$$

of the cascade front and also if minimum singularity conditions are assumed. The parameter λ is determined by the condition of regularity at the upstream infinity ($w - iv = 0$ for $x = -\infty$).

(2.5) *Stall Propagation Velocity*

At both ends $[y = (2k \pm \nu)\pi]$ of the stalled zones the R-angle of attack of the blades is necessarily equal to its critical value $\hat{\alpha}$ and there follows

$$\tan \beta = \tan \hat{\alpha}, \quad b = U \cot \hat{\alpha} - W \quad (11)$$

both relations being independent of the assumption concerning c and γ. Thus, the rate of stall propagation,

$$V = U - W(1 + \tan^2 \alpha_*)/(2 \tan \hat{\alpha}) \quad (12)$$

and the pressure increase through the stalled cascade,

$$(\bar{p} - P)/\rho = (U^2/2) - (W^2/2)(1 + \tan^2 \alpha_*) - W^2(1 + \tan^2 \alpha_*)\{[U/(W \tan \hat{\alpha})] - 1\} \quad (12')$$

(which derive from Eqs. (7), (8), and (11), without any assumption on the actual behavior of the stalled blades) give the following very simple expression for the rate of stall propagation at the onset point of the rotating stall ($U = W \tan \hat{\alpha}$):

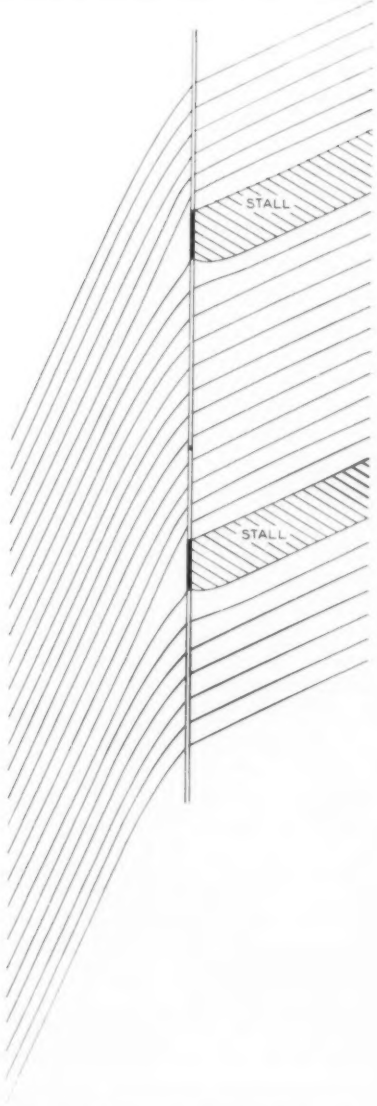

FIG. 2. S-streamlines of rotating stall.

$$V = U\{(1/2) + [(\bar{p} - P)/\rho U^2]\} \quad (13)$$

Furthermore the R-angle of attack of the blades remains constant all along the unstalled blade front, the incidence of the flow being "saturated" to the critical value $\hat{\alpha}$.

(2.6) *Example of a Flow Field*

As an example of the flow field induced by the rotating stall, Fig. 2 shows the S-streamlines corresponding to the operation of the mean section of the test compressor A, the performances of which are described in Section (4).

In Eq. (9) c and γ were taken to be zero—i.e., no through flow was assumed for the stalled blade channels. The following aerodynamic parameters define the flow:

$$W/U = 0.47, \quad \tan \alpha = 1.78, \qquad \tan \alpha_* = 1 \quad (\nu = 0.14)$$

The straightness of the downstream S-streamlines justifies a posteriori the use of linearization and in particular the assumption that the rotational S-perturbation velocity remains constant along the lines

$$y - x \tan \theta = \text{const}$$

The whole S-flow field can be described as made up of no-flow zones attached to the moving blades, somewhat analogous to the potential flow in radial compressors where small flow rates induce high angles of attack on the blades and lead to dead fluid zones attached to the blades.[7]

(3) Induced Flow Field in the Case of Finite Perturbations

(3.1) *A Nonlinearized Representation of the Rotating Stall*

As the throttling of the flow increases, the mean R-angle of attack also increases and so does the extent of the stalled zones. Then the intensity of the perturbations becomes important and the above assumption of linearized theory no longer applies.

The following assumptions allow then an extension of the linearized theory to the case of disturbances with finite amplitude, (w, v) designating at this time the components of the S-velocity. (a) No flow is assumed through the stalled blade channels,[8] the stall cell being a kind of constant pressure wake:

$$w_0 = 0 \quad \text{for} \quad -\nu\pi < y < \nu\pi$$

(b) This constant pressure wake is bounded at least at one side by a regular jet line along which the velocity remains constant:

$$w_0 = 0 \quad \text{at} \quad y = -\nu\pi \quad \text{and/or} \quad y = \nu\pi$$

(c) The angle of attack of the blades in the R-motion is equal to its critical value $\hat{\alpha}$ at the regular edge of the front of the stall cell.

Thus, from the general definition of the local R-angle of attack,

$$\tan \alpha_0 = (v_0 + U - V)/w_0 \quad (14)$$

at the regular edge of the stall zone there follows

$$v_0 = V - U \quad (15)$$

Then from the Bernoulli equation, written along the upstream S-streamline which eventually passes through this regular edge of the stall zone one obtains

$$(P/\rho) + (V^2/2) = (\bar{p}/\rho) + [(V - U)^2/2] \quad (16)$$

Since no pressure rise is given at this point by the rotor, $\bar{p}$ designates the downstream uniform pressure—that is, the pressure in the wake.

There follows the value of the speed of stall propagation

$$V = U\{(1/2) + [(\bar{p} - P)/\rho U^2]\} \quad (13)$$

identical to the one obtained in the case of small perturbations, but valid here for finite disturbances also.

(3.2) *Extent of the Stall Zones*

A one-dimensional approach gives then the extent of the stall zones since it can be assumed, by generalizing the results of the linearized theory, that the R-angles of attack along the unstalled blade front are close to the critical angle $\hat{\alpha}$. Due to the conservation of the tangential momentum, there is no mean induced tangential velocity—that is,

$$v_{0,m} = V \quad (17)$$

where the subscript m designates a mean value along the unstalled front of the blade row, where

$$(2k + \nu)\pi < y < (2k + 2 - \nu)\pi$$

The mean axial velocity is very simply related to the rotor speed as

$$w_{0,m} = U \cot \hat{\alpha} \quad (18)$$

Finally, the mass flow conservation equation yields the extent of the stall zones as

$$\nu = 1 - \tan \hat{\alpha}/\tan \alpha \quad (19)$$

(4) Comparison Between Theoretical Predictions and Experimental Results

(4.1) *Simplified Theory in View of Experimental Verification*

The mean conditions (17) and (18) at the unstalled front of the cascade imply also that the conditions at the front of the unstalled zones are independent of the extent of the stalled regions. It follows that the pressure increase through the unstalled blade channels is independent of the extent of the stall, and the stall speed of rotation remains constant along the whole organized stall performance curve. Thus for all experimental verifications, the static pressure $\bar{p}$ necessary for the calculation of V/U should be measured

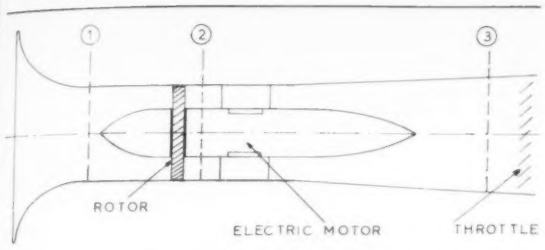

FIG. 3. Experimental compressor A.

during the unstalled operation, at the extrapolated intersection of stalled and unstalled performance curves.

(4.2) *Experimental Compressor A*

Compressor A is a one-stage single rotor with a casing diameter of $2R = 600$ mm. and a hub/tip ratio $R_0/R = 0.625$. The solid body blading consists of untwisted blades with chords proportional to the distance r to the compressor axis, the solidity being thus constant along the blade. The stagger can be characterized by a single angle ζ and the stall always takes place along the whole blade.

On such a compressor the measurements made at the mean radius $R_m = \sqrt{(R^2 + R_0^2)/2}$ represent very closely the mean performances of the whole machine, and in particular the local axial velocity is very little different from the mean axial velocity. Thus a two-dimensional cascade theory may apply at this radius.

The experimental data are taken at three stations (see Fig. 3). Station 1 represents the upstream infinity where all perturbations are already damped, and permits correct measurement of the mean mass flow rate. Station 2 is situated immediately behind the rotor and gives the aerodynamic data (velocity, pressure and angle) of the flow at unstalled operation. A hot-wire anemometer placed in this section records during the rotating stall the periodic flow fluctuations. Station 3 represents the downstream infinity, where all downstream perturbations are damped out, but due to the absence of a stator, the tangential velocity component is not recuperated, and the pressure increase between stations 2 and 3 is due to the recuperation of the axial velocity component only.

The complete operation of a single rotor compressor[9] is represented in Fig. 4, for a stagger angle of $\zeta = 41.5°$ (to which corresponds the mean R-exit angle $\alpha_* = 36.5°$). The performances of the rotor are characterized by means of the following classical flow and pressure parameters:

$$\varphi = W/U, \quad \psi = 2(P_3 - P_1)/\rho U^2 \tag{20}$$

where the reference velocity U is the tangential velocity of the rotor at the mean radius.

The point $\hat{\varphi} = 0.67$ corresponding to the onset of the rotating stall is obtained in Fig. 4(I) by the intersection of the extrapolated stalled branch of the performance curve (φ, ψ) with the unstalled branch. The static pressure, measured only for the unstalled operation, is represented by the static pressure coefficient $\psi_s = 2(p_2 - P_1)/\rho V^2$ shown in Fig. 4(II). Its value, $\hat{\psi}_s = 0.22$ corresponding to $\hat{\varphi}$, determines the theoretical speed of the stall, namely:

$$V = (U/2)\,(1 + \hat{\psi}_s) = 0.61\,U \tag{21}$$

The experimental values of V/U, obtained from the hot-wire oscillograms taken at station 2, are represented in Fig. 4 (III); they correspond to $V/U = T'/nT''$ where T' is the period of the rotor given by a rotating contact mounted on the shaft, T'' the period of the stall and n the number of stall zones ($n = 1$ or 2); the time basis $\tau = 0.01$ second is also recorded on the oscillograms.

The extent of the stall is represented on Fig. 4(IIII) where the theoretical value

$$\nu = 1 - \varphi/\hat{\varphi} \tag{22}$$

derived from Eq. 19 is compared to the experimental measurements $\nu = T'''/T''$ where T''' is the duration of the stall.

(4.3) *Downstream Pressure Evolutions*

Behind the rotor the stalled and unstalled zones undergo a complex mixing process, which in a compressor with large hub/tip ratio is neither a constant section nor a constant pressure mixing. In compressor A, where the tangential velocity component is not recuperated, the pressure increase between stations 2 and 3 can be expressed by

$$\psi - \psi_s = \varphi^2 \tag{23}$$

during the unstalled operation. During the stall, with

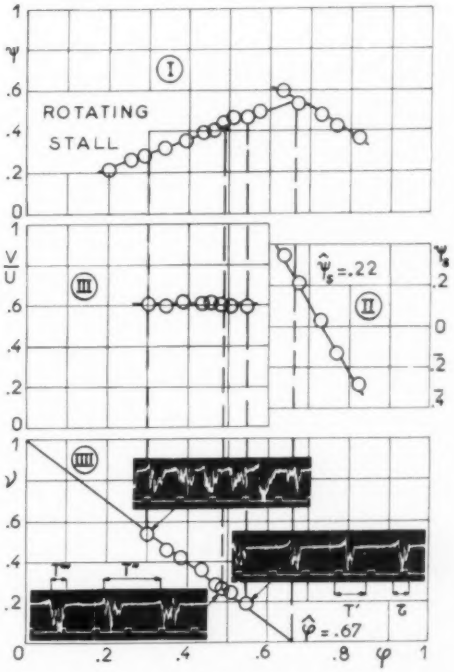

FIG. 4. General performance of a single rotor.

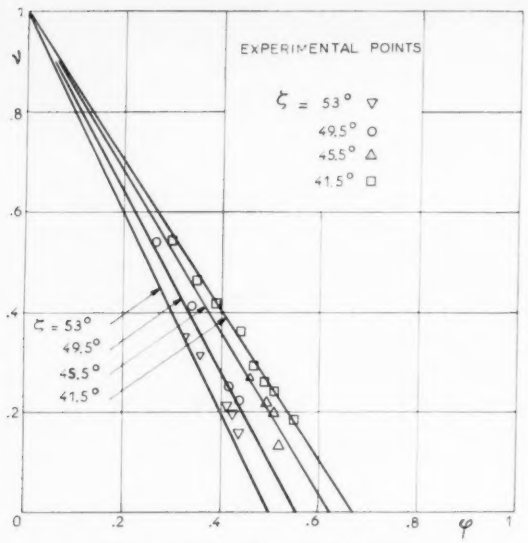

FIG. 5. Extent of the stalled zones.

all conditions at the exit of the unstalled blade channels remaining constant, the pressure variations at downstream infinity depend on the extent of the stall zones only; a constant section mixing would give

$$\psi - \hat{\psi} = -(\varphi - \hat{\varphi})^2 \tag{24}$$

whereas a constant pressure mixing gives

$$\psi - \hat{\psi} = -\hat{\varphi}^2 + \varphi^2 \tag{25}$$

A more general mixing process, which would ensue from a combination of both elementary processes, could be described by

$$\psi - \hat{\psi} = -\epsilon(\varphi - \hat{\varphi})_\epsilon - (1 - \epsilon)\,(\hat{\varphi}^2 - \varphi^2), \quad 0 < \epsilon < 1 \tag{26}$$

In the case of compressor A the straight performance curve of stalled operation [Fig. 4(I)] shows that both processes seem to have equal importance ($\epsilon = 0.5$). It can be verified from Fig. 4(I) that the slope of the stalled ψ vs. ψ curve is really close to $\hat{\varphi}$.

In some compressors where the hub/tip ratio is close to 1 (see reference 10) the mixing is nearly a constant section process and the value $\epsilon = 1$ applies to the downstream pressure recuperation.

(4.4) *Extent and Speed of Rotation of the Stall*

The experimental variations of ν for various stagger angles ($\zeta = 41.5°, 45.5°, 49.5°, 53°$) are represented in Fig. 5. The values of $\hat{\varphi}$ are obtained by correlating the stalled curves (φ, ψ) by means of a straight line of slope $\hat{\varphi}$.

The correct determination of ν is difficult due to the interference between stall zones and blade wake, exact values of ν being measurable only downstream of the rotor. In view of this fact, it may be considered that the divergence of the experimental points from the theoretical (φ, ν) lines is not great.

The corresponding values of $\hat{\psi}_s$ and the theoretical and experimental V/U ratios are given in Table 1.

TABLE 1

ζ	41.5	45.5	49.5	53.0
$\hat{\varphi}$	0.67	0.62	0.55	0.5
$\hat{\psi}_s$	0.22	0.18	0.25	0.2
$(V/U)_{th}$	0.61	0.59	0.62	0.6
$(V/U)_{exp}$	0.61	0.61	0.62	0.6

(4.5) *Upstream Decay of the Disturbances*

The decay of the disturbances can be measured by means of hot-wire recordings at various stations between 1 and 2. In Fig. 6, the hot-wire recordings are compared, for one zone pattern, to the results of the calculations under the conditions of paragraph (2.6) (transformed here into the equivalent electronic signals by means of the calibration curve of the hot-wire anemometer). This comparison is made by expressing all upstream distances, measured from the axis of the blade, in terms of its ratio to the mean radius R_m of the rotor.

This mean radius R_m is the characteristic length of the decay of the upstream disturbances due to the rotating stall with one stall pattern. It is interesting to note that this length is somewhat greater than the characteristic length R/ϵ_1 of the decay of the three-dimensional disturbances of a potential flow in the same annular space between the hub and the casing of the compressor, the eigenvalue of which is ϵ_1, a function of the hub/tip ratio only and generally close to 2π (see reference 11).

(4.6) *Experimental Compressor B*

Experimental compressor B, which is quite similar to compressor A, has also a solid body single rotor, but with a hub/tip ratio of $R_0/R = 0.79$; the casing diameter is $2R = 703$ mm.; and there are 60 blades with a mean R-exit angle of 60°. Due to the great number of blades,

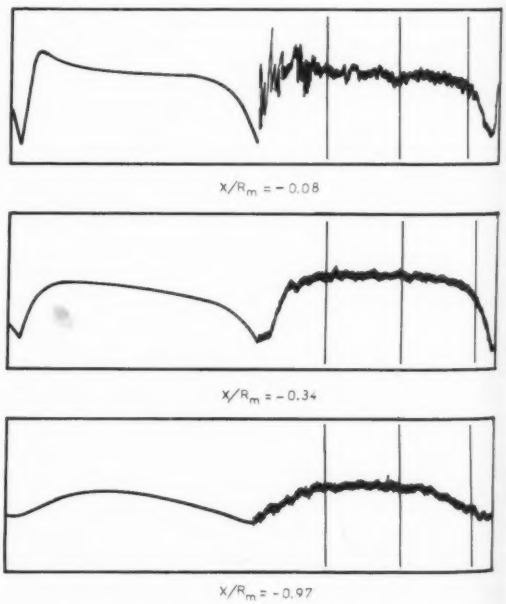

FIG. 6. Upstream decay of the disturbances.

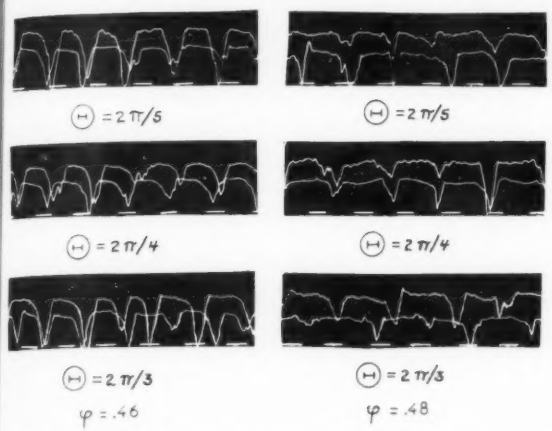

FIG. 7. Determination of the number of stall zones.

the rotating stall appears always with a great number of zones, thus giving a less well defined periodic phenomenon.

The determination of the exact number n of these zones is obtained by means of two hot-wire anemometers placed at angular distances of $\Theta = 2\pi/n'$. Fig. 7 shows the hot-wire recordings obtained for flow coefficients $\varphi = 0.46$ and $\varphi = 0.48$ with $n' = 3, 4$, and 5. It is seen that for $\varphi = 0.48$ there are four stall zones and for $\varphi = 0.46$ there are five stall zones. The speed of rotation remains constant in both cases, $V/U = 0.59$, to which corresponds the value $V/U = 0.61$ derived from the performance curves.

It can also be shown that for incompressible flows the usual similarity laws of compressors apply.[12] This is obvious from the equations of motion and can be verified by means of the experimental measurements shown in Fig. 8 (performance curves of stalled and unstalled operation of compressor B at different speeds of rotation; the stalled operations are represented by means of solid points).

(5) Conclusion

The one-dimensional theory of rotating stall given above necessitates very few assumptions on the behavior of the stalled blade channels. The physical scheme on which it is based, saturation of the R-angle of attack (angles of attack relative to the rotor) and no through flow in the stalled blade channels, seems to have a good physical background.

The predictions of some properties of the rotating stall—such as relation between the rate of stall propagation and the static pressure behind the rotor, extent of the stall zones as a function of the flow coefficient, upstream decay of the disturbances, and downstream mixing of the flow—are well verified by experimental measurements, at least as long as the number of blades is high enough to justify the assumption of an infinite number of blades.

The aerodynamic theory of rotating stall verifies correctly the experimental results on stall propagation along a single rotor. The prediction of the stall necessitates however the consideration of the three-dimensional equilibrium of a flow containing uniformly rotating stalled cells, made up of nearly dead fluid.

Appendix A—Harmonic Flow Fields Related by Means of a Linear Combination Along Their Common Boundary

Let us consider two periodic analytical functions $w - iv$ and $w' - iv'$, valid for $x < 0$ and $x > 0$, respectively, vanishing at infinity and related along $x = 0$ by

$$w_0 = a'w_0' + b'v_0' \tag{A1}$$

Let us assume, without loss of generality, that $w' - iv'$ can be represented by Fourier series such as

$$w' - iv' = \sum_{n=0}^{\infty} (A_n' + iB_n')e^{-n(x+iy)} \tag{A2}$$

then the following relations result:

$$w_0' = \sum_{n=0}^{\infty} (A_n' \cos ny + B_n' \sin ny); \qquad v_0' = \sum_{n=0}^{\infty} (A_n' \sin ny - B_n' \cos ny) \tag{A3}$$

$$w_c = \sum_{n=0}^{\infty} [(a'A_n' - b'B_n') \cos ny + (a'B_n' + b'A_n') \sin ny] \tag{A4}$$

$$w - iv = \sum_{n=0}^{\infty} [(a'A_n' - b'B_n') - i(a'B_n' + b'A_n')]e^{n(x+iy)} \tag{A5}$$

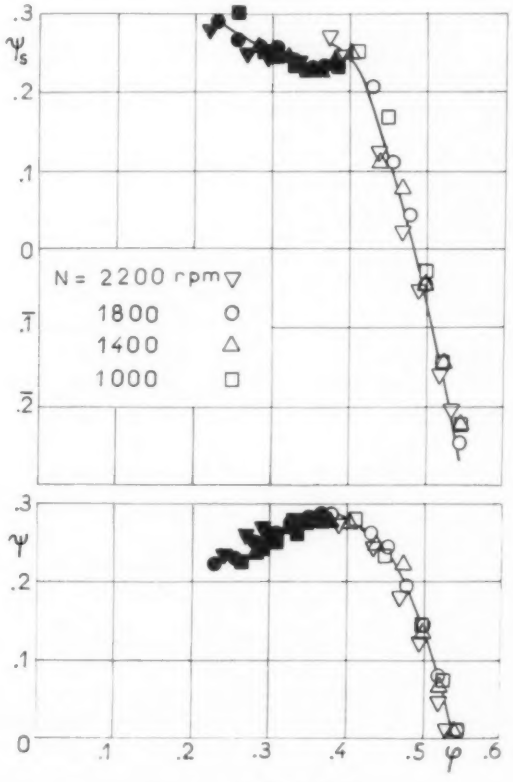

FIG. 8. Similarity rules.

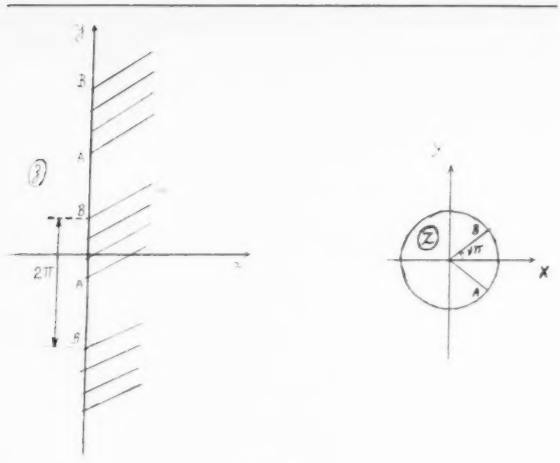

FIG. 9.

$$\left.\begin{aligned} v_0 &= \sum_{n=0}^{\infty} [(a'B_n' + b'A_n') \cos ny - \\ &\qquad (a'A_n' - b'B_n') \sin ny] \\ &= \sum_{n=0}^{\infty} [a'(B_n' \cos ny - A_n' \sin ny) + \\ &\qquad b'(A_n' \cos ny + B_n' \sin ny)] \end{aligned}\right\} \quad (A6)$$

Thus,
$$v_0 = -a'v_0' + b'w_0' \quad (A7)$$

APPENDIX B—THE HILBERT PROBLEM

The transformation $Z = e^{\zeta}$ represents the upstream half-plane $R(z) \leq 0$ on the interior of the circle $|Z| = 1$ (Fig. 9). The images of the stall zones are the arc $\overrightarrow{AB} = 2\nu\pi$. At the boundary $x = 0$ of the half plane, the linear discontinuous system

$$\overrightarrow{AB}: \qquad w_0 - v_0 \cot \gamma = c \quad (B1)$$

or Eq. (8), and

$$\overrightarrow{BA}: \qquad w_0 - v_0 \cot \beta = b \quad (B2)$$

or Eq. (9) relates the real and imaginary parts of the complex velocity $w - iv$.

An evident particular solution is obtained by solving the above linear system. The constant

$$F_0 = w_0 - iv_0 = \frac{b \tan \beta - c \tan \gamma + i(c - b) \tan \beta \tan \gamma}{\tan \beta - \tan \gamma} \quad (B3)$$

which is obtained, satisfies on the whole circle the conditions (B1) and (B2). The flow defined by these conditions results from the superposition on this particular solution of the more general solution of the homogeneous system ($c = b = 0$).

In this case, the analytic function $F(Z) = w - iv$ is defined by the condition that its argument $\tan^{-1}(-v/w)$ be equal to $-\gamma$ on $\overrightarrow{AB}$ or $-\beta$ on $\overrightarrow{BA}$. The basic function of which the imaginary part is discontinuous in A and B is $\log [(B - Z)/(A - Z)]$ and its value at the origin is $2i\nu\pi$ whereas its imaginary part takes the value $(\nu + 1)\pi$ on $\overrightarrow{AB}$ and $\nu\pi$ on $\overrightarrow{BA}$.

In the combination $G = E \log [(B - Z)/(A - Z)] + iH$ where E and H are constant coefficients, the correct values $-\gamma$ and $-\beta$ along the arcs $\overrightarrow{AB}$ and $\overrightarrow{BA}$ are obtained if

$$E = (\beta - \gamma)/\pi, \quad H = -\beta - E\nu\pi \quad (B4)$$

Thus,

$$e^G = \left(\frac{B - Z}{A - Z} e^{-i\gamma\pi}\right)^{(\beta-\gamma)/\pi} e^{-i\beta} \quad (B5)$$

is a solution of the homogeneous problem. Of course such a solution is not unique and any *real* function regular inside the circle, could multiply e^G. However, such a function is necessarily singular in A and B, and is a *real* function λ (see reference 13) of the variable $\zeta = e^{-i\gamma\pi}(B - Z)/(A - Z)$, the argument of which, according to the above calculations, is alternatively equal to 0 and π. Thus the general solution of the problem is

$$F = w - iv = F_0 + \lambda(\zeta) e^{G(Z)} \quad (B6)$$

But generally, $0 \leq (\gamma - \beta)/\pi \leq 1/2$ (it can be seen in Section (2) that $\beta = \hat{\alpha}$ and $\gamma = \pi/2$ in the particular case when no through flow is assumed in stalled blade channels). If infinite velocities are assumed at the front of the stall (point B), which seems to be a correct assumption, the solution with minimum singularity corresponds to $\lambda = \text{const}$, which gives Eq. (10).

In particular, along the blade front ($x = 0$),

$$\left.\begin{aligned} \overrightarrow{AB} \qquad w_0 &= \frac{b \tan \beta - c \tan \gamma}{\tan \beta - \tan \gamma} + \lambda \cos \gamma \left\{\frac{\sin [(\nu\pi - y)/2]}{\sin [(\nu\pi + y)/2]}\right\}^{(\beta-\gamma)/\pi} \\ \overrightarrow{BA} \qquad w &= \frac{b \tan \beta - c \tan \gamma}{\tan \beta - \tan \gamma} + \lambda \cos \beta \left\{\frac{\sin [(y - \nu\pi)/2]}{\sin [(y + \nu\pi)/2]}\right\}^{(\beta-\gamma)/\pi} \end{aligned}\right\} \quad (B7)$$

REFERENCES

[1] Sears, W. R., *Rotating Stall in an Axial Compressor*, Zeitschrift für angewandte Mathematik und Physik, Vol. 6, No. 6, pp. 429–455, 1955.

[2] Emmons, H. W., Pearson, C. E., and Grant, H. P., *Compressor Surge and Stall Propagation*, Transactions of the American Society of Mechanical Engineers, Vol. 77, No. 4, pp. 455–469, 1955.

[3] Stenning, A. H., *Stall Propagation in Cascades of Airfoils*, Journal of the Aeronautical Sciences, Vol. 21, No. 10, pp. 711–712, October, 1954.

(*Continued on page 820*)

A Simple Method of Matric Structural Analysis: Part II—Effects of Taper and Consideration of Curvature

BERTRAM KLEIN*

National Rocket Corporation

SUMMARY

The matric method of structural analysis presented previously in Part I is extended to include the effects of panel geometry and gage taper, stringer taper, and a consideration of curved elements. The resulting matrices are of the same form as the previous matrix and of comparable simplicity. Several problems are presented to illustrate the mechanics and simplicity of the extended method.

SYMBOLS

A	=	effective cross-sectional area, or area
a, b	=	shear panel dimensions
D	=	point in shear panel
E, G	=	Young's and shear moduli
F	=	shear force
$\mathfrak{F}, f, g$	=	functions
h	=	rib spacing
L	=	length of centroidal line of curved element
M	=	bending moment
P	=	axial load, or load
q	=	panel shear flow
R	=	radial force
r	=	radius
S	=	stiffness
s	=	coordinate
s_i	=	distance
T	=	tangential force
u, v	=	displacements
x	=	coordinate
β	=	angle subtended by curved element
γ	=	parameter
Δ	=	determinant
θ	=	angular rotation
κ, λ	=	parameters
ξ	=	effective area parameter
σ	=	stringer stress
τ	=	shear stress
ϕ	=	$(\beta/2)$
ψ	=	function

Subscripts

c	=	centroidal
i, n	=	numerical indices
max	=	maximum value of
min	=	minimum value of
o	=	outer
p	=	panel
q	=	due to shear flow
r	=	rib
rr, tt, etc.	=	denoting various stiffnesses

Superscripts

$\bar{}$	=	average value of
*	=	effective value of

Received March 12, 1957.

* Formerly, Chief of Stress, National Rocket Corporation. Now, Head, Structures Methods Group, Convair (Astronautics) Division of General Dynamics Corporation.

INTRODUCTION

IN A PREVIOUS PAPER,[1] the fundamentals of a method of matric structural analysis have been presented. In the present paper, the work is extended by the derivation of the equations necessary for treating tapered structures and structures containing curved elements, both of which are found extensively in practice.

The aim of this series of articles is to present a method of matric structural analysis in which the setup routine is reduced to such simplicity that the structural engineer can proceed directly and rapidly in the initial stages of the solution of a complicated problem. The task of obtaining final numerical values is assigned to the computer engineer. The size and form of the matrix therefore is not the direct concern of the structural engineer, although he must be cognizant of the limitations of the science of automation.

In the proposed method, once a structure has been idealized, the necessary final equations of equilibrium and compatibility are written down directly and rapidly in final matrix form without recourse to any artificial devices (see numerical examples). In many applications, it is of importance to obtain a complete solution to a problem—i.e., both deflections and stresses. Allowance is made for this requirement directly in the proposed method. Also, with the increasing importance of thermal loadings, and combined thermal and regular loadings, an efficient method should be able to treat such problems with no additional complexity. Allowance is made for these cases directly in the proposed method.

It is admitted that the proposed method is not intended to solve all structural problems, or lead to mathematically exact solutions, or is the best method to use in all cases. However, it is believed that, in a variety of problems, the method should prove to be efficient.

(1) TAPERED PANELS AND STRINGERS

It has been learned through experience that, in many practical cases, it is permissible to idealize a tapered reinforced sheet structure by assuming the structure to be composed of two types of elements—panels taking only shear, and reinforcing elements, assumed to bound the panels, taking direct stresses. Therefore this assumption is maintained. However, when a shear panel

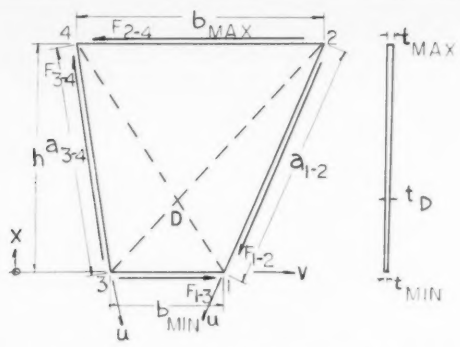

FIG. 1. Shear panel tapered in plan form and thickness.

is tapered in plan form, such as the one shown in Fig. 1, the shear flow in the panel is found to vary in order to maintain a state of equilibrium. The magnitude of the shear flow is largest at the smaller end of the panel, and denoted there as q_{max}. The panel is assumed to have two parallel edges. The shear flow is assumed to be constant at any section parallel to these parallel edges—i.e., for a constant value of x. The thickness of the panel is assumed to vary approximately linearly, increasing in the x direction, and to be approximately constant at any section parallel to the parallel edges.

(a) *Force-Displacement Equations*

For the assumptions made, the necessary expression relating the deflections of the four corners of the panel of Fig. 1 to the shear in the panel is [see Appendix (1)]

$$(u_1 + u_2)a_{1-2} + (v_1 + v_3)b_{max} - (v_2 + v_4)b_{min} - (u_3 + u_4)a_{3-4} = (2A_p/Gt_D)\bar{q} \quad (1)$$

where $\bar{q}$ is the average shear flow in the panel and is

$$\bar{q} = q_{max}(b_{min}/b_{max}) \quad (1a)$$

t_D is the thickness of the panel at the point D, located at the intersection of the diagonals of the panel as shown in Fig. 1, and A_p is the area enclosed by the panel. Note the inversion of the multipliers of the terms containing the v displacements.

A stringer is assumed to be tapered so that the effective cross-sectional area increases in the x direction, as shown in Fig. 2. In accordance with the assumptions made regarding the state of shear stress in the adjoining panels, the desired relation between end displacement in the direction of the stringer, the force at the smaller end of the stringer, and the average shear flows in the adjoining panels is [see Appendix (1)]

$$(E\bar{A}/a)(u_i - u_{i+1}) = P_i + a\sum_n \bar{q}_n f[(b_{min}/b_{max}), (A_{max}/A_{min})] \quad (2)$$

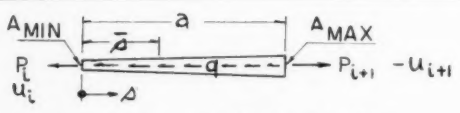

FIG. 2. Tapered stringer and loading.

where $\bar{A}$ is the harmonic average value of A—i.e.,

$$\bar{A} = a\Big/\int_0^a (1/A)ds = A_{\bar{s}} \quad (2a)$$

and f is a function dependent on the type of stringer taper. $\bar{s}$ is the value of s at which $A = \bar{A}$. For example, the values of f and $\bar{s}$ if the variation of A is linear with respect to s are shown plotted in Fig. 3. The value of $\bar{s}/a$ is read from the vertical where $(b_{min} \div b_{max}) = 1$ on the right. Thus if $A_{max}/A_{min} = 2$, and the variation is linear, $\bar{s}/a = 0.44$, from Fig. 3. The positive sign for q acting on the stringer is that shown in Fig. 2. The value of n usually does not exceed 3. Curves similar to the ones presented in Fig. 3 may be drawn for other types of stringer taper variation, such as quadratic, etc.

Since it is assumed that the shear flow is constant along a rib, the expression relating end displacement and end force is of the same form as the equation given previously in reference 1 (Eq. 1). For example for rib 1–3 of Fig. 1,

$$(2E\bar{A}_r/b_{min})(v_1 - v_3) = P_1 + P_3 \quad (3)$$

(b) *Equilibrium Equations*

For a stringer such as shown in Fig. 2, the equilibrium equation is simply [see Appendix (1)]

$$P_{i+1} - P_i = a\sum_n \bar{q}_n \quad (4)$$

For a rib the desired relation is of a similar form. For the ribs shown in Fig. 1, for example, one may write

$$P_3 - P_1 = \sum_n b_n\bar{q}_n, \quad P_2 - P_4 = \sum_n b_n\bar{q}_n \quad (5)$$

The correct sign of each average shear flow acting on the stringer or rib must be used in Eqs. (4) and (5). Note here the inversion of b_{min} and b_{max} such as occurs in Eq. (1).

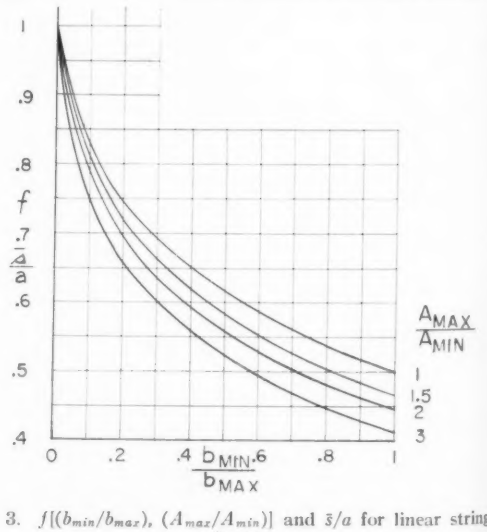

FIG. 3. $f[(b_{min}/b_{max}), (A_{max}/A_{min})]$ and $\bar{s}/a$ for linear stringer taper.

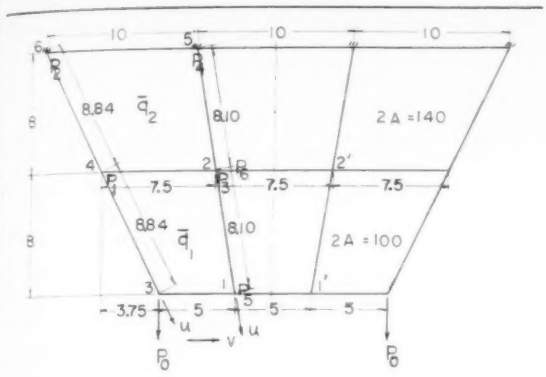

FIG. 4. Geometry and loading of tapered panel.

All the necessary expressions needed for solving tapered quasi-flat reinforced panel structures are now known. It is of interest to note that the coefficients of the unknown quantities appearing in the above equations are panel dimensions or quantities that may be read directly from drawings of a structure or auxiliary curves (such as Fig. 3) or readily calculated from such data. A simple numerical example is presented below to illustrate the workings of the method.

(c) *Numerical Example*

Consider the plane sheet-stringer-rib tapered panel depicted in Fig. 4. For purposes of simplicity, the structure is assumed to have an axis of symmetry, the loading is taken to be symmetrical about that axis, and the structure is assumed to be completely fixed at the supports. The indicated panel dimensions are numbers which could be read from a drawing. The necessary values of the parameters appearing in the force-displacement equations are taken as

stringer	1–2	2–5	3–4	4–6
$E\bar{A}/a$	1	1.5	0.8	1.2

rib	1–3	2–4	1–1′	2–2′
$2E\bar{A}_r/b$	5	7.5	5	7.5

panel	1	2
$2A_p/Gt_D$	100	100
$f[(b_{min}/b_{max}), (A_{max}/A_{min})]$	0.57	0.55

The external load, P_0, is taken as one, and broken up into two components, one acting in the direction of stringers 3–4–6 and of magnitude, $8.84/8 = 1.105$, and one acting in the direction of rib 3–1–1′ and of magnitude $3.75/8 = 0.4685$. The matrix defining the problem in the 16 unknown quantities may be written

$$\begin{bmatrix}
-1 & 0 & 0 & 0\,0\,0 & 8.84 & 0 & & & & & & & & & & \\
1 & -1 & 0 & 0\,0\,0 & 0 & 8.84 & & & & & & & & & & \\
0 & 0 & -1 & 0\,0\,0 & -8.1 & 0 & & & & & & & & & & \\
0 & 0 & 1 & -1\,0\,0 & 0 & -8.1 & & & & & & & & & & \\
0 & 0 & 0 & 0\,1\,0 & -7.5 & 0 & & & & & & & & & & \\
0 & 0 & 0 & 0\,0\,1 & 5 & -10 & & & & & & & & & & \\
0 & 0 & 0 & 0\,0\,0 & 5.04 & 0 & 0 & 0 & -0.8 & 0.8 & & & & & & \\
1 & 0 & 0 & 0\,0\,0 & 0 & 4.86 & 0 & 0 & 0 & -1.2 & & & & & & \\
0 & 0 & 0 & 0\,0\,0 & -4.62 & 0 & -1 & 1 & 0 & 0 & & & & & & \\
0 & 0 & 1 & 0\,0\,0 & 0 & -4.46 & 0 & -1.5 & 0 & 0 & & & & & & \\
0 & 0 & 0 & 0\,1\,1 & 0 & 0 & 0 & 0 & 0 & 0 & -5 & 0 & 5 & 0 & & \\
0 & 0 & 0 & 0\,0\,1 & 0 & 0 & 0 & 0 & 0 & 0 & 0 & -7.5 & 0 & 7.5 & & \\
0 & 0 & 0 & 0\,1\,0 & 0 & 0 & 0 & 0 & 0 & 0 & 5 & 0 & 0 & 0 & & \\
0 & 0 & 0 & 0\,0\,1 & 0 & 0 & 0 & 0 & 0 & 0 & 0 & 7.5 & 0 & 0 & & \\
 & & & & -100 & 0 & 8.1 & 8.1 & -8.84 & -8.84 & 7.5 & -5 & 7.5 & -5 & & \\
 & & & & 0 & -100 & 0 & 8.1 & 0 & -8.84 & 0 & 10 & 0 & 10 & &
\end{bmatrix}
\begin{bmatrix} P_1 \\ P_2 \\ P_3 \\ P_4 \\ P_5 \\ P_6 \\ \bar{q}_1 \\ \bar{q}_2 \\ \\ u_1 \\ u_2 \\ u_3 \\ u_4 \\ v_1 \\ v_2 \\ v_3 \\ v_4 \end{bmatrix}
=
\begin{bmatrix} -1.105 \\ 0 \\ 0 \\ 0 \\ -0.4685 \\ 0 \\ -1.105 \\ 0 \\ \\ 0 \\ 0 \\ -0.4685 \\ 0 \\ 0 \\ 0 \\ 0 \\ 0 \end{bmatrix}$$

The solution is

$$\begin{array}{llll}
P_1 = 0.60892090 & P_5 = -0.88963159 & u_1 = 0.60920638 & v_1 = 0.17792632 \\
P_2 = 0.46945728 & P_6 = 0.12282344 & u_2 = 0.34994332 & v_2 = -0.016376459 \\
P_3 = 0.45455211 & \bar{q}_1 = -0.056117545 & u_3 = 1.4712490 & v_3 = 0.26210263 \\
P_4 = 0.58234118 & \bar{q}_2 = -0.015776428 & u_4 = 0.44353955 & v_4 = -0.032752919
\end{array}$$

As regards the check of equilibrium, it is interesting to note that equilibrium at any section in the direction of P_0 checks almost exactly *provided* it is assumed that the stringers are inclined such that the angles of inclination with the direction of P_0 are exactly arcsin (8/8.84) and arcsin (8/8.1). The check equations for this assumption are

$$(8/8.84)P_1 + (8/8.1)P_3 = 0.999999992$$
$$(8/8.84)P_2 + (8/8.1)P_4 = 0.9999999992$$

On occasion, it may be of benefit to introduce extra, actually nonexistent, stringers and ribs, thereby subdividing actual panels into smaller panels with consequent increase in the size of the matrix. However, this artifice does not change in any way the basic equations or mechanics of the method. (This procedure is the opposite of the more customary method of "lumping" in which the size of the matrix is reduced when existing

stringers and ribs are combined together thereby increasing the sizes of actual panels.)

(2) Curved Elements

In this section, uniform (untapered) elements of constant curvature and acted upon by constant shear flows are considered. Refer to Fig. 5 for the basic geometry and loading of such an element. Notice that each end of the element has associated with it three generalized forces and three generalized displacements (henceforth called simply forces or displacements). Consequently, there exists for the element three equations of equilibrium and three force-displacement equations. These equations are

Equilibrium:

$$\left.\begin{aligned} &\text{sum of vertical forces:} && (T_i + T_{i+1})\tan\phi + (R_i + R_{i+1}) = 0 \\ &\text{sum of horizontal forces:} && (T_i - T_{i+1})\cot\phi - (R_i - R_{i+1}) = 2qr_o \\ &\text{sum of moments about 0:} && (T_i - T_{i+1}) + (1/r_c)(M_i - M_{i+1}) = (r_o/r_c)2qr_o\,\phi \end{aligned}\right\} \tag{6}$$

where r_o is the radius of the outermost fiber of the element, and r_c is the radius of the centroidal line of the element (see Fig. 5); and force-displacement [see Appendix (2)]:

$$\left.\begin{aligned} (M_i + M_{i+1}) &= (\theta_i - \theta_{i+1})S_{mm} + (v_i + v_{i+1})S_{mr} + (u_i - u_{i+1})S_{mt} \\ (R_i - R_{i+1}) &= (\theta_i + \theta_{i+1})S_{rm} + (v_i - v_{i+1})S_{rr} + (u_i + u_{i+1})S_{rt} - 2R_q \\ (T_i + T_{i+1}) &= (\theta_i - \theta_{i+1})S_{tm} + (v_i + v_{i+1})S_{tr} + (u_i - u_{i+1})S_{tt} \end{aligned}\right\} \tag{7}$$

where R_q is the radial force acting on the left end of the element in Fig. 5 when shear only is considered—i.e., $u = v = \theta = 0$.

The values of all the stiffnesses, S, may be expressed matrically in terms of but two stiffnesses—i.e., S_{rr} and S_{tt}—as follows [see Appendix (2)]:

$$\begin{bmatrix} [S_{mm} - (2EI/L)] & S_{mr} & S_{mt} \\ S_{rm} & S_{rr} & S_{rt} \\ S_{tm} & S_{tr} & S_{tt} \end{bmatrix} = \begin{bmatrix} r_c[(\tan\phi/\phi) - 1]S_{tt} & 0 & 0 \\ 0 & S_{rr} & 0 \\ 0 & 0 & S_{tt} \end{bmatrix} \begin{bmatrix} r_c[(\tan\phi/\phi) - 1] & -\tan\phi & 1 \\ -r_c\tan\phi & 1 & \tan\phi \\ r_c[(\tan\phi/\phi) - 1] & -\tan\phi & 1 \end{bmatrix} \tag{8}$$

The values of S_{rr} and S_{tt} may be calculated from the equations

$$\left.\begin{aligned} S_{rr}(r_c^3/EI) &= 2(1 + \cos\beta)/(\kappa\beta - \lambda\sin\beta) \\ S_{tt}(r_c^3/EI) &= 2(1 + \cos\beta)/[\kappa\beta + \lambda\sin\beta - 4(1/\beta)(1 - \cos\beta)] \end{aligned}\right\} \tag{9}$$

where

$$\kappa = 1 + (1/\gamma)[(1/\xi) + 1], \quad \lambda = 1 - (1/\gamma)[(1/\xi) - 1], \quad \gamma = Ar_c^2/I, \quad \xi = A^*/A \tag{9a}$$

A = axial cross-sectional area of element, I = centroidal moment of inertia of cross section of element, and A^* = effective shear area of cross section of element (see reference 2). The value of R_q is given by the expression

$$R_q = qr\,\frac{[\kappa(\beta - \sin\beta) + \beta(1 + \cos\beta) - 2\sin\beta]}{\kappa\beta - \lambda\sin\beta} \tag{10}$$

provided the effect of eccentricity may be neglected—i.e., e/r is very small. The more correct expression including eccentricity is given in Appendix (2).

Frequently it is permissible to take γ infinitely large so that $\kappa = \lambda = 1$.

It is convenient to rewrite Eqs. (9) in the following forms:

$$S_{rr} = \frac{2(EI/L^3)(1 + \cos\beta)}{[(1/6) - (1/5!)\beta^2 + (1/7!)\beta^4 - \ldots] + (I/AL^2)\{(A/A^*)[1 + (1/\beta)\sin\beta] + [1 - (1/\beta)\sin\beta]\}} \tag{9a}$$

$$= \frac{2(EI/L^3)(1 + \cos\beta)}{(1/\beta^2)\psi_1(\beta) + (I/AL^2)[(A/A^*)\psi_2(\beta) + \psi_1(\beta)]} \tag{9b}$$

$$S_{tt} = \frac{2(EA/L)(1 + \cos\beta)}{(AL^2/I)\mathfrak{F}(\beta) + (A/A^*)\psi_1(\beta) + \psi_2(\beta)} \tag{9c}$$

where

$$\mathfrak{F}(\beta) = \sum_{n=1}(-1)^{n+1}\beta^{2n}[2n/(2n + 4)!] \tag{9d}$$

$$= \beta^2[(1/360) - (1/100800)\beta^2 + (1/6048000)\beta^4 - \ldots] \tag{9e}$$

Eq. (10) may be written as

$$R_q = qr\{(1/2)\psi_1(\beta)[1 + (S_{rr}/S_{tt})] + f(\beta)(S_{rr}L^3/EI)\} \tag{10a}$$

where $f(\beta)$ is given in Appendix (2).

Infinite γ

If γ is taken to be infinitely large, the above equations become

$$S_{rr} = \frac{2(EI/L^3)(1 + \cos\beta)}{(1/\beta^2)\psi_1(\beta)} \qquad S_{tt} = \frac{2(EI/L^3)(1 + \cos\beta)}{\mathfrak{F}(\beta)} \tag{9'}$$

A very close approximation to R_q is given as

$$R_q = qr_o[0.1\beta^2 - (e/r_c)(1 + 0.4\beta^2)] \tag{10'}$$

for infinite γ and values of β less than about one radian. This expression includes the effect of eccentricity.

Straight Element

When $\beta = 0$, the element becomes a straight element, and

$$\left.\begin{aligned} S_{mm} = (2EI/L), \quad S_{rr} = -(2/L)S_{rm} = (24EI/L^3)/[1 + 12(I/A^*L^2)], \quad S_{tt} = 2EA/L \\ R_q = -eq/[1 + 12(I/A^*L^2)] \end{aligned}\right\} \tag{11}$$

All other S values become zero. Eqs. (6) and (7) become

$$R_i + R_{i+1} = 0, \quad T_i - T_{i+1} = qL, \quad M_i - M_{i+1} + L(R_i - R_{i+1}) = 2eqL \tag{6'}$$

$$\left.\begin{aligned} M_i + M_{i+1} &= (\theta_i - \theta_{i+1})(2EI/L) \\ R_i - R_{i+1} &= \frac{[(v_i - v_{i+1}) - (L/2)(\theta_i + \theta_{i+1})](24EI/L^3) + 2eq}{1 + 12(I/A^*L^2)} \\ T_i + T_{i+1} &= (u_i - u_{i+1})(2EA/L) \end{aligned}\right\} \tag{7'}$$

All the necessary equations for treating untapered curved and straight elements taking combined loading in their own planes and under constant shear flow are now known.

Numerical Example

Let us consider the circular ring loaded antisymmetrically, as shown in Fig. 6. For purposes of analysis, only one half of the ring need be considered. This half is broken up into two curved elements, segments 1–2, and 2′–3, referred to as 1 and 2 hereafter. The ring cross section is assumed to have the following properties:

$$A = 0.250, \quad I = 0.1666, \quad \xi = 0.16, \quad EI = 10^6, \quad e/r = 0$$

The values of κ and λ are computed from Eq. (9a) to be $\kappa = 1.0120785$, $\lambda = 0.9912535$.
The following values of the stiffnesses times 10^{-3} have been computed using Eqs. (8) and (9):

$$\begin{bmatrix} S_{mm_1} & S_{mr_1} & S_{mt_1} \\ S_{rm_1} & S_{rr_1} & S_{rt_1} \\ S_{tm_1} & S_{rt_1} & S_{tt_1} \end{bmatrix} = \begin{bmatrix} 214.4147079 & -19.78466685 & 8.195077336 \\ -2.09982022 & 0.0434887007 & 0.104991011 \\ 8.195077336 & -0.942802111 & 0.390521421 \end{bmatrix}$$

$$\begin{bmatrix} S_{mm_2} & S_{mr_2} & S_{mt_2} \\ S_{rm_2} & S_{rr_2} & S_{rt_2} \\ S_{tm_2} & s_{tr_2} & S_{tt_2} \end{bmatrix} = \begin{bmatrix} 251.8798715 & -47.0855601 & 113.674598 \\ -37.6270642 & 4.54198844 & 1.88135321 \\ 113.674598 & -42.9721225 & 103.743881 \end{bmatrix}$$

The following values of $2(R_q)$ have been computed from Eq. (10): $2(R_q)_1 = 25.26276318$, $2(R_q)_2 = 2.770052856$. The ring is assumed to be fixed at point 1. Twelve unknown quantities are found to exist. These unknowns consist of seven forces—R_1, M_2, R_2, T_2, $R_{2'}$, $T_{2'}$, and R_3—and five displacements—θ_2, v_2, u_2, θ_3, and u_3. The necessary twelve equations consist of six for each element—i.e., Eqs. (6) and (7) written for each element. The matric equation defining the problem is

$$\begin{bmatrix} \tan\phi_1 & 0 & 1 & 1 & & & & & & & & \\ -\cot\phi_1 & 0 & -1 & 1 & & & & & & & & \\ -1 & -0.05 & 0 & 0 & & & & & & & & \\ 0 & 0 & 0 & 0 & \tan\phi_2 & 1 & 1 & & & & & \\ 0 & 0 & 0 & 0 & \cot\phi_2 & -1 & 1 & & & & & \\ 0 & 0.05 & 0 & 0 & 1 & 0 & 0 & & & & & \\ 0 & 1 & 0 & 0 & 0 & 0 & 0 & S_{mm_1} & -S_{mr_1} & S_{mt_1} & & \\ 0 & 0 & -1 & 1 & 0 & 0 & 0 & S_{rm_1} & -S_{rr_1} & S_{tr_1} & & \\ 1 & 0 & 0 & 0 & 0 & 0 & 0 & S_{tm_1} & -S_{tr_1} & S_{tt_1} & & \\ & -1 & 0 & 0 & 0 & 0 & 0 & S_{mm_2} & S_{mr_2} & S_{mt_2} & -S_{mm_2} & -S_{mt_2} \\ & & & & 0 & -1 & 1 & S_{rm_2} & S_{rr_2} & S_{rt_2} & S_{rm_2} & S_{tr_2} \\ & & & & -1 & 0 & 0 & S_{tm_2} & S_{tr_2} & S_{tt_2} & -S_{tm_2} & -S_{tt_2} \end{bmatrix} \begin{bmatrix} T_2 \\ M_2 \\ R_1 \\ R_2 \\ T_{2'} \\ R_{2'} \\ R_3 \\ \theta_2 \\ v_2 \\ u_2 \\ \theta_3 \\ u_3 \end{bmatrix} = \begin{bmatrix} 0 \\ 2qr \\ 2qr\phi_1 \\ 0 \\ 2qr \\ 2qr\phi_2 \\ 0 \\ 2(R_q)_1 \\ 0 \\ 0 \\ 2(R_q)_2 \\ 0 \end{bmatrix}$$

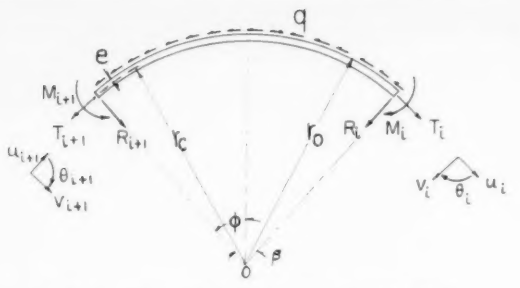

FIG. 5. Curved element geometry and loading.

Let $P = 100$ and $q = 1.1253953925$. The solution is

T_2 =	−28.89457266	R_3 =	−36.62899535
M_2 =	−482.768716	θ_2 =	−2.91185135
R_1 =	18.35518868	v_2 =	94.5672443
R_2 =	51.4024805	u_2 =	−93.2107074
$T_{2'}$ =	41.81610529	θ_3 =	1.23966596
$R_{2'}$ =	19.30819743	u_3 =	−137.333729

The check of vertical equilibrium of half the ring is

$$R_1 - R_3 + 2qr = 18.35518868 + 36.62899535 + 45.01581570 = 99.99999973$$

The calculations are repeated assuming that $\kappa = \lambda = 1$—i.e., assuming γ to be infinitely large. The final results are found to be

T_2 =	−28.93162	R_3 =	−36.57660
M_2 =	482.0277	θ_2 =	−2.947629
R_1 =	18.40758	v_2 =	91.460459
R_2 =	51.43953	u_2 =	−93.66575
$T_{2'}$ =	41.77905	θ_3 =	1.1977498
$R_{2'}$ =	19.27114	u_3 =	−136.1715

The resulting forces are seen to differ but little from the forces calculated previously, and the deflections are of approximately the same magnitude as those found before.

Certain problems involving three-dimensional reinforced cylindrical structures containing curved elements and curved panels may be solved using the data derived herein for curved elements and allied equations. However, for certain problems, such as flexible frames loaded so that the induced panel shear flow varies radically over relatively small arcs, the method presented here may have to be modified.

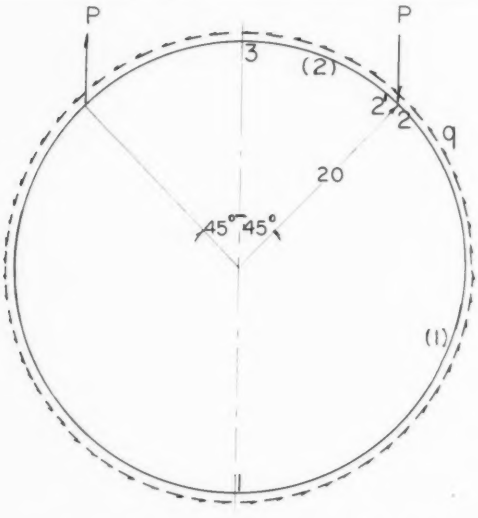

FIG. 6. Circular ring under antisymmetric loading.

APPENDIX (1)

First consider the derivation of the force-displacement for a shear panel simultaneously tapered in plan form and thickness in one direction (x) as shown in Fig. 1. The required relation may be derived by using an elastic energy principle as follows. Equate the work done in shear by the four external loads, F_{1-2}, F_{1-3}, F_{2-4}, and F_{3-4}, to the energy stored in the panel due to shear:

$$(F_{1-2}/2)(1/2)(u_1 + u_2) + (F_{1-3}/2)(1/2)(v_1 + v_3) - (F_{2-4}/2)(1/2)(v_2 + v_4) - (F_{3-4})(1/2)(u_3 + u_4) = (1/2G)\int_0^h \tau^2 t b dx = (q_{max}{}^2 b_{min}/2G) \times \int_0^h (1/t)(b_{min}/b)^3 dx \quad \text{(A-1)}$$

since $\tau = (q/t) = q_{max}(b_{min}/b)^2(1/t)$

Substitution of $b = b_{min} + (b_{max} - b_{min})(x/h)$ and integration yields, for constant t,

$$[q_{max}{}^2/(2Gt)](h/2) \times (b_{max} + b_{min})(b_{min}/b_{max})^2 = [\bar{q}^2/(2Gt)]A_p \quad \text{(A-2)}$$

When t varies approximately linearly in the x direction, the following close approximation applies:

$$[\bar{q}^2/(2Gt_D)]A_p \quad \text{(A-3)}$$

where t_D is the panel gage at point D, as shown in Fig. 1, at the intersection of the diagonals of the panel.

The following examples are given to illustrate the accuracy of this approximation.

First let $(b_{max}/b_{min}) = 2$, and $(t_{max}/t_{min}) = 2$. The correct value of the integral is

$$\int_0^h (t_{min}/t)(b_{min}/b)^3 dx = \int_0^h dx/[1 + (x/h)]^4 = 0.292h$$

In the approximate method, the thickness t_D occurs at $(x/h) = 0.31$ in this case, and the corresponding approximate value of the integral is

$$(h/2)3(1/2)^2/(1 + 0.31) = 0.286h$$

in error by about 2 per cent.

If $(b_{max}/b_{min}) = 3$, and $(t_{max}/t_{min}) = 2$, the results are, by direct integration,

$$\int_0^h \frac{dx}{[1 + (x/h)][1 + 2(x/h)]^3} = 0.183h$$

and by the approximate method, using the thickness at

$(x/h) = 0.25$ in this instance,

$$(h/2)4(1/3)^2/(1 + 0.25) = 0.178h$$

in error by about 3 per cent.

Since the tapers in the latter example are extreme, the approximate method is considered accurate (as long as the thickness variation is approximately linear and only in the x-direction).

Return to the evaluation of Eq. (A-1). The forces appearing on the left-hand side of the equation may be expressed as follows by taking moments about appropriate points:

$$\left.\begin{aligned} F_{1-2} &= F_{1-3}(a_{1-2}/b_{max}) = \bar{q}\, a_{1-2} \\ F_{2-4} &= F_{1-3}(b_{min}/b_{max}) = \bar{q}\, b_{min} \\ F_{3-4} &= F_{1-3}(a_{3-4}/b_{max}) = \bar{q}\, a_{3-4} \end{aligned}\right\} \qquad \text{(A-4)}$$

where

$$F_{1-3} = q_{max}b_{min} = q_{max}(b_{min}/b_{max})b_{max} = \bar{q}\, b_{max}$$

Substitution of these results into Eq. (A-1) and division by $\bar{q}/4$ yields Eq. (1) of the text.

Consider next the derivation of the force-displacement relation for a tapered stringer bounded by n shear panels. Refer to Fig. 2. The axial strain at any section located by the coordinate s is

$$du/ds = \sigma/E = \left(P_i + \sum_n \int_0^s q_n ds\right)\Big/ AE \qquad \text{(A-5)}$$

Integration yields

$$u_i - u_{i+1} = \int_0^a \left[\left(P_i + \Sigma \int_0^s q ds\right)\Big/ AE\right] ds \qquad \text{(A-6)}$$

Each q may be expressed in the form

$$q = q_{max}[s_i/(s_i + s)]^2, \quad s_i = a/[(b_{max}/b_{min}) - 1] \qquad \text{(A-7)}$$

s_i is the distance from the intersection of the sloping edges of the element to point i. Integration yields

$$\int_0^s q ds = q_{max}[s_i s/(s_i + s)] \qquad \text{(A-8)}$$

Final evaluation of the integral in Eq. (A-6) results in

$$(E\bar{A}/a)(u_i - u_{i+1}) = P_i + a\sum_n (\bar{q}_n f_n) \qquad \text{(A-9)}$$

If the variation of A is linear with s—i.e., $A = A_{min} + (A_{max} - A_{min})(s/a)$,

$$f = \frac{b_{max}/b_{min}}{[(b_{max}/b_{min}) - (A_{max}/A_{min})]}\left\{1 - \left[\frac{(A_{max}/A_{min}) - 1}{(b_{max}/b_{min}) - 1}\right]\frac{\log (b_{max}/b_{min})}{\log (A_{max}/A_{min})}\right\} \qquad \text{(A-10)}$$

There remains to discuss the derivation of Eq. (4) of the text. This result follows directly from the relation

$$\int_0^a ds = a\bar{q}$$

obtained by letting $s = a$ in Eq. (A-8) above.

Appendix (2)

Eqs. (7) of the text and the stiffnesses, S and R_q, appearing therein may be derived with the aid of the concepts and equations presented in reference 2. Using the notation of reference 2, for example, one may write

$$\left.\begin{aligned} T_i &= u_i tt_M + v_i tr_M + \theta_i tn_M - u_{i+1} tt_F + v_{i+1} tr_F - \theta_{i+1} tn_F + t_q \\ T_{i+1} &= -u_{i+1} tt_M + v_{i+1} tr_M - \theta_{i+1} tn_M + u_i tt_F + v_i tr_F + \theta_i tn_F - t_q \end{aligned}\right\} \qquad \text{(A-11)}$$

Adding, one obtains

$$T_i + T_{i+1} = (u_i - u_{i+1})(tt_M + tt_F) + (v_i + v_{i+1})(tr_M + tr_F) + (\theta_i - \theta_{i+1})(tn_M + tn_F) \qquad \text{(A-12)}$$

Therefore, the following relations hold:

$$S_{tt} = tt_M + tt_F, \quad S_{tr} = tr_M + tr_F, \quad S_{tn} = tn_M + tn_F \qquad \text{(A-13)}$$

In a similar manner, the remaining two equations of Eqs. (7) may be derived and the following relations established:

$$\left.\begin{aligned} S_{nn} &= nn_M + nn_F \quad S_{nt} = n_{tM} + nt_F \quad S_{rn} = rn_M - rn_F \\ S_{nr} &= nr_M + nr_F \quad S_{rr} = rr_M - rr_F \quad S_{rt} = rt_M - rt_F \end{aligned}\right\} \qquad \text{(A-14)}$$

The task of the determination of the actual value of S, therefore, resolves itself into the evaluation of the sums (or differences) of the quantities, tt_M, tt_F, etc., presented in reference 2. The complete development of these evaluations is lengthy and will not be presented here. First one eliminates the quantities with subscript, F, by writing the matric relation [from Eq. (34) of reference 2]:

$$\begin{bmatrix} S_{nn} & S_{nr} & S_{nt} \\ S_{rn} & S_{rr} & S_{rt} \\ S_{tn} & S_{tr} & S_{tt} \end{bmatrix} = \begin{bmatrix} 2 & r_c \sin\beta & r_c(1 - \cos\beta) \\ 0 & (1 + \cos\beta) & \sin\beta \\ 0 & -\sin\beta & (1 + \cos\beta) \end{bmatrix} \begin{bmatrix} nn_M & nr_M & nt_M \\ rn_M & rr_M & rt_M \\ tn_M & tt_M & tt_M \end{bmatrix} \qquad \text{(A-15)}$$

Next, the quantities with subscript M are expressed in the form of the ratio of the determinants given in Eqs. 22 of reference 2.

$$\left.\begin{aligned}(\Delta/r_c^2) &= (\beta/4)(\beta\kappa - \lambda\sin\beta)[\beta\kappa + \lambda\sin\beta - 4(1/\beta)(1-\cos\beta)]\\ (r_c/EI)[-\Delta_{rt}\sin\beta + \Delta_{tt}(1+\cos\beta)] &= (\beta/2)(1+\cos\beta)(\beta\kappa - \lambda\sin\beta)\\ (r_c/EI)[\Delta_{rr}(1+\cos\beta) + \Delta_{rt}\sin\beta] &= (\beta/2)(1+\cos\beta)[\beta\kappa - \lambda\sin\beta - 4(1/\beta)(1-\cos\beta)]\end{aligned}\right\} \quad \text{(A-16)}$$

By taking the necessary quotients of the above results, Eqs. (9) are derived. In a similar manner, the relations among the S's given in Eq. (8) eventually may be found. The equilibrium Eqs. (6) also prove of use in establishing some of the relations. For example, from the first equation of Eqs. (6), it follows that

$$S_{tr} = -S_{tt}\tan\phi$$

The value of R_q is derived with the aid of Eq. (19b) of reference 2 (with the right-hand side set equal to zero) and the equilibrium equations (6) of this paper. The derivation is lengthy and not given here. The result, including the effect of shear flow eccentricity, is

$$R_q = qr_o\{\kappa(\beta - \sin\beta) + (r_o/r_c) \times [\beta(1+\cos\beta) - 2\sin\beta]\}/(\kappa\beta - \lambda\sin\beta) \quad \text{(A-17)}$$

Elimination of κ and λ using Eq. (9) results in the form

$$R_q = qr_o\{(1/2)\psi_1(\beta)[1 + (S_{rr}/S_{tt})] + [f(\beta) - (e/r_c)g(\beta)](S_{rr}L^3/EI)\} \quad \text{(A-18)}$$

where $e = (r_o - r_c)$ as shown in Fig. 6, and

$$\beta^3 f(\beta) = \phi + \{-1 + (1/2)\psi_1(\beta)(\tan\phi/\phi)\}\tan\phi = \beta^5[(1/1440) + (1/3780)\beta^2 + (323/7257600)\beta^4 + \ldots]$$

$$g(\beta) = (1/8\phi^2)[(\tan\phi/\phi) - 1] = (1/24) + (1/60)\beta^2 + (17/252)\beta^4 + \ldots$$

When e is set equal to zero, the expressions given in Eqs. (10) are obtained.

References

[1] Klein, B., *A Simple Method of Matric Structural Analysis*, Journal of the Aeronautical Sciences, Vol. 24, No. 1, pp. 39–46, January, 1957.

[2] Hoff, N. J., Klein, B., and Libby, P. A., *Influence Coefficients of Curved Bars for Distortions in Their own Plane*, NACA TN 999, 1946.

Rotating Stall in Axial Flow Compressors

(*Continued from page 812*)

[4] Marble, F. E., *Propagation of Stall in a Compressor Blade Row*, Journal of the Aeronautical Sciences, Vol. 22, No. 8, pp. 541–554, August, 1955.

[5] Fabri, J., and Siestrunck, R., *Sur le calcul despetites perturbations propagées à son apparition par le décollement tournant d'une roue axiale*, Comptes Rendus Académie des Sciences, Vol. 243, pp. 1718–1721, 1956.

[6] Cornell, W. C., *The Stall Performances of Cascades*, Proceedings of the Second National Congress of Applied Mechanics, pp. 705–713, New York, 1955.

[7] Roy, M., *Ecoulement théorique et médian dans un rotor à palettes radiales*, Comptes Rendus Académie des Sciences, Vol. 227, pp. 496–498, 1948.

[8] Kriebel, A. R., *Stall Propagation in a Cascade of Airfoils*, Journal of the Aeronautical Sciences, Vol. 23, No. 9, pp. 897–898, September, 1956.

[9] Fabri, J., and Jarlan, L., *Correspondance entre la caractéristique de compression d'une roue axiale et les grandeurs cinématiques du régime de décollement tournant*, La Recherche Aéronautique, No. 54, pp. 21–22, 1956.

[10] Costilow, E. L., and Huppert, M. C , *Some Effects of Guide Vane Turning and Stators on the Rotating Stall Characteristics of a High Hub/Tip Ratio Single-Stage Compressor*, NACA TN 3711, April, 1956.

[11] Siestrunck, R., and Fabri, J., *Ecoulements tourbillonnaires dans les machines axiales*, ONERA, Publ. 45, 1950.

[12] Jaumotte, A., and Goldstein, S., *Propriétés de similitude d'une roue axiale isolée en régime de décollement tournant*, Comptes rendus Académie des Sciences, Vol. 243, pp. 2014–2017, 1956.

[13] Villat, H., *Leçons sur l'hydrodynamique*, Gauthier Villars, Paris, 1929.

Diffraction of Disturbances Around a Convex Right Corner With Applications in Acoustics and Wing-Body Interference†

LU TING*

Polytechnic Institute of Brooklyn

SUMMARY

The problem of the diffraction of a small disturbance or an arbitrary pulse by a convex right-angled corner is reduced to two unsteady problems in half space. The matching of the boundary conditions of the solutions to these two problems leads to a nonhomogeneous integral equation for the pressure distribution along the boundary. The solution is obtained by the method of successive substitution. It is shown that the series given by this procedure converges faster than the power series of one half. The convergence of the series is accelerated by regrouping the terms so that the solutions corresponding to any one of the ordinal numbers of substitution possesses the correct behavior at the boundary of the domain.

When the given disturbance is a plane weak (acoustic) shock, the solution corresponding to the second substitution is already in good agreement with the linearized conical solution. For the other two nonconical fundamental problems considered in this paper, the series converges so rapidly that there is no necessity to go beyond the second substitution.

By superposition of these fundamental solutions, the pressure distribution on a rectangular barrier after it is contacted by a weak shock is obtained. The problem of interference of a prismatic body of rectangular cross section with a planar wing in supersonic flight can be reduced to the problem presented in this paper and the one amenable to solution by Evvard's method. The pressure distribution is obtained for four different wing-body configurations. The value of the integral of the pressure distribution agrees with the value obtained directly by means of a certain integral relationship.

SYMBOLS

A, A_0, A_1, A_2	= constants
B	= $\sqrt{M^2 - 1}$
C	= speed of sound
G	defined in Eq. (11)
$H_1^{(N)}$	defined in Eq. (23)
$2L$	= width of the barrier or the body
M	= Mach Number of undisturbed stream
N	= an integer, 1, 2, 3, 4, . . .
R	defined in Eq. (28)
S_0	= incoming disturbance
S_1, S_2	= additional disturbances
g	defined in Eq. (13)
$h_0, h_1, h^{(0)}, h^{(1)}$	defined in Eqs. (12), (13), (18), (19), (20)
n	= an integer 0, 1, 2, 3, . . .
p	= pressure
t	= time
x, y, z	= Cartesian coordinates with z in the direction of the free stream
ξ	= z/B
$\alpha, \beta, \alpha,' \beta'$	= characteristic coordinates
Δ	= Laplace operator
ξ, τ, ζ	= variables in place of x, t, and z, respectively
ρ	= density of the free stream
ϵ	= pressure jump across a weak shock
δ	= inclination of the upper surface of the wedge with reference to the free-stream direction

Received January 7, 1957.

† This research was supported by the United States Air Force through the Air Force Office of Scientific Research, Air Research and Development Command, under Contract No. AF 18(600)-693, Project No. R-352-30-12 under the supervision of Prof. Antonio Ferri, to whom the author is indebted for his invaluable discussions.

* Research Associate.

INTRODUCTION

THE FLOW FIELDS produced by the motion and diffraction of infinitesimally weak (scalar) two-dimensional waves are governed by the wave equation

$$\Delta\varphi - (1/C^2)\,\varphi_{tt} = 0$$

whereas linearized three-dimensional steady supersonic flows obey the differential equation

$$\Delta\varphi - B^2\varphi_{zz} = 0$$

which is equivalent to the wave equation. Therefore, problems in these two fields can often be solved by the same technique or may even be represented by the same type of solution. In this paper an analysis is given of the flow field associated with the diffraction of a two-dimensional wave which comes in contact with a convex right-angled corner. The solutions obtained are applied to the analysis of the equivalent steady flow problem of the flow field produced by the interference of wings and prismatic bodies of rectangular cross section.

The diffraction of a two-dimensional wave by a wedge was analyzed by Sommerfeld.[1] Since then numerous investigations of diffraction problems have been reported. An extensive account of them can be found in reference 2. Much of the work cited deals with time-harmonic problems in which the incident wave is time-harmonic or "monochromatic." For these problems the simple wave equation reduces to the time-free elliptic equation $\Delta\varphi + k^2\varphi = 0$. In principle, the solutions of these problems can be extended with the aid of the Fourier integral to produce solutions to diffraction problems in which the incidence wave is not time-harmonic. However, the inverses of these Fourier-transform solutions have not yet been determined.

For linearized three-dimensional supersonic flow, the above technique is not practical because the flow field to be analyzed is usually nonperiodic with respect

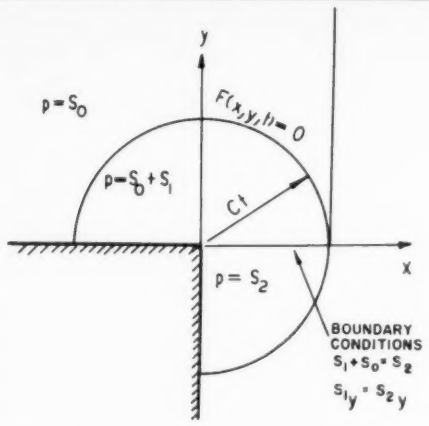

FIG. 1. Pressure distribution at an instant $t > 0$.

to the coordinate (z) in the direction of the undisturbed flow. A different approach was introduced by Busemann[3] who pointed out the frequent existence of conical fields in supersonic flow. In conical fields the governing equation for the velocity components or pressure distribution can be reduced to a Laplace equation of two independent variables. Busemann's original treatment has been applied to delta wings by Stewart[4] and to quadrilateral wings with dihedral by Snow,[5] and has been developed in detail by many others (see reference 6).

The general problem of lifting planar wings in supersonic stream cannot be resolved into conical fields. Two different approaches to this problem were presented in 1947. Gunn[7] applied the method of Laplace transform. Evvard[8, 9] expressed the solution in terms of the equivalent source distribution. The simplicity of Evvard's method has resulted in its being preferred usually for practical applications (see p. 184, reference 6). Nevertheless, Gunn's method has certain advantages for wings of low aspect ratio.

Busemann's method of conical flow has been applied by Keller and Blank[10] to the case of a uniform plane pulse incident on a corner or wedge. Diffraction problems of this type correspond to the problem of wings with dihedral in supersonic flow.[5]

The problem of a uniform plane pulse incident on a thin barrier (or an infinite strip) was analyzed by Ting[11] and Miles[12] on the same physical ground as the supersonic flow over a rectangular plate of infinite chord length. In the treatment of reference 11, the time-history of the diffraction problem is subdivided into equal time intervals. At the end of each interval the disturbance originating at one edge of the strip reaches the other edge, and the response in each case is equivalent to the basic problem of diffraction by a half plane. This basic problem is solved by Evvard's method and detailed pressure variations on the thin barrier (or the strip) are obtained. On the other hand, in reference 12 the method of Laplace transform by Gunn[7] and Fox[13] is used and the complete time-history of the total force acting on the strip is obtained.

In reference 11, it has been pointed out that the time-history of the diffraction of a pulse by a rectangular barrier (or block) can also be subdivided into time intervals. At the end of each time interval the disturbance originating at one corner of the block reaches the other, and the response in each case is equivalent to that of the basic problem of the diffraction of an arbitrary pulse by a convex right corner. The approach to this basic problem suggested in reference 11 may be briefly indicated with the aid of Fig. 1. The incident pulse and its reflection by one side of the corner (the negative x-axis) is given by the pressure disturbance $S_0(x, y, t)$, which is defined in the region $y \geq 0$ for $t \leq 0$ and crosses the corner at the instant $t = 0$. If the same expression of S_0 is extended to the same region $y > 0$ for $t > 0$, a discontinuity of pressure $\Delta p = S_0(x, 0, t)$, will be created along the positive x-axis. This is a violation of the physical conditions of the problem. The discontinuity is removed by the superposition of two addition disturbances S_1 and S_2 created at the corner at the instant $t = 0$ for the region above and below the x-axis—i.e.,

$$S_1 + S_0 = S_2 \tag{1}$$

on the positive x-axis. In addition to the requirement that the resultant pressure be continuous, it is necessary[11] that its normal derivative vanish on the wall and be continuous along the positive x-axis. The solutions S_1 and S_2 to the simple wave equation in half space can be expressed in terms of their normal derivatives on the x-axis—i.e., $S_{1y}(x > 0, 0, t)$—and consequently Eq. (1) yields an integral equation for S_{1y} or S_{2y} along the positive x-axis. The solution to the integral equation is not presented in reference 11.

A more general problem, the case of an arbitrary pulse incident on an infinite wedge of *any angle*, has been considered by Kay.[14] Kay's approach differs from that of reference 11 in the following respect. The definition of the incident wave together with the reflections from the side of the wedge for $t < 0$—i.e., before crossing the corner located at the origin—is extended in the same expression only to the region outside the characteristic cone $ct = \sqrt{x^2 + y^2}$ in the space-time continuum. The problem is then to find a solution of the wave equation inside the cone. For this solution the condition of continuity of the solution across the cone determines a certain nonhomogeneous boundary condition on the cone in addition to the homogeneous boundary condition already imposed on the wedge. Hence for the special case of a wedge angle equal to 90°, Kay's solution inside the cone should be identical with the solutions in reference 11—i.e., with $S_0 + S_1$ and S_2 in the regions $y > 0$ and $y < 0$, respectively—whereas both S_1 and S_2 fulfill a homogeneous boundary condition on the characteristic cone. Kay has obtained, in principle, the solution to his problem. However, the intricacy of his method precludes the possibility of obtaining the final results of any problem other than the conical problem treated by Keller and Blank.[10]

Turner[15] proposed to determine the Green's function for the wave equation for the case of the wedge by "two transformations and two inversions." The procedure, in principle, is straightforward. Nevertheless, it is only illustrated by the problem of diffraction of a cylindrical pulse by a half plane.

Graphs of the theoretical pressure distribution[10] resulting from the diffraction of a weak shock by a rigid right-angled corner are compared with graphs of measured pressure distribution by Keller.[16] The agreement is found to be satisfactory except at the corner of the wedge and at the "triple-point" where the incident (or reflected) pulse front is tangent to the characteristic cone.

At the corner of the wedge, the velocity components based upon the linearized theory or acoustic theory become infinite although the pressure remains finite. The experimental result shows the existence of a small region of finite vorticity near the corner. Theoretical investigations of the relevant vortex generation have been made by Howard and Matthews[17] and Rott.[18] In the vicinity of the "triple-point" Lighthill's technique[19, 20] fails. A semiempirical approach has been advanced recently by Sun.[21]

In the present paper, the problem of diffraction of disturbance or an arbitrary pulse by a convex right corner is again considered. The classical acoustic approximation for weak pulses is used, while the generation of vortices is ignored and improvement of the acoustic solution near the characteristic cone is not included. The main purpose is to present an elementary and intuitive method which permits final numerical results to be obtained conveniently, rather than to derive a solution purely in principle. The approach is based on the same physical ground outlined in reference 11. Instead of an integral equation for the normal derivative of pressure along the positive x-axis, an integral equation for the pressure distribution along the x-axis is set up. The necessity for doing this will be explained later. A solution to this new integral equation is presented. The final results can be obtained by simple quadratures.

Three fundamental types of incident pulses are considered and the response obtained in each case. Two of them do not possess the properties of a conical field.

By superposition of these fundamental solutions, many diffraction problems and wing-body interference problems can be solved. This is illustrated in the present paper by the treatment of the diffraction of a weak shock by a rectangular structure. Likewise, the corresponding problem in supersonic flow (the interference problem of a prismatic body of rectangular cross section with a planar wing having supersonic edges) is treated. In addition a method of solution for wings with subsonic edges is presented. This type of wing-body interference problem was first considered by Lagerstrom and Van Dyke.[22] Discussions of additional applications of the results to be presented here can be found in references 23 and 24.

(1) Formulation of the Diffraction Problem

In Fig. 1, the 90° convex corner is represented by the third quadrant of the x-y plane. The given two-dimensional pressure disturbance, $S_0(x, y, t)$, which is a solution of the simple wave equation, is defined in the region $y > 0$ and vanishes when $x > Ct$, where C is the speed of sound. It is understood that S_0 fulfills the boundary condition $(\partial/\partial y)S_0(x, 0^+, t) = 0$.

When $t > 0$, the pressure disturbance $S_0(x, y, t)$ creates a discontinuity in pressure, $\Delta p = S_0(x, 0^+, t)$, along the portion of the x-t plane where $0 < x < Ct$.* The additional disturbance, which will be confined inside the cone,

$$F(x, y, t) = Ct - \sqrt{x^2 + y^2} = 0$$

should be such that the total pressure disturbance, $p(x, y, t)$, and also its first derivatives should be continuous[11] across the portion of the x-t plane where $0 < x < Ct$. Let $S_1(x, y, t)$ and $S_2(x, y, t)$ be the additional pressure disturbances in the region $y > 0$ and $y < 0$, respectively. The problem now is to find S_1 and S_2. Both of them are solutions to the simple wave equation

$$(\partial^2 p/\partial x^2) + (\partial^2 p/\partial y^2) - (1/C^2)\,(\partial^2 p/\partial t^2) = 0 \quad (2)$$

and fulfill the following initial conditions:

$$\left.\begin{aligned} S_1(x, y, t < 0) &= 0 \\ S_2(x, y, t < 0) &= 0 \end{aligned}\right\} \quad (3)$$

and boundary conditions:

$$S_2(x > 0, 0^-, t > 0) - S_1(x > 0, 0^+, t > 0) = S_0(x > 0, 0^+, t > 0) \quad (4)$$

$$(\partial/\partial y)S_2(x > 0, 0^-, t > 0) = (\partial/\partial y)\,S_1(x > 0, 0^+, t > 0) \quad (5)$$

$$(\partial/\partial y)S_1(x < 0, 0^+, t > 0) = 0 \quad (6)$$

$$(\partial/\partial x)S_2(0^+, y < 0, t > 0) = 0 \quad (7)$$

$$S_1 = S_2 = 0 \quad \text{on and outside the cone } F = 0 \quad (8)$$

(2) The Integral Equation and Its Solution

It is clear that Eq. (7) can be replaced by the condition of symmetry,

$$S_2(x, y < 0, t > 0) = S_2(-x, y < 0, t > 0) \quad (9)$$

Due to the boundary conditions (5), (6), and (9), the solutions of the wave equation in half space, S_1 and S_2 can be expressed in terms of the following integrals:

$$S_1 = -\frac{1}{\pi}\iint \frac{G(\xi, \tau)d\xi d\tau}{\sqrt{(t-\tau)^2 - [(x-\xi)^2 + y^2]/C^2}} \quad (10)$$

$$S_2 = \frac{1}{\pi}\iint \frac{G(|\xi|, \tau)\,d\xi d\tau}{\sqrt{(t-\tau)^2 - [(x-\xi)^2 + y^2]/C^2}} \quad (11)$$

* The case in which the discontinuity is created in the supersonic region is treated at the end of Section (5).

where $G(x < 0, t) = 0$

$$G(x > 0, t) = S_{1y}(x > 0, 0^+, t) = S_{2y}(x > 0, 0^-, t)$$

Elimination of the unknown function $G(x, t)$ from Eqs. (10) and (11) will yield an integral relationship between S_2 and S_1. With this relationship, S_2 will be eliminated from Eq. (4) and an integral equation for the pressure disturbance along the positive x-axis is obtained. This approach is carried out as follows.

Following Evvard's method[8, 9] the characteristic coordinates are introduced, with

$$\alpha = Ct - x, \quad \beta = Ct + x$$

Eqs. (10) and (11) then become

$$h_1(\alpha, \beta) = \frac{-1}{2\pi} \int_0^\alpha \frac{d\alpha'}{\sqrt{\alpha - \alpha'}} \int_{\alpha'}^\beta \frac{g(\alpha', \beta')d\beta'}{\sqrt{\beta - \beta'}} \tag{12}$$

$$h_2(\alpha, \beta) = \frac{1}{2\pi} \int_0^\alpha \frac{d\alpha'}{\sqrt{\alpha - \alpha'}} \int_{\alpha'}^\beta \frac{g(\alpha', \beta')d\beta'}{\sqrt{\beta - \beta'}} + \frac{1}{2\pi} \int_0^\alpha \frac{d\alpha'}{\sqrt{\alpha - \alpha'}} \int_0^{\alpha'} \frac{g(\beta', \alpha')d\beta'}{\sqrt{\beta - \beta'}} \tag{13a}$$

$$h_2(\alpha, \beta) = -h_1(\alpha, \beta) + \frac{1}{2\pi} \int_0^\alpha \frac{d\alpha'}{\sqrt{\beta - \alpha'}} \int_{\alpha'}^\alpha \frac{g(\alpha', \beta')d\beta'}{\sqrt{\alpha - \beta'}} \tag{13}$$

where $h_1(\alpha, \beta) = S_1(x, 0^+, t)$
$h_2(\alpha, \beta) = S_2(x, 0^-, t)$

$$g(\alpha, \beta) = G(x, t)$$

Both Eq. (12) and Eq. (13) holds for $\beta > \alpha > 0$ (or $x > 0$) only. The second term in Eq. (13) is actually equivalent to $-h_1(\beta, \alpha)$ [or $-S_1(-x, 0^+, t)$], therefore,

$$h_2(\alpha, \beta) = -h_1(\alpha, \beta) - h_1(\beta, \alpha) \tag{14}$$

and Eq. (4) becomes

$$2h_1(\alpha, \beta) + h_1(\beta, \alpha) = -h_0(\alpha, \beta) \tag{15}$$

with $h_0(\alpha, \beta) = S_0(x > 0, 0^+, t)$ and $\beta > \alpha$. $h_1(\beta, \alpha)$ can be expressed in terms of $h_1(\alpha, \beta)$ as follows:[9]

$$\left.\begin{aligned} h_1(\beta, \alpha) &= -\frac{1}{2\pi} \int_0^\alpha \frac{d\alpha'}{\sqrt{\beta - \alpha'}} \int_{\alpha'}^\alpha \frac{g(\alpha', \beta')d\beta'}{\sqrt{\alpha - \beta'}} \\ &= \frac{1}{\pi} \int_0^\alpha \frac{d\alpha'}{\sqrt{\beta - \alpha'}} \times \frac{\partial}{\partial \alpha'} \int_0^{\alpha'} \frac{h_1(\alpha'', \alpha)d\alpha''}{\sqrt{\alpha' - \alpha''}} \\ &= \frac{\sqrt{\beta - \alpha}}{\pi} \int_0^\alpha \frac{h_1(\alpha', \alpha)d\alpha'}{(\beta - \alpha')\sqrt{\alpha - \alpha'}} \end{aligned}\right\} \tag{16}$$

and then Eq. (15) becomes an integral equation for $h_1(\alpha, \beta)$,

$$2h_1(\alpha, \beta) + \frac{\sqrt{\beta - \alpha}}{\pi} \int_0^\alpha \frac{h_1(\alpha', \alpha)d\alpha'}{(\beta - \alpha')\sqrt{\alpha - \alpha'}} = -h_0(\alpha, \beta) \tag{17}$$

for all values of $\beta > \alpha > 0$.

Although this equation appears to be an equation of Fredholm's type,[25] it is actually quite different because of the replacement of β by α in the function h_1, and the appearance of the factor $(\beta - \alpha')$ in the integrand.

Nevertheless the integral Eq. (17) is solved by the method of successive substitution, as is the Fredholm's type—i.e., for $\beta > \alpha$,

$$h_1(\alpha, \beta) = h^{(0)}(\alpha, \beta) + h^{(1)}(\alpha, \beta) + h^{(2)}(\alpha, \beta) + \ldots \tag{18}$$

where

$$h^{(0)}(\alpha, \beta) = -[h_0(\alpha, \beta)/2]$$

$$h^{(1)}(\alpha, \beta) = -\frac{\sqrt{\beta - \alpha}}{2\pi} \int_0^\alpha \frac{h(\alpha', \alpha)d\alpha'}{(\beta - \alpha')\sqrt{\alpha - \alpha'}} \tag{19}$$

$$h^{(n)}(\alpha, \beta) = -\frac{\sqrt{\beta - \alpha}}{2\pi} \int_0^\alpha \frac{h^{(n-1)}(\alpha', \alpha)\, d\alpha'}{(\beta - \alpha')\sqrt{\alpha - \alpha'}} \tag{20}$$

For most of the physical problem, $h^{(1)}(\alpha, \beta)$ is always bounded,* therefore, there exists a constant A, so that

$$|h^{(1)}(\alpha, \beta)| < A$$

for all values of $\beta > \alpha$. It follows that

$$|h^{(2)}(\alpha, \beta)| \leq \frac{\sqrt{\beta - \alpha}}{2\pi} \int_0^\alpha \frac{Ad\alpha'}{(\beta - \alpha')\sqrt{\alpha - \alpha'}} = \frac{A}{\pi} \tan^{-1} \sqrt{\frac{\alpha}{\beta - \alpha}} \leq \frac{A}{2}$$

and similarly if

$$|h^{(n-1)}(\alpha, \beta)| < 2^{-(n-2)}A$$

it follows that

$$|h^{(n)}(\alpha, \beta)| < (max/2)|h^{(n-1)}(\alpha, \beta)| < A/2^{n-1}$$

Hence, the solution by successive substitution, Eq. (18), converges faster than the power series of $1/2$.

The method of successive substitution for this problem can be interpreted on physical ground. For the zero order approximation, the diffraction problem by the convex right corner represented by the third quadrant is approximated by the corresponding problem with a flat plate along the negative x-axis. Due to the condition of antisymmetry, it is obvious that the pressure disturbances in the regions of $y > 0$ and $y < 0$ which balance the discontinuity in pressure along the positive x-axis are, respectively, $h^{(0)}(\alpha, \beta)$ and $-h^{(0)}$ as defined by Eq. (19) for $\beta > \alpha$. Consequently $-h^{(1)}(\beta, \alpha)$ defined by Eq. (20) represents the corresponding pressure disturbance on the lower surface of the "imaginary" flat plate.

The presence of the solid surface along the negative y-axis has the effect of a mirror. The image of the approximate solution in the third quadrant is added to the corresponding solution in the fourth quadrant. As

* This is valid if $h_0(\alpha, \beta)$ or (S_0) is bounded and still true even if h_0 possesses a logarithmic singularity or a singularity of $\alpha^{-1/2}$ as $\alpha \to 0$.

a result, a new discontinuity in pressure $\Delta p = h^{(1)}(\alpha, \beta)$ is created along the positive x-axis and one cycle of the successive substitution is completed.

In reference 11, an integral equation for the normal derivative of pressure along the positive x-axis was obtained by substitution of Eqs. (12) and (13a) into Eq. (4),

$$\int_0^\alpha \frac{g(\beta', \alpha)}{\sqrt{\beta - \beta'}}\, d\beta' + 2\int_\alpha^\beta \frac{g(\alpha, \beta')}{\sqrt{\beta - \beta'}}\, d\beta' = \frac{\partial}{\partial \alpha}\int_0^\alpha \frac{h_0(\alpha', \beta)}{\sqrt{\alpha - \alpha'}}\, d\alpha' \quad (21)$$

Omission of the first term will change the equation into one of the Abel's type.[25] Consequently, the method of substitution can be applied and has actually the same physical meaning as the one for Eq. (18). However, a proof of convergence of the solution for Eq. (21) was lacking in reference 11 due to the difficulty of assessing the property of the derivative of pressure in the flow field. In addition to the complicacy of the operation in each substitution, a double integration is required to obtain the pressure distribution from the solution of Eq. (21), whereas the solution of Eq. (17), which is the pressure distribution, can be obtained by simple quadrature. Hence, the new formulation, Eqs. (17)–(19), is well suited for obtaining numerical results.

The convergence of the series of Eq. (18) will be faster if it is regrouped as follows:

$$h_1(\alpha, \beta) = (2/3)h^{(0)}(\alpha, \beta) + (1/3)\,[h^{(0)}(\alpha, \beta) + 2h^{(1)}(\alpha, \beta)] + (1/3)\,[h^{(1)}(\alpha, \beta) + 2h^{(2)}(\alpha, \beta)] + \ldots = (2/3)h^{(0)}(\alpha, \beta) + (1/3)\sum_{n = 1, 2, 3}^{\infty} [h^{(n-1)}(\alpha, \beta) + 2h^{(n)}(\alpha, \beta)] \quad (22)$$

In the series of Eq. (18) the zero order approximation for $h_1(\alpha, \beta)$—i.e.,

$$h^{(0)}(\alpha, \beta) = -(1/2)h_0(\alpha, \beta)$$

is obtained from Eq. (17), or Eq. (15), by assuming $h_1(\beta, \alpha) = 0$ for $\beta > \alpha$; while in the series of Eq. (22) the zero order approximation for $h_1(\alpha, \beta)$—i.e.,

$$(2/3)h^{(0)}(\alpha, \beta) = -(1/3)h_0(\alpha, \beta)$$

is obtained by assuming

$$h_1(\alpha, \beta) = h_1(\beta, \alpha)$$

The latter assumption fulfills the condition that the value of the pressure at $\alpha = \beta$ is unique—i.e.,

$$\lim_{\beta - \alpha \to 0} [h_1(\alpha, \beta) - h_1(\beta, \alpha)] = 0$$

The former assumption leads to a discontinuity of $(1/2)h_0(\beta, \beta)$ at $\alpha = \beta$. Hence, it is expected that the series of Eq. (22) converges faster than the series of Eq. (19). Another reason in favor of the series of Eq. (22) is that the solution corresponding to the Nth substitution—i.e.,

$$H_1^{(N)} = (2/3)h^{(0)} + (1/3)\sum_{n = 1, 2, 3}^{N} [h^{(n-1)} + 2h^{(n)}] \quad (23)$$

yields the correct behavior for h_1 at both end points, $\alpha = 0$, and $\alpha = \beta$.* On the other hand, the series of Eq. (18) converges to the correct value of $-(1/3)h_0(\beta, \beta)$ at the end point where $\alpha = \beta$ in the same manner as the series $(1/2) - (1/4) + (1/8) \ldots$ does to 1/3. In case $h_0(\beta, \beta) = 0$ for all values of $\beta > 0$, then there is no longer any reason to prefer the series of Eq. (22) to the series of Eq. (18).

After $h_1(\alpha, \beta)$, or $H_1^{(N)}(\alpha, \beta)$, is determined for $\beta > \alpha$, the pressure distribution can be obtained from the following formulas:

$$p(x, y > 0, t) = S_0 + S_1 = S_0 - \frac{1}{\pi}\frac{\partial}{\partial y}\iint \frac{S_1(\xi, 0, \tau)d\xi d\tau}{R} \quad (24)$$

$$p(x, y < 0, t) = S_2 = \frac{1}{\pi}\frac{\partial}{\partial y}\iint \frac{S_2(\xi, 0, \tau)d\xi d\tau}{R} \quad (25)$$

where

$$S_1(x > 0, 0, t) = h_1(\alpha, \beta) \quad (26)$$

$$S_1(x < 0, 0, t) = -S_0(-x, 0, t) - 2S_1(-x, 0, t) \quad (27)$$

$$S_2(x > 0, 0^-, t) = S_2(-x, 0^-, t) = S_0(x, 0^+, t) + S_1(x, 0^+, t) \quad (28)$$

$$R = \sqrt{(t - \tau)^2 - [(x - \xi)^2 + y^2]/C^2}$$

(3) Fundamental Solutions

In many practical problems, the incoming disturbance S_0 is a conical solution with apex located at a point other than the origin, say at $x = -1$, $y = 0$. The discontinuity in pressure, created by S_0, in the first quadrant of the x-t plane, in general is expressed by a series,

$$S_0(x, 0^+, t) = A_0 + A_1\sqrt{1 - [(x + 1)/(Ct + 1)]} + A_3\{1 - [(x + 1)/(Ct + 1)]\}^{3/2} + \ldots \quad (29)$$

where $A_0, A_1, A_3, \ldots$ are constants if S_0 is bounded.† The sum of the first three terms usually differs less than 5 per cent from the value of S_0 for $1 \geq t > x \geq 0$ [see Sections (4) and (5)]. It is, therefore, worthwhile to find the additional disturbances $S_1(x, y > 0, t)$ and $S_2(x, y < 0, t)$ corresponding to

$$S_0(x, 0^+, t) = 1, \sqrt{(Ct - x)/(1 + Ct)}$$

* It can be shown that

$$\lim_{\alpha \to 0} H_1^{(N)}(\alpha, \beta) = h^{(0)}(0, \beta) = -(1/2)h_0(0, \beta)$$

$$\lim_{\beta - \alpha \to 0^+} H_1^{(N)}(\alpha, \beta) = (2/3)h^{(0)}(\beta, \beta) = -(1/3)h_0(\beta, \beta)$$

† Otherwise, the terms representing the singularities of S_0 will appear in the series of Eq. (29).

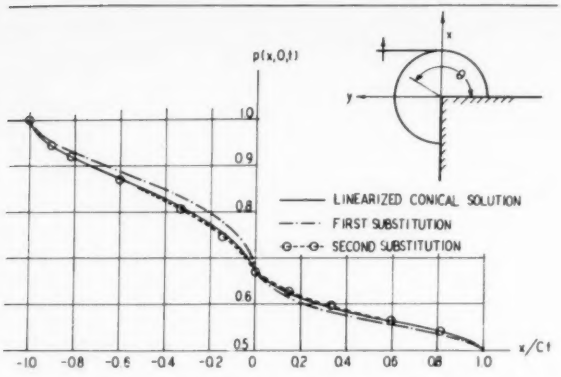

FIG. 2. Pressure distribution corresponding to $S_0(x, 0, t) = 1$.

and $[(Ct - x)/(1 + Ct)]^{3/2}$, respectively. S_1 and S_2 are called the fundamental solutions.

(i) $S_0^{\mathrm{I}}(x > 0, 0^+, t) = 1$

The discontinuity in pressure $S_0^{\mathrm{I}}(x, 0^+, t) = 1$ is created when a plane weak shock (or sonic pulse), $x = Ct$, is passing over the 90° convex corner (Fig. 2). The pressure distribution can be obtained as a conical solution[5, 10]

$$p_c\left(\frac{x}{t}, \frac{y}{t}\right) = 1 - \frac{1}{\pi}\tan^{-1}\frac{(1 - \Omega^2)\sqrt{3}}{(1 + \Omega^2) - 4\Omega\cos\omega} \qquad (30)$$

where $\tan^{-1}$ is taken between 0 to π,

$$\Omega = [(1 - \sqrt{1 - r^2})/r]^{2/3}$$
$$\omega = 2\vartheta/3$$
$$r = \sqrt{x^2 + y^2}/Ct$$
$$\vartheta = \tan^{-1}(y/x) + (\pi/2)$$

Therefore, the fundamental solution corresponding to $S_0^{\mathrm{I}} = 1$ is

$$S_1^{\mathrm{I}}(x, y > 0, t) = p_c - S_0 = p_c(x, y > 0, t) - 1 \qquad (31)$$

$$S_2^{\mathrm{I}}(x, y < 0, t) = p_c(x, y < 0, t) \qquad (32)$$

This problem is now re-solved by the method presented in this paper in order to learn how fast the series of Eq. (23) converges. With $S_0(x, 0^+, t) = 1$, Eqs. (19) and (20) yield

$$\left.\begin{aligned} h^{(0)} &= -(1/2) \\ h^{(1)}(\alpha/\beta) &= (1/2\pi)\tan^{-1}\sqrt{(\alpha/\beta)/[1 - (\alpha/\beta)]} \\ h^{(2)}(\alpha/\beta) &= (-1/2\pi\beta)\sqrt{\alpha(\beta - \alpha)}\times \\ &\qquad \int_0^1 \frac{h^{(1)}(\lambda)d\lambda}{[1 - \lambda(\alpha/\beta)]\sqrt{1 - \lambda}} \end{aligned}\right\} \qquad (33)$$

The last integral can be evaluated by numerical integration. Fig. 2 shows the pressure distribution along $y = 0$, given by Eqs. (24), (26) and (27) where $h_1(\alpha, \beta)$ is approximated by the results of first and second substitutions, $H_1^{(1)}$ and $H_1^{(2)}$, respectively. It is clear that the result based upon the second substitution is already very close to that of the exact linearized conical solution—i.e., Eq. (30).

(ii) $S_0^{\mathrm{II}}(x > 0, 0^+, t) = \sqrt{(Ct - x)/(Ct + 1)}$

In order to be able to carry out the first and the second substitution without resorting to numerical integration, $S_0^{\mathrm{II}}(x > 0, 0^+, t)$ is expressed as a power series of $(\beta - \alpha)/(2 + 2\beta)$,

$$S_0^{\mathrm{II}}(x > 0, 0^+, t) = h_0(\alpha, \beta) =$$
$$\sqrt{2a/(2 + \beta + \alpha)} = \sqrt{2/[2(1 + \beta) - (\beta - \alpha)]} =$$
$$\sqrt{\alpha/(1 + \beta)}\left\{1 + [(\beta - \alpha)/4(1 + \beta)] + (3/32)[(\beta - \alpha)/(1 + \beta)]^2 + \ldots\right\} \qquad (34)$$

The error in using only the first three terms is less than 3 per cent for $2 \geq \beta > \alpha \geq 0$. Corresponding to these three terms, the integrals in Eq. (20) can be evaluated.[26] The solutions for the first and second substitutions differ less than 2 per cent from each other. Because of Eq. (20), the series of Eq. (22) is an alternating series. The exact solution lies in between two successive substitutions. Hence, the result from the second approximation is satisfactory and there is no necessity to carry out the third substitution.

Since the denominator in the integrand in Eq. (20) vanishes as $\alpha' \to \alpha$, the value of $h^{(1)}(\alpha, \beta)$ depends predominantly on the value of $h^{(0)}(\alpha', \alpha)$ as $\alpha' \to \alpha$. It is clear that S_0^{II} approaches the first term on the right side of Eq. (34) as $\alpha \to \beta$. When this first term is used for the evaluation of $h^{(1)}$, the solution from the first substitution is

$$H_1^{(1)}(\alpha, \beta) = h^{(0)} + (2/3)h^{(1)} =$$
$$(-1/2)\sqrt{2\alpha/(2 + \alpha + \beta)} + [1/(6\sqrt{1 + \alpha})]\times$$
$$[\sqrt{\beta} - \sqrt{\beta - \alpha}] \qquad (35)$$

The maximum difference between the simple solution of Eq. (35) and that from the second substitution corresponding to the first three terms in series Eq. (34), is 2.5 per cent.

The additional pressure disturbance $S_1^{\mathrm{II}}(x, y > 0, t)$ and $S_2^{\mathrm{II}}(x, y < 0, t)$ can be obtained from Eqs. (24) to (28) where $h_1(\alpha, \beta)$ is approximated by $H_1^{(1)}$ in Eq. (35).[26] The error due to this approximation is less than 2.5 per cent.

(iii) $S_0^{\mathrm{III}}(x > 0, 0^+, t) = [(Ct - x)/(Ct + 1)]^{3/2}$

The additional disturbance pressure $S_1^{\mathrm{III}}(x, y > 0, t)$ and $S_2^{\mathrm{III}}(x, y < 0, t)$ due to S_0^{III} can be obtained in the same manner as S_1^{II} and S_2^{II} (see reference 26).

(4) Diffraction of Weak Shock by a Rectangular Barrier

In Fig. 3 is shown a rectangular barrier of height L and width $2L$. (The generality of the problem is not lost by specifying the ratio between the height and the

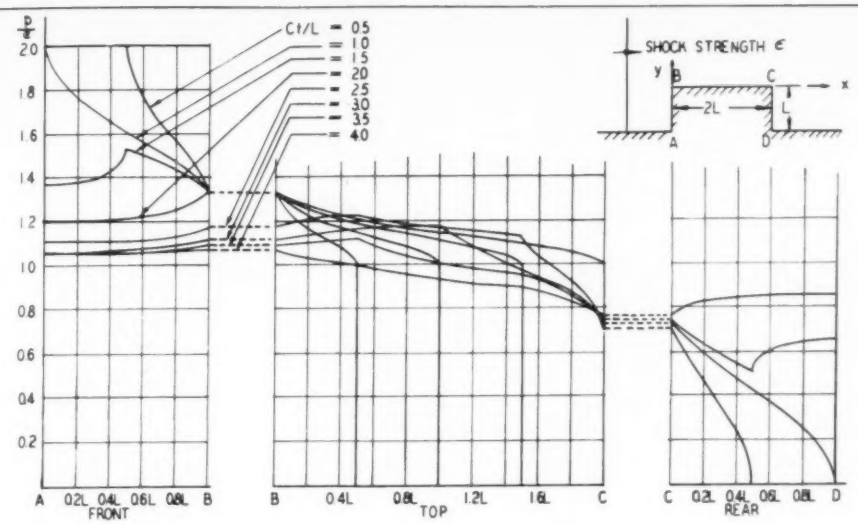

FIG. 3. Pressure distribution on the barrier.

width). The weak shock of strength ϵ hits the barrier at $t = 0$. During the interval $0 < t < L/C$, the pressure distribution is given by the conical solution.[10, 11]

$$(1/\epsilon)p^{(1)}(x, y, t) = 2 - p_c(-x, y, t)$$

where $p_c(x, y, t)$ is defined in Eq. (30). During the interval $L/C < t < 2L/C$, an additional disturbance $(1/\epsilon)p^{(2)}(x, y, t) = p_c(-x, -y - 2L, t)$ is created when $p^{(1)}$ is reflected from the 90° concave corner at A. When $t > 2L/C$, the pressure disturbance, $p^{(1)}$, is diffracted by the convex right corner at C and the disturbance, $p^{(2)}$, by the corner at B. The continuations of the solutions $p^{(1)}$ and $p^{(2)}$ for $t > 2L/C$ create discontinuities in pressure along the portion of the x-axis where $x > 2L$ and along the positive y-axis, respectively. The discontinuities are expressed by the general form of Eq. (29)—i.e.,

$$(1/\epsilon)p^{(1)}(x > 2L, 0, t) = 1 + 0.17327 \times \sqrt{(Ct_1 - x_1)/(2L + Ct_1)} + 0.0551 \times [(Ct_1 - x_1)/(2L + Ct_1)]^{3/2} + \ldots$$

$$(1/\epsilon)p^{(2)}(0, y > 0, t) = -0.519798 \sqrt{(Ct_1 - y)/(2L + Ct_1)} - 0.06257 [(Ct_1 - y)/(2L + Ct_1)]^{3/2} + \ldots$$

where

$$x_1 = x - 2L > 0 \quad \text{and} \quad t_1 - 2L/C > 0$$

The additional pressure disturbances around the 90° convex corners B and C can be obtained by superposition of the fundamental solutions in Section (3). The pressure distribution on the barrier at the instants $Ct/L = 0.5$, 1, 1.5, 2, 2.5, 3, 3.5, and 4 is shown in Fig. 3. After the instant $t = (2n + 1)L/C$, where n is a positive integer, additional disturbances are created due to the reflection from the ground. After the instant $t = 2nL/C$, the disturbances created previously are diffracted by the right corners at A and C and the response for each case can be obtained by the method presented in Section (2).

(5) Interference of a Prismatic Body of Rectangular Cross Section With a Planar Wing in Supersonic Flight

The problem of wing-body interference at supersonic speeds has been subjected to intensive investigation in recent years. A comprehensive study and survey was made by Lagerstrom and Van Dyke[22] by Lawrence and Flax[27] and recently by Ferrari.[28] Many results have been obtained for slender or conical wing-body configurations. For the flow field about a wing-body combination employing planar wings with supersonic edges and bodies deviating only slightly in shape from a right circular cylinder, theoretical methods are presented by Ferrari and Cramer,[28] by Nielsen,[29] and by Morikawa.[30] The direct correlation between the first two methods is shown in reference 28 and the similarity between the third and the second method is pointed out in reference 27. These methods are feasible for practical computations due to the availability of the tabulation of the "characteristic functions."[29, 31]

Besides the representation of fuselage by circular cylinders, another representation by prismatic bodies of rectangular cross sections was discussed by Lagerstrom and Van Dyke.[22] In this Section, the problem of the interference of a prismatic body of rectangular cross section with a planar wing (with supersonic or subsonic edges) is reduced to two basic problems—the diffractions of disturbances by the subsonic edges of the wing and by the right corners of the body. They are solved, respectively, by Evvard's method and the method presented in Section (2).

This solution of the wing-body problem can be applied to study (i) the effect of "slight contouring" of the prismatic body, that is, the favorable shape of the body which differs slightly from a basic prismatic body

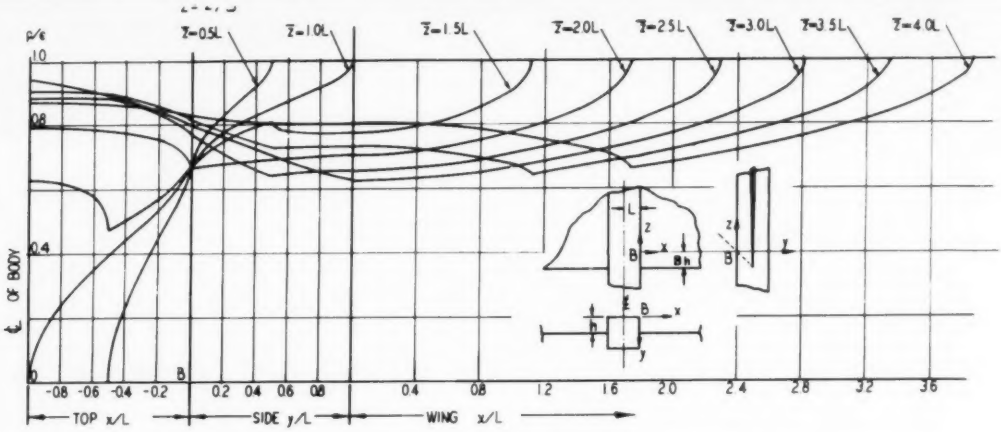

FIG. 4. Pressure distribution on body and wing [height/width = 1].

of rectangular cross section;[23] (ii) the favorable interference of wing-body configurations among the prismatic bodies of rectangular cross section with the same volume (or cross-section area) but different height-width ratio; and (iii) the resultant effects of "slight contouring," (i), and variation of height-width ratio, (ii).

On the other hand, the solution of the interference problem for circular cylindrical bodies[27–31] can be applied to study the effect of "slight contouring," (i), but not the corresponding nonlinear effects of (ii) and (iii).

(a) *Wing-Body Interference—Wings With Supersonic Edges*

For wings with supersonic edges a basic configuration is shown in Fig. 4. An infinitely long prismatic body of rectangular cross section is mounted on a wing represented by a semi-infinite wedge (or flat plate). The body is parallel to the free-stream direction and the upper surface of the wedge is inclined at a small angle δ. The origin is located at the point where the plane of the weak shock at the leading edge ($y = h$, $z = -Bh$) hits the 90° convex corner B.* The discontinuity in pressure across the weak shock is denoted by ϵ which is equal to $M^2\rho C^2\delta/B$. When the shock is passing over the 90° corner at B—i.e., $z > 0$—an additional disturbance $p^{(1)}(x, y, z)$ is created,

$$p^{(1)}(x, y, z) = \epsilon p_c(-y, x, z)$$

where $p_c(x, y, z)$ is the conical solution defined in Eq. (30) and Ct is replaced by z/B. For $z \geq hB$, $p^{(1)}$ is reflected from the surface of the wing ($y = L$). The additional disturbance due to reflection, which is

$$p^{(2)}(x, y, z) = p^{(1)}(x, -y + 2L, z) - \epsilon$$

passes over the right corner B for $z > 2Bh$. The continuation of $p^{(2)}$ into the region $z > 2Bh$ creates a discontinuity in pressure across the y-z plane—i.e.,

$$\begin{aligned}\Delta p(y < 0, z_1 > 0) &= p^{(2)}(0, y < 0, z_1) \\ &= -0.1734\,\epsilon[(z_1 + By)/(z_1 + 2Bh)]^{1/2} - 0.55\,\epsilon[(z_1 + By) \div (z_1 + 2Bh)]^{3/2} + \ldots\end{aligned}$$

where $z_1 = z - 2Bh$. The additional disturbances which balance the discontinuity are obtained by superposition of the second and the third fundamental solutions in Section (3). Similarly, the pressure disturbance $p^{(1)}$ is reflected from the plane of symmetry ($x = -L$) for $z > BL$. The reflected disturbance,

$$\bar{p}^{(1)}(x, y, z) = p^{(1)}(-x - 2L, y, z)$$

is again diffracted by the right corner B for $z > 2BL$ and the discontinuity in pressure across the x-z plane, which is

$$\begin{aligned}\Delta p(x, z_1) = \bar{p}^{(1)}(x > 0, 0, z_1) = {} & 0.519798\epsilon\sqrt{(z_1 - xB)/(2LB + z_1)} + \\ & 0.06257\epsilon[(z_1 - xB)/(2LB + z_1)]^{3/2} + \ldots\end{aligned}$$

for $z_1 = z - 2BL > 0$, is removed by the superposition of the fundamental solutions.

As in the problem of diffraction by a rectangular barrier, after the section of $x = (mL + nh)B$, where n and m are positive integers, additional disturbances will be produced due to the reflection of disturbances from the wing surface or the plane of symmetry or due to diffraction of disturbances by the right corner at B. The basic diffraction problem is treated in Section (3).

Figs. 4, 4(a), 4(b), and 4(c) show the pressure distribution at various sections on the surface of the body and the upper surface of the wing for width-height ratios equal to 1, 0.5, 2, and 1.5, respectively. The integrals of the pressure distribution fulfill the integral relationship,[23, 24] i.e.,

$$\int_{-L}^{0} p(x, 0, z)\,dx = \int_{0}^{\infty} [\epsilon - p(x, y = h, z + BL)]\,dx$$

Thus it serves as a check to the numerical results.

* It is sufficient to discuss only what happens on the right side of the plane of symmetry ($x = -L$).

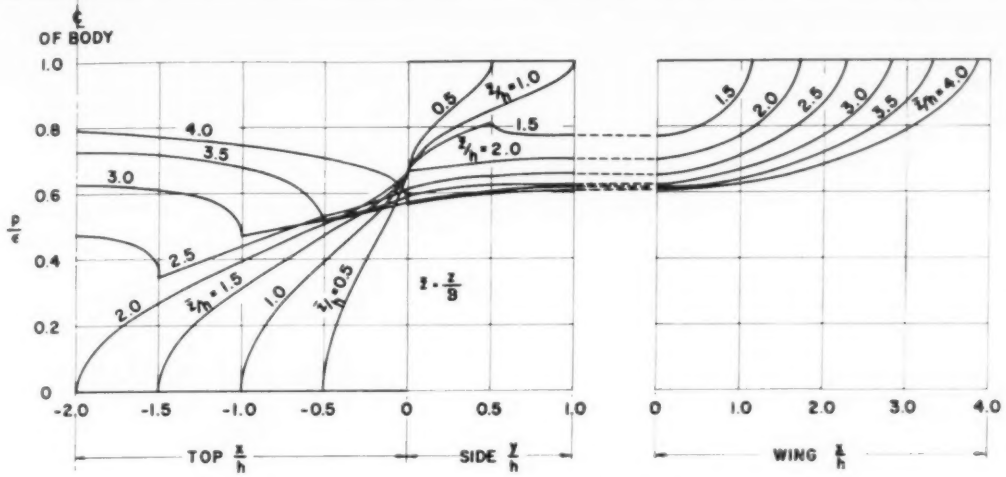

FIG. 4(a). Pressure distribution on body and wing [height/width = 0.5].

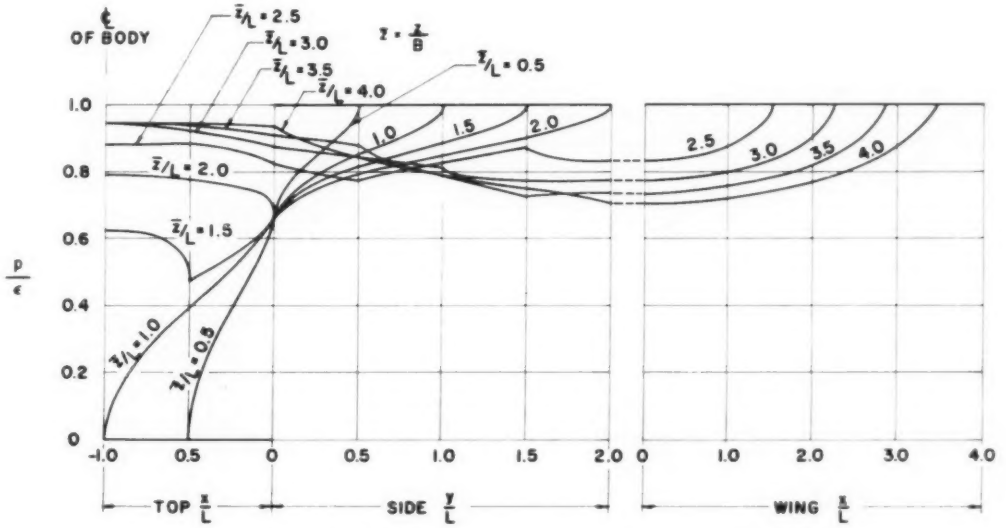

FIG. 4(b). Pressure distribution on body and wing [height/width = 2].

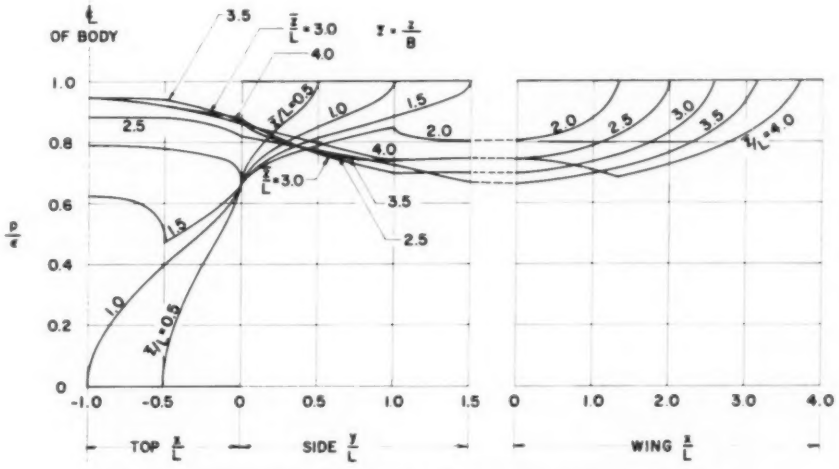

FIG. 4(c). Pressure distribution on body and wing [height/width = 1.5].

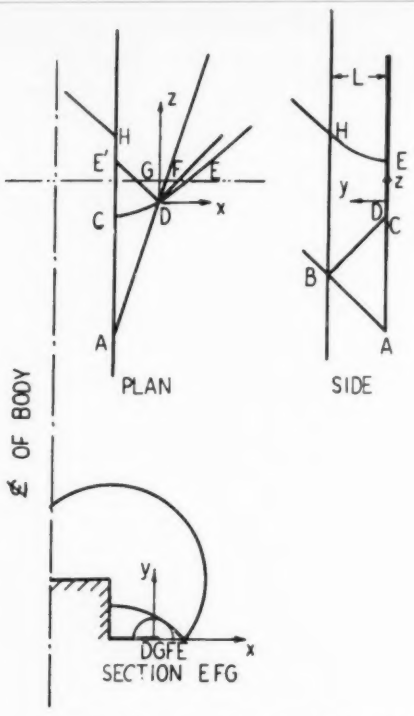

FIG. 5. Wing-body interference (subsonic leading edge).

(b) *Wing-Body Interference—Wings With Subsonic Edges*

For wings with subsonic edges, the pressure distributions can be obtained by repeatedly using Evvard's method[8, 9] and the method presented in Section (2) with or without modification. The required modification can be illustrated by an example as shown in Fig. 5. The disturbance that originates at point B on the 90° convex corner of the body is reflected from the wing surface and passes over the subsonic leading edge at point D, the origin of the x, y, z coordinates. The incoming disturbance $p_0(x, +y, z) + p_0(x, -y, z)$ creates the discontinuity in pressure, $2p_0(x, 0, z)$ in the x-z plane between the leading edge, ADG, and the hyperbola, CDE. The additional pressure disturbance can be split into two parts—namely,

$$p_1(x, y, z) = p_1^{(1)}(x, y, z) + p_1^{(2)}(x, y, z)$$

The discontinuity in the supersonic region—i.e., between the sonic line DF and the hyperbola—is removed by $p_1^{(1)}$, where

$$p_1^{(1)}(x, y > 0, z) = -p_1^{(1)}(x, y < 0, z) = \frac{1}{\pi}\iint \frac{h(\xi, \zeta),\, d\xi d\zeta}{\sqrt{(z-\zeta)^2 - [(x-\xi)^2 + y^2]B^2}}$$

$$h(x, z) = (\partial/\partial y)p_0(x, 0^+, z) \quad \text{for} \quad x > z/B$$

$$h(x, z) = 0 \quad \text{for} \quad x < z/B$$

The discontinuity in the subsonic region—that is, between the leading edge and the sonic line, is now $2p_0(x, 0^+, z) + 2p_1^{(1)}(x, 0^+, z)$. This discontinuity is removed by $p_1^{(2)}$, which can be obtained by Evvard's method.

Similar modification is necessary when a disturbance originates at the leading edge (point D) and passes over the 90° convex corner of the body (point H)

Conclusion

The problem of the diffraction of a two-dimensional disturbance or an arbitrary pulse by a convex right-angled corner is solved by a method which permits final numerical results to be obtained conveniently. The solutions obtained are applied to the analysis of the two-dimensional unsteady flow field associated with the diffraction of a weak shock by a rectangular barrier and to the analysis of the equivalent three-dimensional steady supersonic flow field produced by the interference of wings and prismatic bodies of rectangular cross section.

References

[1] Sommerfeld, A., *Mathematische Theorie Der Diffraction*, Mathematische Annalen, Vol. 47, p. 368, 1894.

[2] Baker, B. B., and Copson, E. T., *The Mathematical Theory of Huygens' Principle*, 2nd Ed., pp. 125–189; Oxford University Press, 1950.

[3] Busemann, A., *Infinitesimale Kegelige Überschallströmung*, Schr. Dtschen. Akad. Luftfahrtforschung, 7B, pp. 105–122, 1943 (Transl. NACA TM 1100).

[4] Stewart, H. J., *The Lift of a Delta Wing at Supersonic Speeds*, Quart. Appl. Math., Vol. 4, pp. 246–254, 1946.

[5] Snow, Robert M., *Aerodynamics of Thin Quadrilateral Wings at Supersonic Speeds*, Quart. Appl. Math., Vol. 5, pp. 417–428, January, 1948.

[6] Ward, G. N., *Linearized Theory of Steady High-Speed Flow*, pp. 135–161, 184–186; Cambridge University Press, 1955.

[7] Gunn, J. C., *Linearized Supersonic Aerofoil Theory*, Phil. Trans. Soc. A., No. 240, pp. 327–373, 1947.

[8] Evvard, J. C., *Distribution of Wave Drag and Lift in the Vicinity of Wing Tips at Supersonic Speeds*, NACA TN 1382, July, 1947.

[9] Evvard, J. C., and Turner, R. L., *Theoretical Lift Distribution and Upwash Velocity of Thin Wings at Supersonic Speeds*, NACA TN 1484, November, 1947.

[10] Keller, J. B., and Blank, A., *Diffraction and Reflection of Pulses by Wedges and Corners*, Communication on Pure and Applied Mathematics, Vol. 4, No. 1, June, 1951.

[11] Ting, L., *Diffraction and Reflection of Weak Shocks by Structures*, Journal of Mathematics and Physics, XXXII, 2–3, pp. 102–116, July–October, 1953.

[12] Miles, J. W., *Impulsive Motion of a Flat Plate*, Quart. J. Mech. and Appl. Math., Vol. VI, Part 2, pp. 129–140, 1953.

[13] Fox, E. N., *The Diffraction of Sound Pulses by Infinitely Long Strip*, Phil. Trans. Soc. (A), Vol. 241, No. 828, pp. 71–103, June, 1948.

[14] Kay, I., *The Diffraction of an Arbitrary Pulse by Wedges and Corners*, Communication on Pure and Applied Mathematics, Vol. 6, p. 419, 1953.

[15] Turner, Robert D., *The Diffraction of a Cylindrical Pulse by a Half-plane*, Quart. Appl. Math., Vol. XIV, No. 1, pp. 63–73, 1956.

[16] Keller, J. B., *Diffraction of a Shock or An Electromagnetic Pulse by a Right-Angled Wedge*, J. Appl. Phys., Vol. 23, No. 11, pp. 1267–1268, November, 1952.

[17] Howard, L. N., and Matthews, D. C., *On the Vortices Produced in Shock Diffraction*, J. Appl. Phys., Vol. 27, No. 3, pp. 223–231, March, 1956.

(*Continued on page 844*)

Transonic Flow With a Detached Bow Wave Past a Wedge Between Two Parallel Plane Walls

SHIGEKI MORIOKA*

Yoshida College, University of Kyoto

SUMMARY

In the present paper the two-dimensional transonic flow with a detached bow wave past a doubly symmetrical double-wedge section placed midway between two parallel walls is investigated. The subsonic flow field over the front half of the profile is determined by applying the relaxation technique to the transonic perturbation equation in the hodograph plane. The method of characteristics is adopted for the supersonic flow over the rear half. Detailed computation has been carried out for three values of the ratio of the chord length to the tunnel width, assuming the value of the transonic parameter to be 0.921 in every case.

Of the results, the following may be noted. When the tunnel width is gradually decreased, the bow wave moves forward and the pressure coefficients over the profile increase uniformly. However, a definite limit for the reduction of the tunnel width to maintain steady flow of a given (supersonic) Mach Number seems to exist. It is not clear what happens exceeding this limit. The distance between the bow wave and the profile is comparatively small even in this limiting stage.

SYMBOLS

a_* = critical velocity
c = airfoil chord
C_p = pressure coefficient
$\tilde{C}_p$ = reduced pressure coefficient $(\gamma + 1)^{1/3} \times (t/c)^{-(2/3)} C_p$
e, f, g, h, k = length of irregular lattice intervals relative to that of basic interval
H = width of tunnel
I_w = integral defined by Eq. (23)
J_i = $(i = 1, 2, 3)$ component integral [see Eq. (20)]
K, L = functions of e, f, g, h, and $\tilde{\eta}_0$ [see Eqs. (15) and (16)]
k = numerical constant [see Eq. (9)]
M = Mach Number
M_0 = Mach Number of uniform flow in front of bow wave
p = pressure at exit of tunnel
$S(\tilde{\eta}_0)$ = function defined by Eq. (17)
t = airfoil thickness
V = local speed of flow
x, y = Cartesian coordinates in physical plane
α = absolute value of $\tilde{\eta}$ at return point of shock polar
β = absolute value of $\tilde{\eta}$ at left-hand limit of lattice
γ = ratio of specific heats (1.4 for air)
Δ = basic lattice interval
η = hodograph variable defined by Eq. (2)
η_0 = value of η corresponding to uniform flow velocity in front of bow wave
$\tilde{\eta}$ = reduced hodograph variable defined by Eq. (1)
θ = local inclination of flow relative to x-axis
$\tilde{\theta}$ = reduced hodograph variable defined by Eq. (1)
$\tilde{\theta}'$ = variable of integration [see Eq. (8)]
θ_w = half-angle of wedge
$\tilde{\theta}_w$ = value of θ_w corresponding to wedge half-angle
ξ = speed function $(M^2 - 1)/[(\gamma + 1)(t/c)]^{2/3}$
ξ_0 = transonic similarity parameter $(M_0^2 - 1) \div [(\gamma - 1)(t/c)]^{2/3}$
ρ_* = fluid density at critical speed
ψ = stream function
ψ_w = value of ψ on tunnel wall

Subscript

0, 1, 2, etc. = value at a prescribed lattice point

Received February 1, 1957.

* Department of Physics.

INTRODUCTION

A THEORETICAL INVESTIGATION of the aerodynamic characteristics has been performed by W. G. Vincenti and C. B. Wagoner[1] at zero angle of attack of a thin, doubly symmetrical double-wedge profile in the range of supersonic flight speed in which the bow wave is detached. They have determined the subsonic flow field between the bow wave and the profile by applying the relaxation technique to a boundary value problem for the transonic small disturbance equation in the hodograph plane. On the other hand, they have used the method of characteristics in calculating the purely supersonic flow over the rear half of the wedge profile.

The flow field as considered by Vincenti and Wagoner can be realized in a closed wind tunnel, the width of which is sufficiently large compared with the model size. The reflected shocks from the tunnel walls, in this case, do not affect the flow over the model profile. Now we consider what happens when the width of the wind tunnel is gradually decreased. As far as the shock angle at the wall of the bow wave lies within the range 1 of Fig. 1, the bow wave will be reflected regularly from the wall. When the tunnel is more narrowed and the shock angle enters the region II, the reflection will become of Mach's type. Further, if the stage is reached in which the reflection occurs at a subsonic shock angle, the bow wave becomes normal at the wall and the reflected wave will disappear. It is this stage to be considered in the present paper.

The flow field under consideration is in general governed by four parameters:[2] (1) Mach Number M_0 of the uniform flow in front of the bow wave, (2) the pressure p at the exit of the tunnel, (3) wedge angle $2\theta_w$, and (4) ratio c/H of the model length to the tunnel width. The parameter (2) has little influence upon

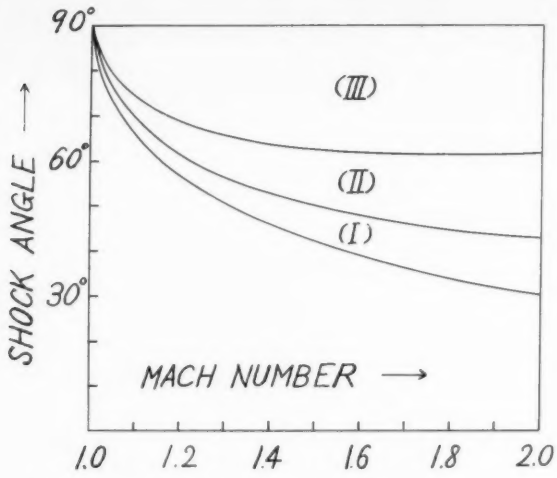

FIG. 1. Transition of reflection type of bow wave on wall.

the flow upstream of the exit by taking p to be a supersonic pressure. The parameter (4) represents the so-called tunnel effect and it is closely related, as is seen later, to the location of the return point of the shock polar in the hodograph plane (the return point is the image of the inflection point of the shock wave in the physical plane). As the return point moves to the point of normal shock condition, the width of the tunnel decreases to a minimum and then increases until the (subsonic) choked condition is reached when the two points coincide with each other.

The return point is a singularity in the hodograph transformation. The transformation Jacobian actually becomes zero at this point. However, it has been shown[3] that this singularity is isolated provided it lies in subsonic region some distance apart from the sonic line. (The necessary distance is smaller as the shock is weaker). Therefore the correspondence between the physical and the hodograph plane is one to one. Thus, the flow field in question forms a regular boundary value problem for the Tricomi equation in the hodograph plane. However, it seems difficult to treat the problem analytically because of the complicated boundary conditions. In the present paper, a numerical method similar to that used in reference 1 is adopted—the flow over the front half of the wedge is determined by the relaxation method, while the flow over the rear half is calculated by the method of characteristics. Actual computation has been carried out for three cases of the flow, each for different value of the ratio c/H. The transonic parameter for each case is assumed to have a value 0.921. (This value is adopted for the sake of comparison of the results with those for free flight condition due to Vincenti and Wagoner).

Boundary Value Problem

We now consider the two-dimensional transonic flow with a detached bow wave past a thin double-wedge profile placed midway between two parallel plane walls (Fig. 2). (In the following description only the flow in the upper half-plane will be described, since the flow is symmetrical about the chord line.) The hodograph representation of the flow field is shown in Fig. 3. Fig. 4 shows the reduced hodograph plane in the transonic approximation. In these Figures it may be noted that the shock polar returns back at some point B (return point) in the subsonic region. The characteristic DF corresponds to the so-called limiting Mach wave.

Using the reduced hodograph variables

$$\tilde{\eta} = \eta/\eta_0, \quad \tilde{\theta} = 2^{1/2}(\theta/\eta_0^{3/2}) \tag{1}$$

with

$$\eta = (\gamma + 1)^{1/3}\,[(V - a_*)/a_*] \tag{2}$$

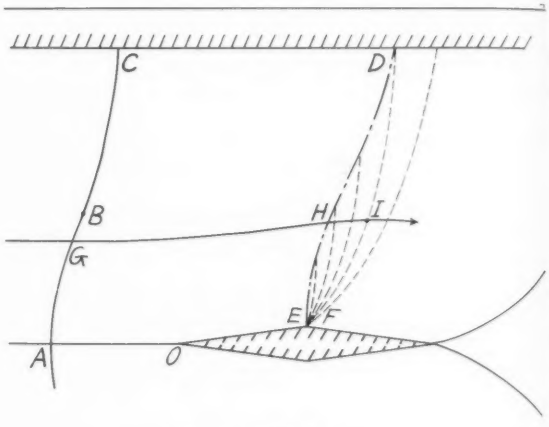

FIG. 2. Physical plane.

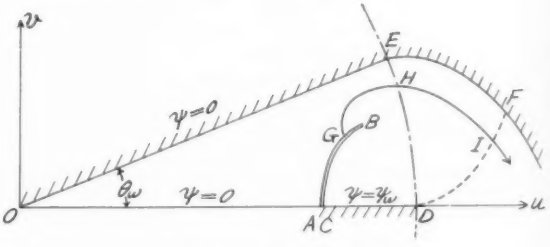

FIG. 3. Hodograph plane.

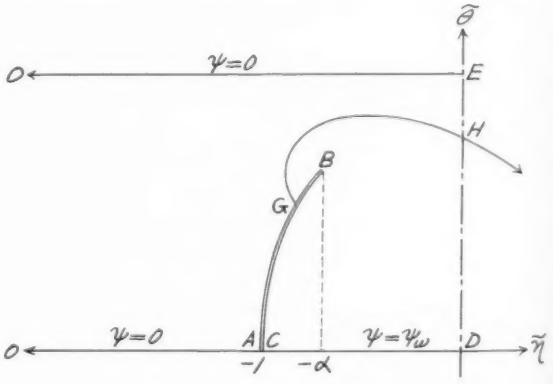

FIG. 4. Reduced hodograph plane.

the boundary value problem in the $\tilde{\eta}\tilde{\theta}$-plane can be summarized as follows.

Differential Equation

$$\psi_{\tilde{\eta}\tilde{\eta}} - 2\tilde{\eta}\psi_{\tilde{\theta}\tilde{\theta}} = 0 \tag{3}$$

Boundary Conditions

On the basic streamline AOE,

$$\psi = 0 \quad \text{for} \quad \tilde{\eta} \leqq -1, \quad \tilde{\theta} = 0 \tag{4}$$

$$\psi = 0 \quad \text{for} \quad \tilde{\eta} \leqq 0, \quad \tilde{\theta} = \tilde{\theta}_w \tag{5}$$

$$\psi \to 0 \quad \text{for} \quad \eta \to -\infty, \quad 0 \leqq \tilde{\theta} \leqq \tilde{\theta}_w \tag{6}$$

On the shock polar ABC,

$$\psi_{\tilde{\eta}} - [(1 + 7\tilde{\eta})/(3 + 5\eta)]\sqrt{1 + \tilde{\eta}}\,\psi_{\tilde{\theta}} = 0 \tag{7}$$

for $\quad -1 \leqq \tilde{\eta} \leqq -\alpha, \quad \tilde{\theta} = (1 - \tilde{\eta})\sqrt{1 + \tilde{\eta}}$

On the sonic line DE,

$$\psi_{\tilde{\eta}}(0, \tilde{\theta}) + k \int_{\tilde{\theta}_w}^{\tilde{\theta}} [\psi_{\tilde{\theta}}(0, \tilde{\theta}')/(\tilde{\theta}' - \tilde{\theta})^{2/3}]d\tilde{\theta}' = 0 \tag{8}$$

for $\quad \tilde{\eta} = 0, \quad 0 \leqq \tilde{\theta} \leqq \tilde{\theta}_w$

where

$$k = 2^{4/3} \cdot \pi/3^{1/3}\Gamma^3(1/3) = 0.341 \tag{9}$$

On the solid wall CD,

$$\psi = \psi_w \quad \text{for} \quad -1 \leqq \tilde{\eta} \leqq 0, \quad \tilde{\theta} = 0 \tag{10}$$

Reduction to the Finite-Difference Equation

The formulation of the finite-difference equation can be accomplished by grouping conveniently the lattice points into six categories similar to reference 1. The arrangement of the relative lattice points and the difference equation to each point in the present problem are as follows.†

(1) *Regular Internal Points*

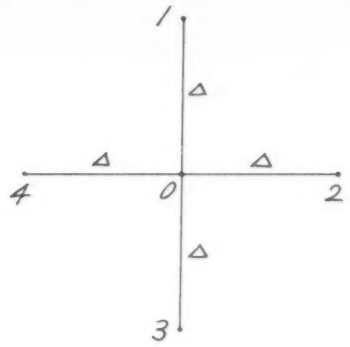

FIG. 5.

$$\psi_2 + \psi_4 - 2\tilde{\eta}_0(\psi_1 + \psi_3) - 2(1 - 2\tilde{\eta}_0)\psi_0 = 0 \tag{11}$$

(2) *Points Far to the Left*

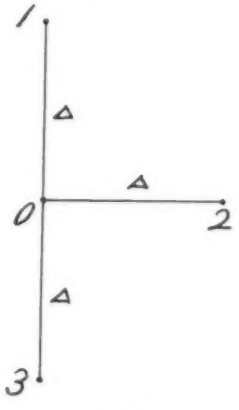

FIG. 6.

$$\psi_2 + 2\beta(\psi_1 + \psi_3) + \tfrac{1}{4}[1 - (\Delta/4\beta)] \times \exp[-(\pi\Delta/\tilde{\theta}_w)\sqrt{2\beta}] - 2(1 + 2\beta)\}\psi_0 = 0 \tag{12}$$

(3) *Points Adjacent to the Shock Polar*

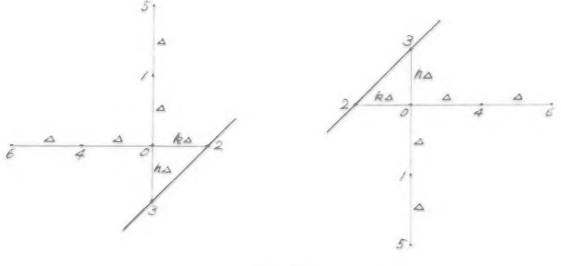

FIG. 7.

$$\frac{6}{k(1+k)(2+k)}\psi_2 + \frac{2(2-k)}{1+K}\psi_4 - \frac{1-k}{2+k}\psi_6 - 2\tilde{\eta}_0\left[\frac{6}{h(1+h)(2+h)}\psi_3 + \frac{2(2-h)}{1+h}\psi_1 - \frac{1-h}{2+h}\psi_5\right] - \left[\frac{3-k}{K} - 2\tilde{\eta}_0\frac{3-h}{n}\right]\psi_0 = 0 \tag{13}$$

† For the details of derivation of the difference equations see reference 1.

(4) *Points on the Shock Polar*

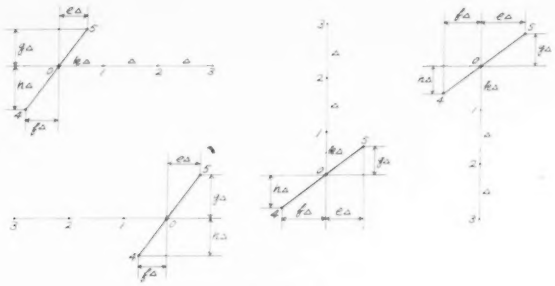

FIG. 8.

$$\frac{(1+k)(2+k) \pm 2(3+2k)L}{2k}\psi_1 - \frac{k(2+k) \pm 4(1+k)L}{1+k}\psi_2 + \frac{k(1+k) \pm 2(1+2k)L}{2(2+k)}\psi_2 \pm egK\psi_4 \mp$$

$$fhK\psi_5 - \left[\frac{2+6k+3k^2}{k(1+k)(2+k)} \pm \frac{6L}{k(2+k)} \pm (eg-fh)K\right]\psi_0 = 0 \quad (14)$$

$$K = \left\{[gh(e+f)/S(\tilde{\eta}_0)] + ef(g+h)\right\}^{-1}, \quad L = (eh-fg)\,[(gh/4\tilde{\eta}_0) - (ef/2)]K \quad (15)$$

$$K = [gh(e+f) + ef(g+h)S(\tilde{\eta}_0)]^{-1}, \quad L = (eh-fg)\,[(gh/2) - ef\tilde{\eta}_0]K \quad (16)$$

$$S(\tilde{\eta}_0) = [(1+7\tilde{\eta}_0)/(3+5\tilde{\eta}_0)]\sqrt{1+\tilde{\eta}_0} \quad (17)$$

Where upper and lower signs in Eq. (14) correspond to the developments to the positive and negative directions of the axes respectively. Also K and L in Eqs. (15) and (16) correspond respectively to horizontal and vertical developments.

(5) *Point on the Sonic Line*

The difference equation for these points may be obtained by putting the following expression into Eq. (7):

$$\psi_{\tilde{\eta}}(0,\tilde{\theta}) = (1/\Delta)\,[(7/6)\psi_0 - (4/3)\psi_i + (1/6)\psi_{ii}] \quad (18)$$

together with the relations

$$\int_{\tilde{\theta}_w}^{\tilde{\theta}} \frac{\psi_{\tilde{\theta}}(0,\tilde{\theta}')}{(\tilde{\theta}'-\tilde{\theta})^{2/3}}\,d\tilde{\theta}' = 3.533\,(\psi_0/\Delta^{2/3}) \quad (19)$$

for the first point below the upper boundary, and

$$= J_1 + J_2 + J_3 \quad (20)$$

$$J_1 = [1/(n\Delta)^{2/3}] \sum_{m=0} [4/(4+3m)]\,[(2/3)m/m!\,n^m]\,\psi_{n-1},$$
$$(2/3)_0 = 1, \quad (2/3)_m = (2/3)\,(5/3)\ldots[(3m-1)/3]$$

$$J_2 = (3/\Delta^{2/3}) \sum_{m=1}^{n-2} [(m+1)^{1/3} - m^{1/3}]\,(\psi_m - \psi_{m+1})$$

$$J_3 = (1/\Delta^{2/3})\,[(2/7)\psi_2 - (87/28)\psi_1 + (33/14)\psi_0 + (13/28)\psi_{-1}]$$

for general point below the first lattice point. (See Fig. 9.)

(6) *Return-Point of the Shock Polar*

Accounting for the symmetry of the shape of shock wave in the vicinity of its inflection point in the physical plane, the value of ψ at the return point may be taken as the average of ψ at two neighboring points which are facing each other on both sides of the shock polar.

SOLUTION IN HODOGRAPH PLANE

As is described in the preceding section, a finite-difference equation can be set up for each lattice point in the hodograph plane. Thus, our boundary value problem is replaced by a large number of simultaneous algebraic equations involving an equal number of unknown values of ψ. Since the number of unknowns in each equation is small, they can be solved conveniently by the relaxation technique. The mechanics of the relaxation process have been well described by various authors[4] and need not be gone into here.

Actual calculation has been carried out for three cases, each having different position of the return point—i.e., for three values of the ratio c/H of the model length to the tunnel width in the physical plane. The value of the transonic parameter is assumed to be a fixed value 0.921 for all cases. (This value is selected out of those treated in reference 1). Figs. 5 to 7 show calculated patterns of the streamlines in the reduced

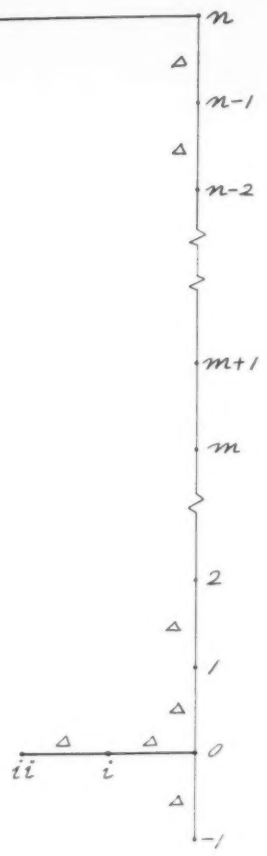

FIG. 9.

hodograph plane, together with the distribution of the lattice points used in the relaxation calculation. (See Figs. 10–12.)

TRANSFORMATION TO PHYSICAL PLANE

The relation between the physical x,y-plane and the reduced hodograph $\tilde{\eta}\tilde{\theta}$-plane is given by the following pair of equations (see reference 1):

$$d(x/c) = (1/4I_w)\,(2\tilde{\eta}\psi_{\tilde{\theta}}\,d\tilde{\eta} + \psi_{\tilde{\eta}}\,d\tilde{\theta}) \tag{21}$$

$$d(y/c) = (1/4I_w)\,[2\tilde{\theta}_w/(\gamma+1)\,(t/c)]^{1/3}\,d\psi \tag{22}$$

with

$$I_w = \rho_* a_* c/2^{3/2}(\gamma+1)^{1/3}\eta_0^{1/2} = \int_{-\infty}^{0} \tilde{\eta}\psi_{\tilde{\theta}}\,(\tilde{\eta},\,\tilde{\theta}_w)d\tilde{\eta} \tag{23}$$

By integrating these equations numerically from $-\infty$ to the point considered, we can find the corresponding physical coordinates.

Fig. 13 shows the calculated shapes of the bow wave and the sonic line relative to the wedge profile and the tunnel wall for three cases of flow for specific values of the Mach Number 1.164, $\gamma = 1.4$ and the thickness ratio $t/c = 0.1$. In this Figure are also shown Vincenti-Wagoner's and Marschner's results[5] for compari-

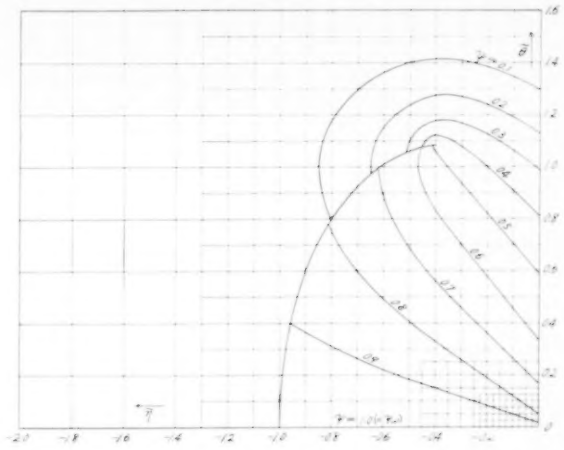

FIG. 10. Distribution of lattice points and streamlines pattern in $\tilde{\eta}\tilde{\theta}$ = plane. Case I.

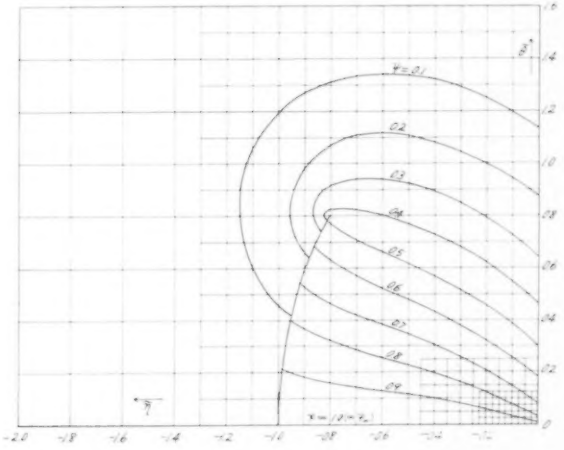

FIG. 11. Distribution of lattice points and streamlines pattern in $\tilde{\eta}\tilde{\theta}$ = plane. Case II.

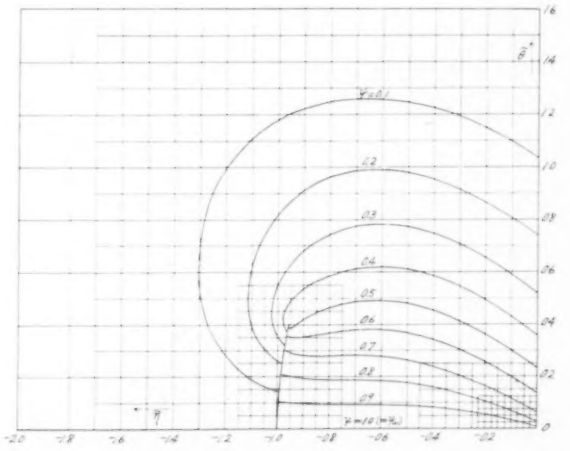

FIG. 12. Distribution of lattice points and streamlines pattern in $\tilde{\eta}\tilde{\theta}$ = plane. Case III.

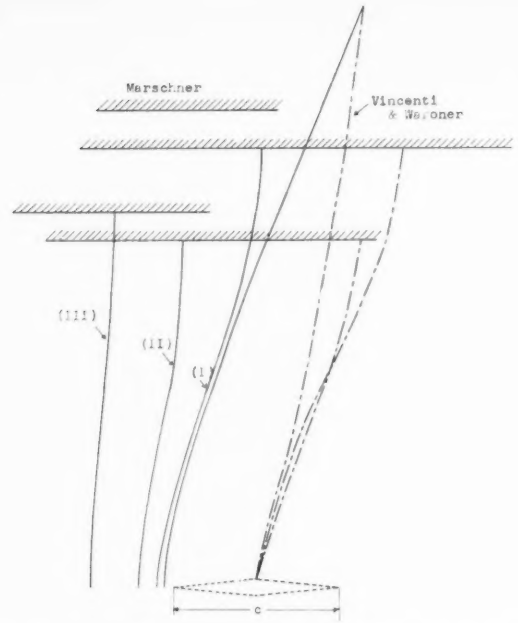

FIG. 13. Shapes of bow wave and sonic line relative to wedge profile and tunnel wall.

son. The Vincenti-Wagoner case is that of the free flight condition and Marschner's is the (subsonic) choked state which may be regarded as the limiting case with the bow wave at infinity upstream.

The speed function ξ in the subsonic region can be found directly from the following relation:

$$\xi = (M^2 - 1)/[(\gamma + 1)\,(t/c)]^{2/3} = \xi_0\tilde{\eta} = (2^{1/3}/\tilde{\theta}_w^{2/3})\tilde{\eta} \quad (24)$$

The speed function in the supersonic region can be obtained, after determining the subsonic region, by the method of characteristics (specialized to the transonic small disturbance theory). Then, the pressure coefficient C_p can easily be calculated by the relation

$$C_p = -2(\gamma + 1)^{-(1/3)}\,(t/c)^{2/3}\,(\xi - \xi_0) \quad (25)$$

Fig. 14 represents the distribution of the reduced pressure coefficient

$$\tilde{C}_p = (\gamma + 1)^{1/3}\,(t/c)^{-(2/3)}C_p$$

along the front and the rear surfaces of the wedge profile. Here the corresponding results for free flight and choked conditions are also shown for the sake of comparison. The total pressure drag can of course be found by integrating over the wedge surface the pressure coefficient just given.

Discussion of Results

From the results obtained in the preceding section, we can understand the wall influence upon a transonic flight condition with a detached bow wave. Figs. 13 and 14 show that the bow wave moves forward and the pressure coefficients over the model surface increase uniformly as the wall approaches the model. However, it is to be noted that there is a definite limit for the approach of the wall (unexpected result to the writer). In this limiting stage, the mean mass flow at the narrowest passage attains its maximum which is clearly larger than that for the (subsonic) choked condition (Marschner's case). Thus, the flow comes to a kind of choked condition (Supersonic choked condition, say). It is not clear what happens beyond this limit. It is probable that the steady flow of the type considered above no longer exists, and the bow wave may suddenly run out of the tunnel entrance. (A similar phenomenon is familiar in a supersonic diffuser.) It may be noticed here that, as is seen from Fig. 13, there are two possible solutions for a range of wall positions between the lower limit of approach and Marschner's choked condition. One solution belongs to the branch just traced above and the other to the branch that bridges over the lower limit and Marschner's case. It is clear, however, that the latter branch may have a chance to be pursued by the continuous transition from the free flight condition only when the wall is moved back from its lowest position. Moreover, this solution is likely to be unstable—as is seen from Fig. 13, a larger distance of the bow wave requires a wider tunnel. Now assume that in the presumably unstable region one of the flow patterns belonging to the second branch has been established and that the distance of the walls is then reduced by a small amount. This will reduce the mass flow through the narrowest cross section and will cause an accumulation of air in front of the body. Consequently the bow wave will be pushed upstream. But then a flow field would arise which requires a wider cross section of the tunnel—i.e., the shock will be unable to find a stable position. As regards the occurrence of two solutions for one given boundary condition, one may remember the well known behavior of the attached shock to an infinite wedge when the wedge angle is increased monotonically. In this case, of two

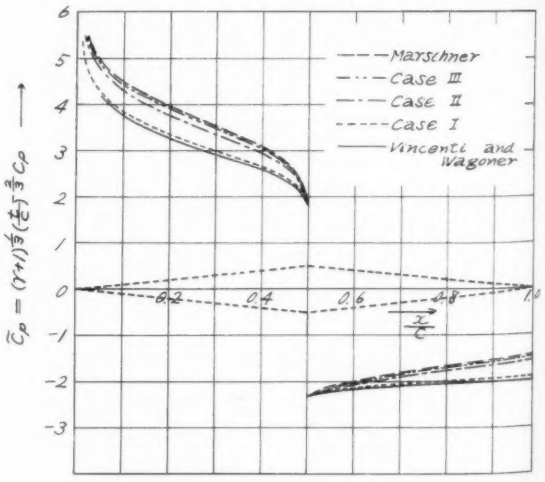

FIG. 14. Chordwise distribution of reduced pressure coefficient.

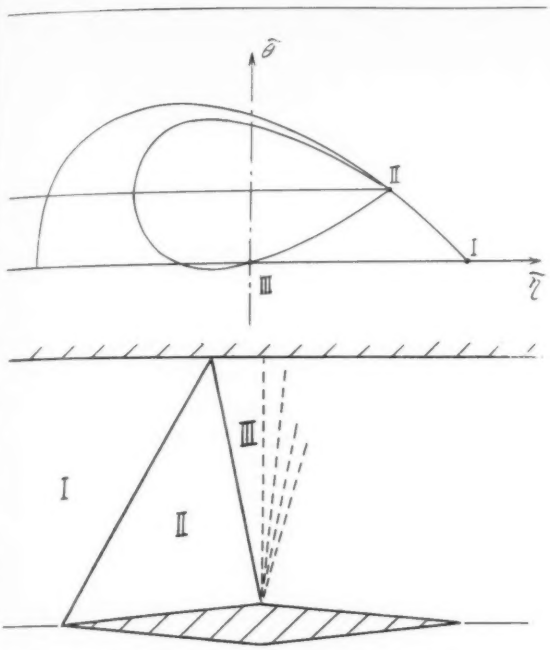

FIG. 15. *Top*, hodograph plane. *Bottom*, physical plane.

possible branches of the solution, the one that is related to the weaker shock is pursued under the usual conditions up to the so-called detachment angle. Thus, it seems natural to the writer that in the present case also the first branch mentioned above will be followed up to (or at least to the proximity of) its limiting point (lowest wall position) if the tunnel wall approaches the model monotonically. Better understanding of the occurrence of the two solutions and of the supersonic choked condition may be obtained by the consideration of the following example. Assume that the nose angle of the wedge is such that in a purely supersonic flow with an attached shock the velocity after the shock reflected from the wall is exactly sonic. Furthermore let the wedge side have such a length that the reflected shock hits exactly at the shoulder (Fig. 15). This flow pattern has certainly a maximum of the mass flow in the narrowest cross section between the model and the wall—i.e., for this flow pattern the distance of the walls has its absolute minimum.

For a greater distance of the walls there may exist two solutions—a supersonic one and the solution with a detached shock. (The latter may involve attached "lambda" shocks for wall distances slightly larger than the absolute minimum.) The two branches correspond clearly to the first and second branches considered above. The flow pattern in Fig. 15 also corresponds to the supersonic choked condition mentioned before. Further, this example shows clearly that the supersonic choked condition can carry a greater mass flow than the subsonic choked condition.

Fig. 14 shows that the pressure distribution over the profile has in general close resemblance to that for the free flight condition with the same value of the transonic parameter. It increases considerably, however, as the lowest wall position is approached and then tends to the distribution for the subsonic choked condition. It may be interesting to note that the distance between the bow wave and the profile also increases on approaching the limit, but the increment remains comparatively small.

Finally, it may be remarked that, although in the present paper only the case where the width of the tunnel is varied for a fixed Mach Number is considered still, it is possible to make a qualitatively similar argument for the case in which the Mach Number of the flow is varied in a given wind tunnel.

This problem has been suggested to the writer by Prof. Z. Hasimoto, to whom the writer wishes to express his hearty thanks. The writer's thanks are also due to Prof. K. Tamada for his advice and kind inspection of the manuscript, and to Prof. M. Tada for his valuable discussions.

REFERENCES

[1] Vincenti, W. G., and Wagoner, C. B., *Transonic Flow Past a Wedge Profile With Detached Bow Wave*, NACA TR 1095, 1952.

[2] Guderley, G., *Considerations of the Structure of Mixed Subsonic-Supersonic Flow Patterns*, AMC Wright Field Technical Report No. F-TR-2168ND, October, 1947.

[3] Hasimoto, Z., and Morioka, S., *On the Flow Just Behind Two-Dimensional Shock with a Singularity in Hodograph Transformation*, (unpublished).

[4] Fox, L., *A Short Account of Relaxation Methods*, Quarterly Journal of Mechanics and Applied Mathematics, Vol. 1, Part 3, pp. 253–280, September, 1948.

[5] Marschner, B. W., *The Flow Over a Body in a Choked Wind Tunnel and in a Sonic Free Jet*, Journal of the Aeronautical Sciences, Vol. 23, No. 4, pp. 368–376, April, 1956.

Experiments on Interaction Between a Traveling Shock Wave and a Turbulent Jet†

DARSHAN S. DOSANJH*

The Johns Hopkins University

SUMMARY

The interaction of a turbulent jet and a plane shock wave traveling in a shock tube was optically observed. Various arrangements of both subsonic and supersonic jets were used. Some typical shadowgraphs are reproduced and discussed.

As a direct result of its passage through the jet, the shock wave developed a bulge. The growth and behavior of this bulge were recorded through a sequence of instantaneous shadowgraphs. The transverse spread and the changing profile of this bulge offer an interesting visual demonstration of the angle of spread and decay of the jet flow. It is shown that beyond an equivalent distance of about twelve jet diameters the bulge-profile reaches a state of similarity.

When the shock and the jet impinged against each other head on, an intense, intermittent, and high frequency acoustic radiation manifested itself in the flow field behind the shock front. Some plausible explanations of this phenomenon are advanced.

INTRODUCTION

THE RISING INTEREST in the development of faster jet-propelled aircraft has accelerated the tempo of jet-flow research. In this challenging research field, the contributions of Tollmien,[1] Kuethe,[2] Corrsin,[3, 4] Pai,[5, 6] Wilder,[7] and Anderson[8] have some direct or indirect bearing on the experiments described here. In recent years the problem of the intense noise generated by modern jet-propelled aircraft, especially the uncomfortably high intensity at take-off and landing, has attracted considerable attention. Generally speaking, the noise originates either due to the structural vibrations and/or flow fluctuations. Therefore a better understanding of the basic mechanism of noise generation processes in jet flow is essential for the successful planning of any extensive scientific program of noise abatement. During the past few years some valuable light has been shed on the subject by Powell[9, 10, 11] Lighthill,[12, 13] Ribner,[14] and Kovasznay.[15] It has been observed that the mean jet flow velocity, jet diameter, turbulence level, and interaction between any existing shock front and turbulent jet flow all contribute to the intensity and other characteristics of aerodynamic noise.[12]

It is well known that a free jet becomes turbulent only a short distance downstream of its exit.[6] To investigate the interaction of a shock front traveling in a turbulent jet flow, jets were mounted either close to the open end or inside a shock tube and the transient passage of the shock front through the turbulent flow field was optically recorded.‡ A brief description of the main units of the experimental equipment follows.

THE SHOCK TUBE

In these experiments the shock tube was used primarily as a convenient source of plane normal shock waves of known strength. The shock tube consisted of a steel box of uniform cross section (approximately 6 by 4 in. inside). To achieve the optimum sensitivity to any disturbances in the flow under investigation, the 6-in. side of the shock tube was laid horizontal. The experimental observations were made in the 12-in. glass section, with top to bottom visibility, mounted at 15 ft., downstream of the diaphragm location (see Fig. 1). For any detailed information about the basic shock-tube theory, the bibliographies in references 16 to 18 are suggested.

SHOCK SPEED MEASUREMENTS

The time taken by the shock wave to travel between the two timing hotwires, mounted a known distance apart in the upper wall of the shock tube (see Fig. 1), was clocked (for details, see reference 19). The shock speed U_s was calculated, and from well-known relations, the shock strength

$$S = \frac{\text{pressure behind the shock wave}}{\text{pressure ahead of the shock wave}}$$

and other pertinent flow parameters such as drift flow velocity u_2 and the corresponding density ρ_2, temperature T_2, and pressure p_2 behind the shock front were calculated.

The hot-wire response pulse originating at the downstream station was simultaneously used to stop the chronograph as well as to actuate the delay system. To decouple the two input loads, a cathode follower was found helpful (see Fig. 2).

ARRANGEMENT FOR TAKING SHADOWGRAPHS

The arrangement used for taking shadowgraphs with the short duration high intensity "point" source of

Received July 9, 1956.

† This work was conducted during 1952 under the combined sponsorship of the Bureau of Ordnance and U.S. Air Force under Contract Nord 8036JBH-3F. The help and contribution of Mr. Jaime de los Cesares for collecting part of the experimental data are gratefully acknowledged. The author appreciates the helpful suggestions of Drs. Francis H. Clauser and Stanley Corrsin.

* Formerly, Graduate Student, Department of Aeronautics. Now, Associate Professor, Department of Mechanical Engineering, Syracuse University, Syracuse, N.Y.

‡ A few hot-wire oscillograms of this interaction were also recorded but are not discussed here.

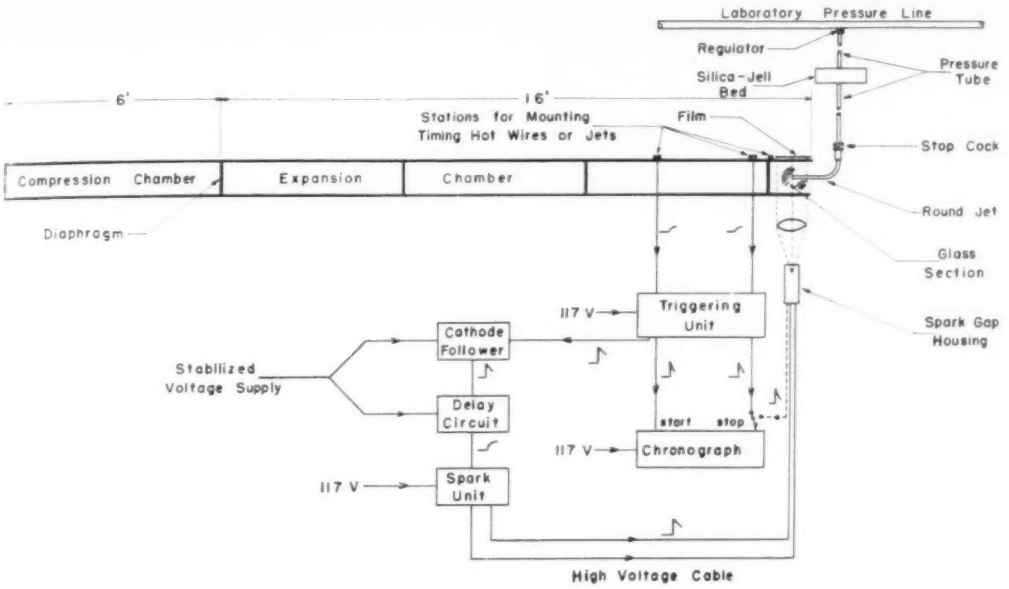

FIG. 1. Block diagram of the experimental arrangement.

light is shown in Fig. 1. For details about the spark unit see reference 20. For recording the instantaneous shadowgraphs of the advancing shock front and/or the flow field behind it, the spark has to be properly synchronized. The passage of the shock front over the triggering hot wire produces a sizeable response signal. The tripping of the spark gap, as a result of this signal, is delayed by a pre-estimated time through a simple R-C delay circuit introduced between the output of the triggering unit and the spark unit (see Fig. 1).

THE JET ARRANGEMENTS

Arrangement A

Different types of jets (round as well as two-dimensional), operating at subsonic or supersonic exit velocities, were mounted just outside the open end of the shock tube and a systematic set of shadowgraphs recording the passage of the shock fronts through the turbulent jet flow was taken. A general distortion of the traveling shock front always occurred. However, for the shock strengths and the jet velocities used in these experiments, no auxiliary sound emission was observed (see Fig. 2).

Arrangement B

In Arrangement A, the rarefaction wave originating at the open end of the shock tube progressively weakens the shock wave (see Fig. 2). To get around this limitation, an axisymmetric jet (circular brass tube with inside diameter = 3/16 in., horizontal stem 8 in., bent at gentle right angle) was centrally mounted inside the shock tube (Fig. 3). The jet flow and the advancing shock front were both directed toward the open end of the shock tube. The air was supplied from the laboratory pressure line (100 lbs. per sq.in.), and to reduce its water-vapor content, it was made to pass through a heavy steel chamber packed with silica jell. The exit velocity was controlled by a regulator near the pressure line and/or by a stopcock close to the shock tube (Fig. 1).

The maximum mean velocity U_m of the jet flow was measured with the total head tube and/or with the hot-wire technique at various stations downstream from the exit of the jet. It is known that the maximum velocity U_m on the axis of the jet decreases approximately fol-

FIG. 2. Jet mounted outside the open end of shock tube (arrangement A). Two-dimensional jet (exit 1/8 in. by 6 in.), exit velocity U_e = 200 ft./sec., shock strength S = 2.5, delay = 84 microsec. (open end corresponds to zero delay), spark light uncollimated.

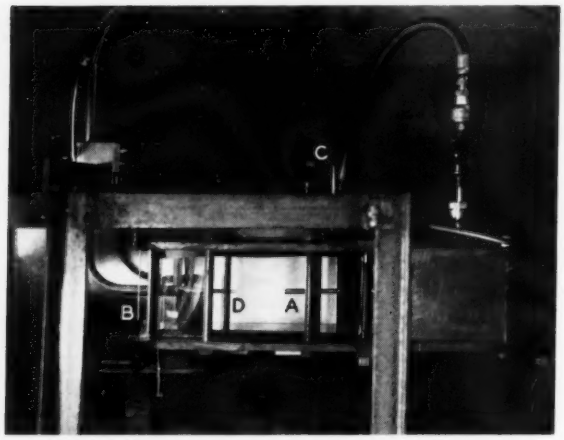

FIG. 3. Jet directed towards the open end of shock tube (arrangement B). A = round jet, B = open end of shock tube, C = triggering hot-wire, D = hot-wire probe for recording jet-shock interaction.

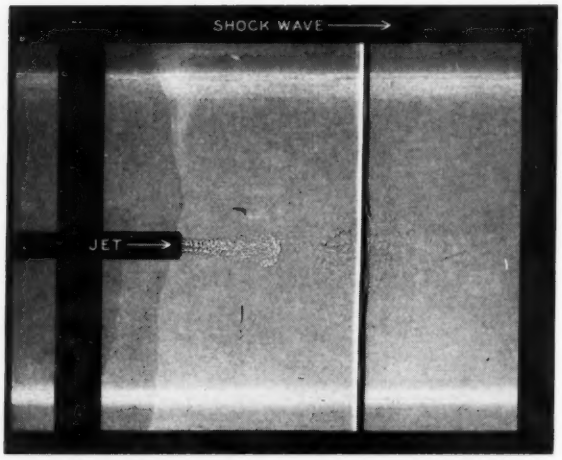

FIG. 4. Interruption of jet flow due to passage of shock front. Round jet with plug, U_e supersonic, $S = 1.58$, delay = 114 microsec., spark light uncollimated.

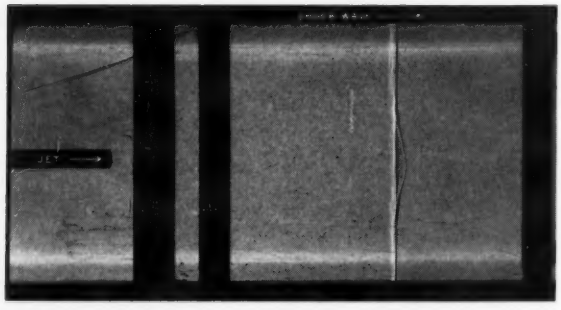

FIG. 5. Shock jet interaction (arrangement B). Round jet, $d = 3/16$ in., $U_e = 340$ ft./sec., $S = 1.58$, delay = 248 microsec., $x_s/d = 23.6$, spark light uncollimated with shock front in line with optical axis of divergent light beam.

lowing a hyperbolic power law[3]

$$U_m/U_e = 6.5(d/x) \tag{1}$$

where x is the distance along the jet axis downstream of the exit and d is the diameter of the circular jet. This relation can roughly be extended to the present case and the approximate exit velocity U_e can be estimated.

The following observations were made from the recorded shadowgraphs. After the traveling shock front advances just past the jet exit, the jet flow is interrupted for a short interval of time (the same happened in Arrangement A). This seems to be caused by the sudden rise in the ambient pressure surrounding the jet. An effort was made to overcome this difficulty. A 1/4-in. long solid plug with five symmetrically drilled holes (diameter = 0.041 in.) was silver soldered in the exit of the jet. The higher pressure ratio across the plug resulted in a choked jet. Mild acoustic radiation eminated from the jet flow near its exit. However, the passage of the shock front still interrupted the jet flow (Fig. 4).

Since the jet flow ahead of the shock front has no way of knowing the state of the "shocked" jet behind the shock wave, the advancing shock front overtakes and passes essentially through the domain of the normal pre-shock jet flow. Some of the already well-known aspects of the jet flow can be optically demonstrated from the sequence of the shadowgraphs of a shock front advancing through jet flow (Fig. 5). For instance, the progressive increase of the transverse distance of the "bulge" in the shock front was exploited to find the angle of spread of the subsonic jet exhausting into quiescent air as follows.

The successive locations x_s of the main shock front, relative to the jet exit, were determined from $x_s = U_s t$ by using the experimentally measured shock speed U_s and the delay time t. The delay time corresponding to the arrival of the shock front at the jet exit was taken as zero. From the corresponding shadowgraphs, the maximum magnitude of the transverse distance (measured up to the point where the bulge profile just becomes tangential to the main shock front) was scaled and plotted at the corresponding locations x_s of the shock front.

For $x_s/d > 10$ and with apex at the center of the jet exit, a semiangle of spread $\theta = 10.5° \pm 1°$ was measured. If one laid the transverse distance r_0 (where $l = 1/2\ l_{max.}$), and with the same apex as before, r_0 lies on a cone of semiangle $(\theta)_{r_0} = 6° \pm 0.5°$ (Fig. 6). These values agree rather well with those quoted in literature for the semiangles of spread of turbulent subsonic jets exhausting in quiescent surroundings.[6] It was observed that in most shadowgraphs the shape of the bulge was symmetrical with respect to the x axis. The occasional exceptions seemed to be due to the local distortion caused by some strong local flow fluctuations.

The depth $l_{max.}$ of the bulge reduced in magnitude the farther downstream from the jet exit the shock front advanced. In the usual manner of the jet-flow investigations,[3, 6, 8] r/r_0 vs. $l/l_{max.}$ was plotted for successive shadowgraphs of the same (strengthwise, $S =$

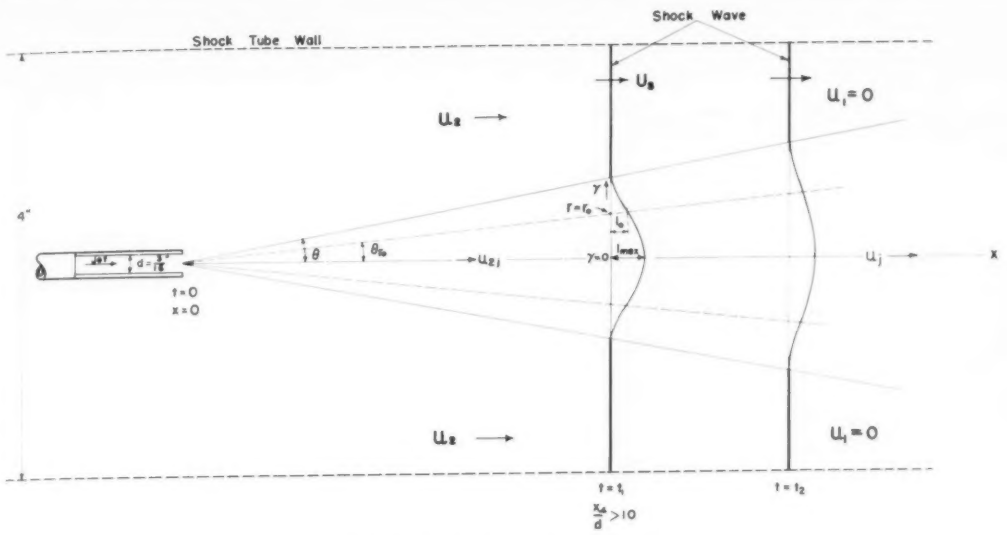

FIG. 6. Angle of spread of jet flow.

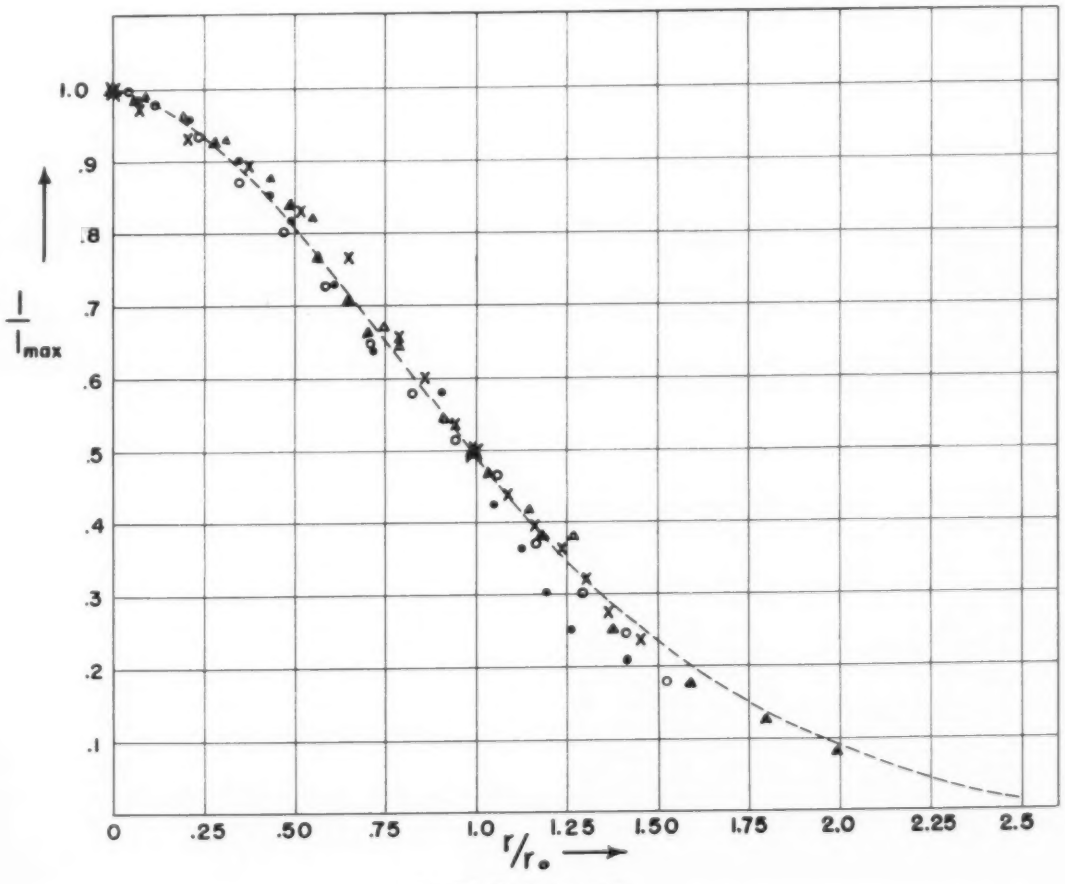

FIG. 7. Similarity profiles.

	Exp. Arrangement	U_e (ft./sec.)	x_s/d
○	B	340	23
●	B	340	30
△	B	340	33
▲	C	1,200	13
×	C	775	17
- - -	theoretical	U/U_m (Prandtl-Tollmien)	

FIG. 8. Shock-jet-interaction with shock front and jet flow directed against each other (arrangement C). Round jet, d = 3/16 in., S = 1.58.

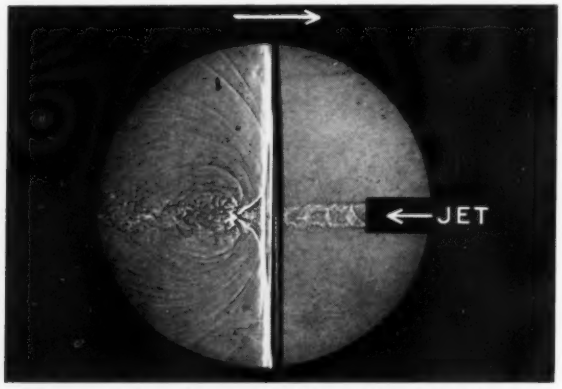

(a) Supersonic jet. $U_e \backsimeq$ 1,200 ft./sec., delay if shock front was to be at jet exist = 414 microsec., delay corresponding to shock front location = 378 microsec., x_s/d = 3.46, spark light collimated.

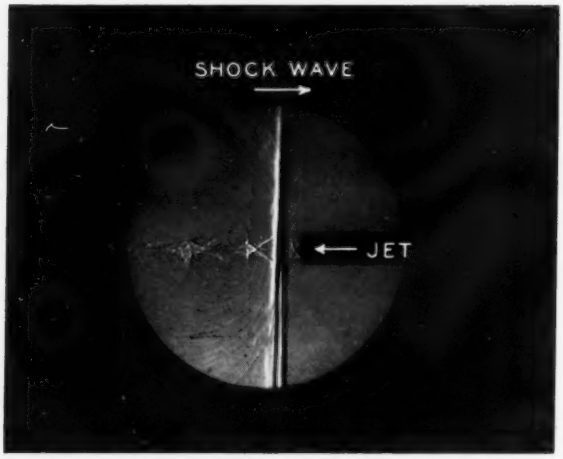

(b) Supersonic jet. $U_e \backsimeq$ 1,200 ft./sec., delay if shock front was to be at jet exist = 385 microsec., delay corresponding to shock location = 377 microsec., x_s/d = 1, spark light collimated.

(c) Subsonic jet. $U_e \backsimeq$ 775 ft./sec., delay if shock front was to be at jet exist = 418 microsec., delay corresponding to shock location = 402 microsec., x_s/d = 1.46, spark light divergent with shock front in line with the optical axis of divergent beam.

1.58) shock front. It was found that for $x_s/d > 12$, the similarity plot agreed with the one for velocity distribution derived by Tollmien[1] using Prandtl's momentum transfer theory[5, 8] (see Fig. 7).

Any physical interpretation of the observations is complicated by the fact that the shock bulge would have spread in transverse direction and decreased in depth even if the jet was removed part way out.

Arrangement C

To circumvent the complications caused by the interruption of a shocked jet (at least till the shock-jet interaction has been recorded), the round jet was centrally mounted through the open end and directed toward the diaphragm of the shock tube (Fig. 1). The jet assembly and the air supply was the same as the one described under Arrangement B. The jet flow and the traveling shock front (and therefore its drift flow) were directed against each other. The maximum velocity of the jet flow was measured with a pitot tube at a number of stations downstream of the jet exit and the approximate exit velocity was estimated by relation 1. Both supersonic (Figs. 8a and 8b) and subsonic (Fig. 8c) jets were tried. Since relation 1 applied only to the subsonic domain of the jet flow, the estimation of the supersonic exit velocity is somewhat arbitrary.

Since the expansion chamber of the shock tube is closed by a diaphragm and the jet is directed upstream (Fig. 1), the jet discharge flows, with a relatively low back-flow velocity, in the opposite direction to the flow in the central jet core.

The following observations were made. The pertinent data are listed under each shadowgraph.

The instantaneous shadowgraphs of the shock front reveal that the central portion of the shock front develops a bubble-top bulge at its rear and seemingly there is a conspicuous splitting or doubling of the shock front (Fig. 8). These distortions of the shock front are obviously related to the relative direction of advance of the shock front and the local jet flow.

If we choose the coordinates such that the shock front is stationary, and it is assumed that the shock front is plane and the back flow velocity is negligible, then the problem reduces to the one with two supersonic parallel streams (jet flow domain in region 3 and the outer flow region 1) with different Mach Numbers such that $M_3 = (U_s + u_j)/a_3 > M_1 = U_s/a_1 > 1$, being convected through a plane stationary shock front. From the well-known one- (or two-) dimensional shock analysis,[7] one may write p_2/p_1 as a function of M_3 and p_4/p_3 as function of M_3 and α. Applying the necessary condition that $p_2/p_1 = p_4/p_3$, one gets $\sin \alpha = M_1/M_3$.

If $M_3 \rightarrow M_1$—i.e., jet velocity $u_j \rightarrow 0$, then $\alpha \rightarrow 90°$. Since $M_3 > M_1$, $\alpha < 90°$, therefore an oblique shock should exist in the jet flow region. The speed of the shock front U_s was known. The approximate speed of the jet flow u_j near the exit (potential core region) was roughly estimated as described before: M_1/M_3 was calculated and the expected value of the inclination α came out to be approximately 48°. As measured from

the shadowgraph $\alpha \approx 40°$ (Fig. 8a). This simplified interpretation ignores the complexity (i.e., three-dimensionality and additional wave pattern) of the bulge shape.

When the turbulent jet, be it subsonic or supersonic, is flowing against the direction of advance of the traveling shock front, an auxiliary wave system originates and propagates in the flow region behind the shock wave. The wave system which resembles an intense acoustic emission seems to have two distinct modes. One is comprised of very high frequency emission (almost continuous) and the other, apparently the stronger of the two, is distinctly intermittent and symmetrical in character (Fig. 8). The apex of these wavelets seem to be coincident with apex of the bulge. The wave system is not clear in the turbulent domain of the jet flow, but is abundant in the outer region of the drift flow. Due to the subsonic drift flow behind the shock, the emitted wave system piles up on the main shock front at its rear[13] while ahead of the shock front, the quiescent region surrounding the jet flow (back flow velocity is overlooked) is devoid, within the sensitivity limitation of the shadowgraphic technique, of any sound field emitted due to the jet flow alone.

By proper choice of the coordinate system, the shock front can be considered to be stationary. In the instantaneous shadowgraphs, the acoustic emission can be analyzed as if eminating from a stationary point source located at the apex of the shock bulge and being radiated into the moving stream behind the shock front (Fig. 9). It is assumed[21] that the propagation velocity normal to the wave fronts is equal to the local speed of sound a_2 in the drift flow region behind the shock front which is related to the frequency f and wavelength λ of the acoustic emission by $a_2 = f\lambda$. If the shock speed U_s is known, then a_2 and the velocity $U_s - u_2$ (stationary-shock coordinates) in region 2 can be calculated, and with the help of the vectorial diagram as shown in Fig. 9, the wavelength λ can be estimated.[21] For the case when the jet was choked and the shock wave ($S = 1.58$) has advanced to a location $x/d = 3.5$ downstream from the jet exit (Fig. 8a),

$$(U_s - u_2)/a_2 = M_2 = 0.81, \qquad \lambda_{ave} \approx 0.24 \text{ in.},$$

$$a_2 = 1{,}230 \text{ ft./sec.}, \qquad f_{ave} \approx 60 \times 10^3 \text{ cycles/sec.}$$

where λ_{ave} and f_{ave} are, respectively, the average order of magnitude of the wavelength and frequency of the intermittent acoustic wavelets. It was observed that the average frequency is somewhat higher ($f_{ave} \approx 80 \times 10^3$ cycles/sec.) for the same operating conditions, but with shock front at $x_s/d = 1$ and is somewhat lower at distances farther downstream from the exit ($f_{ave} \approx 50 \times 10^3$ cycles/sec. at $x_s/d = 13$). For the same shock strength, the frequency and the character of the emitted sound field are strikingly similar in both the supersonic and subsonic jets (Fig. 8). However for the supersonic jet ($U_e \approx 1{,}200$ ft./sec.), the emitted wave system first appeared at $x_s/d = 24 \pm 1$ and for the subsonic jet ($U_e \approx 775$ ft./sec.) at $x_s/d = 15 \pm 1$.

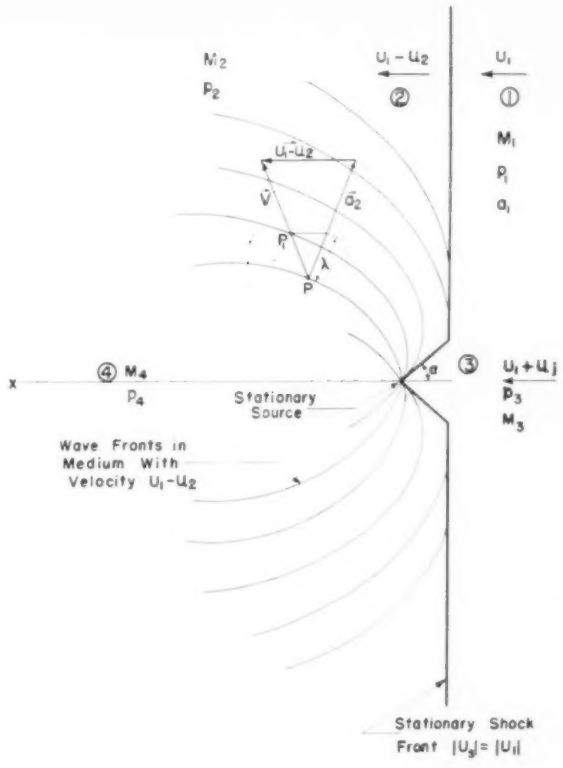

FIG. 9. Acoustic radiation behind shock front.

Since the maximum axial jet velocity U_m was measured at various stations downstream of the exit it is, therefore, possible to estimate U_m for both supersonic and subsonic jets at the respective locations at which the sound emission first clearly manifested itself. Such an estimate revealed that for both supersonic and subsonic jets, the corresponding local $U_m \approx 340 \pm 30$ ft./sec. Based on normal shock considerations, the drift flow velocity $u_2 = 388$ ft./sec.

The drift and the jet flows impinge against each other and develop a common stagnation point close to the shock front. The shocked jet flow is forced to reverse in direction and is continually being pushed outward in the radial direction resulting in a clear swelling of the jet flow (see Fig. 8). The drift flow is called upon to adjust itself around this swelling and any resulting imbalance between the pressure in the jet-flow region and the outer-flow region seems to contribute toward the observed auxiliary wave system whose intermittency is, most likely, due to the oscillating or buffeting of the shock segments constituting the bulge. These oscillations could be caused by the intense velocity or pressure fluctuations convected through the shock front.[9, 10, 11] The characteristics of turbulence—i.e., its intensity and spectrum—will undoubtedly have a direct influence on the nature of the emitted sound field. The present data were not sufficient to estimate the level of the emitted acoustic power. However, it seems apparent

from the shadowgraphs that the level of emission increases as the shock front progresses toward the jet exit.

All these observations were recorded with the shock wave of the same strength ($S = 1.58$). The shock strength may have a direct effect on the characteristics (location of origin and intensity) of the acoustic radiation. In passing, it ought to be pointed out that for the operating conditions of these experiments, $\lambda_{ave} \approx d$, where d is the diameter of the round jet. Therefore, the dependence of λ on the diameter of the jet nozzle (or local diameter of the jet flow) seems likely.

The other mode of the observed acoustic radiation consisting of very high frequency components possibly is due to the convection of the corresponding small scale (higher frequencies) turbulent disturbances through the shock front as expected by Lighthill,[12, 13] Ribner,[14] and Kovasznay.[15]

References

[1] Tollmien, W., *Berechung der turbulenten Ausbreitungs Vorgange*, ZAMM Bd. IV, 1926, p. 468; also translated as NACA TM 1085, 1945.

[2] Kuethe, A. M., *Investigations of the Turbulent Mixing Regions Formed by Jets*, Jour. Appl. Mech. Vol. 2, No. 3, pp. A87–95, September, 1935.

[3] Corrsin, S., *Investigations of Flow in an Axially Symmetrical Heated Jet of Air*, NACA Wartime Report W-94, December, 1943.

[4] Corrsin, S., and Uberoi, M. S., *Spectrum and Diffusion in a Round Turbulent Jet*, NACA TN 2124, July, 1950.

[5] Pai, S. I., *Axially Symmetrical Jet Mixing of a Compressible Fluid*, Quart. Math., vol. 10, No. 2, July, 1952.

[6] Pai, S. I., *Fluid Dynamics of Jets;* Van Nostrand Company, Inc., Princeton, 1954.

[7] Wilder, J. C., and Hindersinn, K., *Spreading of Supersonic Jets in Supersonic Streams*, Aeronautical Engineering Review, Vol. 12, No. 10, pp. 54–68, October, 1953.

[8] Anderson, A. R., and Johns, F. R., *Characteristics of Free Supersonic Jets Exhausting Into Quiescent Air*, Jet Propulsion, Vol. 25, No. 1, January, 1955.

[9] Powell, A., *On the Noise Eminating from a Two Dimensional Jet Above the Critical Pressure*, The Aeronautical Quarterly, Vol. IV, Part II, February, 1953.

[10] Powell, A., *On the Mechanism of Choked Jet Noise*, Proc. Phys. Soc. *B66*, p. 1039, 1953.

[11] Powell, A., *A Note on the Sound From Weak Disturbances of a Normal Shock Wave*, Aero. Research Council, C. P. No. 194.

[12] Lighthill, M. J., *On Sound Generated Aerodynamically, II. Turbulence as a Source of Sound*, Proc. Roy. Soc. A, Vol. 222, pp. 1–32, 1954.

[13] Lighthill, M. J., *On the Energy Scattered From the Interaction of Turbulence With Sound or Shock Waves*, Cambridge Phil. Soc., Vol. 49, Part 3, July, 1953.

[14] Ribner, H. S., *Shock-Turbulence Interaction and the Generation of Noise*, NACA TN 3255, July, 1954.

[15] Kovasznay, L. S. G., *Interaction of a Shock-Wave and Turbulence*, presented in 1955, Heat Transfer and Fluid Mechanics Institute held at Univ. of Calif., Los Angeles, June, 1955.

[16] Dosanjh, D. S., *Use of a Hot-Wire Anemometer in Shock Tube Investigations*, NACA TN 3163, December, 1954.

[17] Dosanjh, D. S., *Interaction of Grids With Traveling Shock Waves*, NACA TN 3680, 1956.

[18] Glass, I. I., and Patterson, G. M., *A Theoretical and Experimental Study of Shock Tube Flows*, Journal of the Aeronautical Sciences, Vol. 22, No. 2, pp. 73–100, February, 1955.

[19] Dosanjh, D. S., *Use of the Hot-Wire Anemometer as a Triggering and Timing Device for Wave Phenomena in a Shock Tube*, Rev. Sci. Instr., Vol. 26, No. 1, 65–70, January, 1955.

[20] Kovasznay, L. S. G., *High Power Short Duration Discharge*, Rev. Sci. Instr., Vol. 20, No. 9, pp. 696, 697, September, 1949.

[21] Krishnamurty, K., *Acoustic Radiation From Two-Dimensional Rectangular Cut-Out in Aerodynamic Surfaces*, NACA TN 3487, August, 1955.

Diffraction of Disturbances Around a Convex Right Corner . . .

(*Continued from page 830*)

[18] Rott, N., *Diffraction of a Weak Shock with Vortex Generation*, J. Fluid Mech., Vol. I, No. 1, pp. 111–128, 1956.

[19] Lighthill, M. J., *A Technique for Rendering Approximate Solutions to Physical Problems Uniformly Valid*, Philosophical Magazine, Series 7, Vol. 40, No. 311, p. 1189, December, 1949.

[20] Lighthill, M. J., *The Shock Strength in Supersonic "Conical Fields,"* Philosophical Magazine, Series 7, Vol. 40, No. 311, p. 1202, December, 1949.

[21] Sun, T. F., *On the "Triple-point" in Shock-Diffraction Problems*, Graduate School of Aeronautical Engineering, Cornell University, September, 1956.

[22] Lagerstrom, P. A., and Van Dyke, M. D., *General Considerations About Planar and Non-Planar Lifting Systems*, Rep. No. SM-13432, Douglas Aircraft Co., Inc., June, 1949.

[23] Ferri, A., Clarke, J. H., and Ting, L., *Favorable Interference in Lifting Systems in Supersonic Flow*, Presented at the Aerodynamics—III Session, Twenty-Fifth Annual Meeting, IAS, New York, January, 1957 (IAS Preprint No. 664).

[24] Ting, L., *Generalization of Integral Relationships with Applications in Wing-Body Interference, Wing Theory and Diffraction of Pulses*, PIBAL Report No. 379, Polytechnic Institute of Brooklyn, April, 1957.

[25] Whittaker, E. T., and Watson, G. N., *A Course of Modern Analysis*, pp. 209–230; Cambridge University Press, American Edition, 1947.

[26] Ting, L., *Diffraction of Disturbances Around a Convex Right Corner with Applications in Acoustics and Wing-Body Interference*, PIBAL Report No. 307, Polytechnic Institute of Brooklyn, August, 1956.

[27] Lawrence, H. R., and Flax, A. H., *Wing-Body Interference at Subsonic and Supersonic Speeds—Survey and New Developments*, Journal of the Aeronautical Sciences, Vol. 21, No. 5, pp. 289–324, May, 1954.

[28] Ferrari, C., *Wing-Body Interference at Supersonic Speeds*, High Speed Aerodynamics and Jet Propulsion, Vol. VII, Chapter 5, Section C, Princeton University Press, 1957.

[29] Nielsen, J. N., *Quasi-Cylindrical Theory of Wing-Body Interference at Supersonic Speeds and Comparison with Experiment*, NACA Report 1252, 1955.

[30] Morikawa, G. K., *A Non-Planar Boundary Problem for the Wave Equation*, Quart. Appl. Math., Vol. 10, No. 2, pp. 129–140, 1952.

[31] Nielsen, J. N., *Tables of Characteristic Functions for Solving Boundary-Value Problems of the Wave Equation with Application to Supersonic Interference*, NACA TN 3873, February, 1957.

Readers' Forum

BRIEF REPORTS of investigations in the aeronautical sciences and discussions of papers published in the JOURNAL are presented in this special department. Entries must be restricted to a maximum of 1,300 words or the equivalent of one JOURNAL page including formulas and illustrations. Publication is completed as soon as possible after receipt of the material. The Editorial Committee does not hold itself responsible for the opinions expressed by the correspondents.

Contents

Reply to "Further Comments on 'Supersonic Diffuser Instability'" ..... ROBERT L. TRIMPI 845
Reply ..... C. L. DAILEY 846

On the Variational Theorem for Creep ..... T. H. H. PIAN 846

On the Minimum Weight Design Problem for Cylindrical Sandwich Shells ..... WALTER F. FREIBERGER 847

The Boundary Layer in Simple Shear Flow Past a Flat Plate ..... M. B. GLAUERT 848
Author's Reply ..... TING YI LI 849

A Series-Expansion Method for Computing Random Gust Responses ..... KENNETH A. FOSS 850

Effect of Air Temperature on Vortex Shedding Frequency of Cylinders ..... WILLIAM D. CLIFFORD 852

Summary of Low-Prandtl-Number Heat-Transfer Results for Forced Convection on a Flat Plate ..... E. M. SPARROW AND J. L. GREGG 852

An Exact Solution of the Navier-Stokes Equations ..... W. CHESTER 853

On One-Dimensional Heat Conduction With an Arbitrary Heating Rate ..... GEORGE W. SUTTON 854

Natural Frequencies of Rectangular Plates With Edges Elastically Restrained Against Rotation ..... C. V. JOGA RAO AND C. LAKSHMI KANTHAM 855

Reply to "Further Comments on 'Supersonic Diffuser Instability'"

Robert L. Trimpi
Aeronautical Research Engineer, Langley Aeronautical Laboratory, NACA, Langley Field, Va.

April 29, 1957

SEVERAL statements[1] made by C. L. Dailey indicate incorrect interpretations of the comments[2] and original publications[3, 4] of the writer on the subject of ram-jet buzz. This brief discussion will attempt to clarify a few of the points so misinterpreted.

The validity of the application of a quasi-one-dimensional unsteady flow approach to the buzzing problem is questioned in reference 1. Consequently an examination of the implications which are associated with the use of such an approach is in order. The quasi-one-dimensional theory permits cross-sectional area variation but considers only one velocity component (axial) and averages fluid properties at a cross section. First, in regards to the use of quasi-one-dimensional theory inside the ram-jet, many experiments have proved that the cross-sectional area versus distance distribution of practical ram-jets is such that a one-dimensional analysis (both steady and nonsteady) gives good correlation. Thus, regardless of what happens *ahead* of the ram-jet cowling, the one-dimensional approach is valid *inside* the ram-jet.

Now the difference between a three-dimensional and a quasi-one-dimensional approach lies principally in the normal variation of flow parameters inside a stream tube. In particular, when the quasi-one-dimensional approach is applied to the stream tube extending from the "normal shock" to the cowling lip at the instant of incidence of inlet instability, the normal gradients of pressure and entropy (the latter is mainly boundary-layer effect) are ignored by averaging across the stream tube. Within these limits the quasi-one-dimensional theory with

Contributors Please Note

Readers' Forum items must be confined to the equivalent of one page in the *Journal*. Contributions that exceed this limit will be returned to the authors for condensation and rewrite. To avoid inconvenience and delay, please adhere to the following specifications:

(1) Five, double-spaced, typewritten, manuscript pages ($8\frac{1}{2}$ by 11 in.), including wide margins, formulas, and headings equal one printed page.

(2) For every illustration, deduct at least one-half or as much as one manuscript page, depending on the size of the illustration.

flexible walls (to account for spillage around the cowling) can yield qualitative information regarding the initiation of buzz. It might be noted that, contrary to the contention of reference 1, no negative values of this stream tube area are required to handle outflow but merely an increased timewise growth of area.

In reference 1 the statement that ". . . a buzz cycle can be generated by the *spontaneous* 'outward' motion of a shock in a one-dimensional channel . . . " was erroneously attributed to reference 2. No such statement was made in reference 2; in fact, the following excerpt from reference 3 expresses the views of the writer in this respect: "The entrance of the vortex sheet, increasing separation, or boundary layer growth (behind the shock), either on the central body or on the inner surface of the cowling, generates a compression wave which *forces* the normal shock outward."

The opinion[2] that the "fill up" portion of the pressure-time curve of a buzz cycle was a series of steps rather than a relaxation cycle was also challenged.[1] The writer interprets a relaxation curve to be a smooth exponential curve and in addition the terms "simple exponential solution" are used in reference 5 to describe the solution to the theoretical pressure-time variation. The experimental pressure-time curves of references 4 and 5 do indeed show such steps and not a smooth exponential trend.

The analysis of reference 1 is inconsistent in regard to another aspect of the "fill up" cycle. In one paragraph it is acknowledged that excellent pressure versus time results may be obtained by the use of the quasi-one-dimensional theory which includes the reflections both at the exit nozzle and at the swallowed shock to satisfy prescribed boundary conditions. Then in the next paragraph the question is raised whether the simple mechanism of reflected compressions are able to build the plenum chamber pressures back up. Such contradictions should not appear if comments result from careful consideration of the problem under discussion.

References

[1] Dailey, Charles L., *Further Comments on "Supersonic Diffuser Instability,"* Journal of the Aeronautical Sciences, Readers' Forum, Vol. 24, No. 1, p. 70, January, 1957.

[2] Trimpi, R. L., *Comments on "Supersonic Diffuser Instability,"* Journal of the Aeronautical Sciences, Readers' Forum, Vol. 23, No. 6, pp. 611, 612, June, 1956.

[3] Trimpi, Robert L., *A Theory for Stability and Buzz Pulsation Amplitude in Ram Jets and An Experimental Investigation Including Scale Effects*, NACA Report 1265, 1956 (formerly NACA RM L53G28, 1953).

[4] Trimpi, Robert L., *An Analysis of Buzzing in Supersonic Ram Jets by a Modified One-Dimensional Nonstationary Wave Theory*, NACA TN 3695, July, 1956 (formerly NACA RM L52A18, 1952).

[5] Dailey, C. L., *Supersonic Diffuser Instability*, Journal of the Aeronautical Sciences, Vol. 22, No. 11, pp. 733–749, November, 1955.

Reply

C. L. Dailey

Research Associate, University of Southern California, Los Angeles Calif.

July 23, 1957

It is hoped that this discussion will not be continued publicly. The many statements and clarifications thereof made to date must surely be sufficient to permit the interested reader to arrive at a point of view of his own.

It is difficult, however, to be entirely satisfied with the present state of knowledge of propulsion system transient analysis. Mr. Trimpi's treatment of inlet buzz affords a convincing example of the extent to which muddled thinking can be seriously regarded as an apparently meaningful explanation.

It is sobering to realize that no method exists at present for predicting either damping and frequency of coupled engine-inlet modes of oscillation or internal pressure noise spectrum of coupled systems. Yet such information is of obvious practical importance to a propulsion engineer.

The phenomenon of inlet buzz is one of the more gross, and hence more obvious, aspects of the general subject of propulsion system transient behavior. While there is no point laboring the description of this phenomenon further, it is worth noting that its cause is not yet thoroughly understood and falls in the general class of things to be cleared up before transient system analysis will enjoy the same rigor that is common in steady flow analysis.

On the Variational Theorem for Creep

T. H. H. Pian

Assistant Professor, Department of Aeronautical Engineering, Massachusetts Institute of Technology, Cambridge, Mass.

July 8, 1957

In a recent NACA publication,[1] Sanders, McComb and Schlechte presented a variational theorem for a body undergoing creep. The authors stated that the integral to be varied was obtained by trial and error. It appears to the present writer that the same integral can be derived in a more rigorous manner using the generalized Reissner's Principle for bodies with initial stresses and initial strains.[2]

As shown by Wang and Prager[3] the present boundary problem may be stated in the following manner: In the interval between the instant t and dt, the surface stress is assumed to be changed by $d\bar{T}_i$ on S_1 and the displacement by $d\bar{u}_i$ on S_2. Creep deformations will occur during this interval. What are the corresponding changes of stresses $d\sigma_{ij}$ and the corresponding displacements du_i throughout the body?

For this problem the state of stress at the beginning of the time interval may be considered as initial stress and the creep strains during the interval dt may be considered as initial strains.

For a body with initial stresses and initial strains the integral π_R to be varied may be written as

$$\pi_R = \int_V [(\sigma_{ij} + d\sigma_{ij})d\epsilon_{ij} - W - d\sigma_{ij}\epsilon_{ij}^{(0)}]\, dV - \int_{S_1} (\bar{T}_i + d\bar{T}_i)du_i dS - \int_{S_2} (du_i - d\bar{u}_i)(\bar{T}_i + dT_i)\, dS \quad (1)$$

where

σ_{ij} = stress at the beginning of the interval dt
$d\sigma_{ij}$ = increment in stress during dt
$d\epsilon_{ij}$ = increment in strain during dt
$\epsilon_{ij}^{(0)}$ = initial strain
W = a function of incremental stresses defined by $d\epsilon_{ij} = \partial W/\partial d\sigma_{ij}$

For problems of finite elastic deformations the strains can be expressed as

$$\epsilon_{ij} = (1/2)(u_{i,\,j} + u_{j,\,i} + u_{k,\,i}\, u_{k,\,j}) \quad (2)$$

Hence,

$$d\epsilon_{ij} = (1/2)(du_{i,\,j} + du_{j,\,i} + u_{k,\,i}\, du_{k,\,j} + u_{k,\,j}\, du_{k,\,i} + du_{k,\,i}\, du_{k,\,j}) \quad (3)$$

The integral π_R may be separated into two parts,

$$\pi_R = \pi_R' + \pi_R'' \quad (4)$$

where

$$\pi_R' = \int_V (1/2)\sigma_{ij}(du_{i,j} + du_{j,\,i} + u_{k,\,i}\, du_{k,\,j} + u_{k,\,j}\, du_{k,\,i})\, dV - \int_{S_1} \bar{T}_i du_i dS - \int_{S_2} (du_i - d\bar{u}_i)\bar{T}_i\, dS \quad (5)$$

$$\pi_R'' = \int_V [(1/2)d\sigma_{ij}(du_{i,\,j} + du_{j,\,i} + u_{k,\,i}\, du_{k,\,j} + u_{k,\,j}\, du_{k,\,i}) + (1/2)\sigma_{ij} du_{k,\,i}\, du_{k,\,j} - W - d\sigma_{ij}\epsilon_{ij}^{(0)}]\, dV - \int_{S_1} d\bar{T}_i du_i dS - \int_{S_2} (du_i - d\bar{u}_i)\, dT_i dS \quad (6)$$

It can be shown that the variation of π_R' vanishes because the initial stresses σ_{ij} satisfy the equations of equilibrium and boundary conditions.

If the rate of creep strain is expressed as a function of stress only, such as in the case of secondary creep, where $\dot{\epsilon}_{ij}^{(c)} = f(J^2) S_{ij}$, the creep strain may be written as $\epsilon_{ij}^{(c)} = \dot{\epsilon}_{ij}^{(c)}\, dt$. Furthermore, increments in stresses and displacements may be expressed in terms of the corresponding time derivatives, $d\sigma_{ij} = \dot{\sigma}_{ij}\, dt$, $dT_i = T_i\, dt$, $du_i = u_i\, dt$.

The resulting integral π_R'' is

$$\pi_R'' = \frac{1}{t}\int_V [\dot{\sigma}_{ij}\dot{\epsilon}_{ij} + (1/2)\sigma_{ij}\dot{u}_{k,i}\dot{u}_{k,j} - \bar{W} - \dot{\sigma}_{ij}\dot{\epsilon}_{ij}^{(c)}]\, dV - \int_{S_1} \dot{T}_i \dot{u}_i\, dS - \int_{S_2} (\dot{u}_i - \hat{\dot{u}}_i)\dot{T}_i\, dS \Big\} dt^2 \quad (7)$$

where $\bar{W}$ is of the same form as W except that $d\sigma_{ij}$ is replaced by $\dot{\sigma}_{ij}$. The integral to be varied is now reduced to that in the brace of Eq. (7). It is equivalent to the integral I given in reference 1. It is clear that the variational operations should be applied to incremental stresses and displacements only—i.e., to time derivatives of quantities but not to the quantities themselves.

References

[1] Sanders, J. L., Jr., McComb, H. G., Jr., and Schlechte, F. R., *A Variational Theorem for Creep with Applications to Plates and Columns*, NACA TN 4003, May, 1957.

[2] Washizu, K., *On the Variational Principles of Elasticity and Plasticity*, M.I.T. Aeroelastic and Structures Research Lab. Tech. Report 25-18, March, 1955.

[3] Wang, A. J., and Prager, W., *Thermal and Creep Effects in Work-Hardening Elastic-Plastic Solids*, Journal of the Aeronautical Sciences, Vol. 21, No. 5, pp. 343, 344, 360, May, 1954.

On the Minimum Weight Design Problem for Cylindrical Sandwich Shells*

Walter F. Freiberger
Assistant Professor, Brown University, Providence, R.I.

July 8, 1957

Introduction

The problem of the plastic design of a structure for minimum weight is a problem of constrained optimalization. The unknown functions—stress-resultants and thickness-parameters for plates and shells—are constrained to lie in a domain defined by the plastic yield condition of the material and the equilibrium equations of the structure; the objective function to be optimized is the weight of the structure, usually in integral form.

A frontal attack on this problem is most naturally by the Lagrange multiplier method of the calculus of variations. For plates, both solid and sandwich, this has been done in reference 1. For cylindrical shells the problem is complicated by the fact that the thickness parameter no longer enters homogeneously into the yield-condition; this homogeneity can, however, be preserved for sandwich shells, and this latter problem is solved in the present paper.

An intuitive criterion applicable to structures obeying a piecewise smooth yield condition led in earlier papers[2, 3] to a minimum weight design procedure for shells. Although formal proof of the optimality of this procedure is as yet lacking, the heuristic criterion has been successful in all cases studied.[4] However, it is by its nature not applicable to smooth yield surfaces.

Recently, the theorems of limit analysis have been applied to a general discussion of minimum weight design.[5, 6] It is shown, for instance, that problems of plane stress and membrane deformation will lead to designs whose weight is an absolute minimum under the criterion derived in reference 1; in the latter paper, as in the present one, the minima derived are the relative ones in the sense of the calculus of variations, and which of these is absolute has to be decided in each particular case. For beams and plates, however, the method of references 5 and 6 can do no better than reference 1. No general method for determining an absolute minimum is yet available.

Further progress in the field is likely to accrue from the two parallel lines of attack—the method of limit analysis (see references 5, 6, and 7) on the one hand, and the calculus of variations (reference 1 and the present paper) on the other.

Solution of the Problem

The sandwich shell of length $2L$, radius R, is to have a core of negligible weight and prescribed constant thickness H, and the thickness h of its faces is to be designed for minimum weight. The shell faces are to flow in the plastic-rigid mode; the yield condition can be written

$$F(N_x, N_\varphi, M_x) = \sigma^2 h^2 \quad (1)$$

where N_x, N_φ, M_x are the stress and moment resultants and σ is the yield stress in pure tension. The von Mises criterion, generalized to three resultants, is

$$F = N_x^2 + N_\varphi^2 - N_x N_\varphi + (3/4H^2) M_x^2 = \sigma^2 h^2 \quad (2)$$

The generalization of Tresca's criterion for shells was given independently.[8, 9]

For homogeneous functions F, Euler's theorem applies; when F is of second degree,

$$N_x(\partial F/\partial N_x) + N_\varphi(\partial F/\partial N_\varphi) + M_x(\partial F/\partial M_x) = (1/2)F \quad (3)$$

The rates of extension and curvature are

$$\epsilon_\varphi = w/R, \qquad \epsilon_x = du/dx, \qquad \kappa = d^2w/dx^2 \quad (4)$$

where u and w are rates of displacement and x is the coordinate in the axial shell direction. From the theory of the plastic potential, the following flow rule may be associated with the yield condition (1):

$$\epsilon_\varphi = \alpha\, \partial F/\partial N_\varphi, \quad \epsilon_x = \alpha\, \partial F/\partial N_x, \quad \kappa = \alpha\, \partial F/\partial M_x \quad (5)$$

where α is a function of position, expressible in terms of the yield condition and the energy dissipation rate.

The rate of energy dissipation per unit area of shell surface is

$$D = N_\varphi \epsilon_\varphi + N_x \epsilon_x + M_x \kappa \quad (6)$$

Hence,

$$D = (1/2)\alpha F = (1/2)\alpha\sigma^2 h^2 \quad (7)$$

and thus

$$\partial F/\partial N_\varphi = (h^2/2D)(w/R), \quad \partial F/\partial N_x = (h^2/2D)(du/dx), \quad \partial F/\partial M_x = (h^2/2D)(d^2w/dx^2) \quad (8)$$

The equations of equiiibrium of the shell are

$$M_x'' + (N_\varphi/R) = p(x) \quad \text{and} \quad N_x' = q(x) \quad (9)$$

where primes denote differertiation with respect to x, and p and q are the radial and axial loads on the shell per unit area.

The weight of the sheil will be a constant magnitude (the core) plus a quantity proportional to

$$\int_{-L}^{L} h(x)dx$$

The variational problem thus reduces to the following: to minimize

$$\int_{-L}^{L} h dx \quad (10)$$

under the conditions

$$F(N_x, N_\varphi, M_x) - h^2 = 0 \quad (11)$$

* The results presented in this paper were obtained in the course of research sponsored by the Ballistic Research Laboratories of Aberdeen Proving Ground under Contract DA-19-020-ORD-798.

$$M_x'' + (1/R)N_\varphi - p = 0 \tag{12}$$

$$N_x' - q = 0 \tag{13}$$

With Lagrange multipliers λ, μ, ν for Eqs. (11), (12), and (13), respectively, the Euler equations become

$$1 - 2\psi h = 0 \tag{14}$$

$$\lambda(\partial F/\partial M_x) + \mu'' = 0 \tag{15}$$

$$\lambda(\partial F/\partial N_x) - \nu' = 0 \tag{16}$$

$$\lambda(\partial F/\partial N_\varphi) + (\mu/R) = 0 \tag{17}$$

Eliminating λ and μ from Eqs. (14), (15), and (17), we obtain

$$[(R/h)(\partial F/\partial N_\varphi)]'' = (1/h)(\partial F/\partial M_x) \tag{18}$$

and substituting Eq. (8) into Eq. (18)

$$(hw'/D)'' = hw''/D \tag{19}$$

Putting $D/h = \Delta$, the rate of energy dissipation per unit volume, Eq. (19) can be written

$$2w'(1/\Delta)' + w(1/\Delta)'' = 0$$

or, integrating,

$$(w^2/\Delta^2)\Delta' = \beta \tag{20}$$

where β is a constant of integration. It can be shown by considering the boundary conditions at the ends of the shell, that $\beta = 0$ at $x = \pm L$, and thus for all x.

We conclude, then, that we must, for minimum weight, have

$$\Delta' = 0 \quad \text{or} \quad \Delta = D/h = \text{constant} \tag{21}$$

A relative minimum for the shell weight in the sense of the calculus of variations is thus found for sandwich shells designed to give constant rate of energy dissipation per unit volume of face material. In view of the local plane stress conditions prevailing in the faces, this condition will also give an absolute minimum and thus an overall optimum design according to reference 6.

For the von Mises yield condition (2), Eq. (18) gives

$$[(2N_\varphi - N_x)/h]'' = (3R/2H^2)(M_x/h) \tag{22}$$

and it can readily be shown that in this case the functions $M_x(x)$ and $h(x)$ are determined by the following two differential equations:

$$-2M_x'''' + 4t'M_x''' - 2(t'^2 - t'')M_x'' - (3/H^2R^2)M_x = a(x) + b(x)(t'^2 - t'') + c(x)t'$$

$$(M_x'')^2 + d(x)M_x'' + (3/4H^2)M_x^2 + e(x) = \sigma^2 e^{2t}$$

where we have put $t = \log h$, and the quantities a, b, c, d, e are known functions of x depending on the applied loads $p(x)$ and $q(x)$.

References

[1] Freiberger, W., and Tekinalp, B., *Minimum Weight Design of Circular Plates*, J. Mech. & Phys. Solids, Vol. 4, No. 4, pp. 294–299, August, 1956.

[2] Onat, E. T., and Prager, W., *Limit of Economy of Material in Shells*, De Ingenieur, Vol. 67, pp. 46–49, 1955.

[3] Freiberger, W., *Minimum Weight Design of Cylindrical Shells*, J. Appl. Mech., Vol. 23, No. 4, pp. 576–580, December, 1956.

[4] Bodner, S., *On the Minimum Weight Design of Cylindrical Shells* (to appear in the J. Appl. Mech.).

[5] Drucker, D. C., and Shield, R. T., *Design for Minimum Weight*, Brown University, Division of Engineering, O.O.R. Contract 3172, Report No. 11, September, 1956.

[6] Drucker, D. C., and Shield, R. T., *Bounds on Minimum Weight Design*, Brown University, Division of Applied Mathematics, O.N.R. Contract C11, Report No. 18, October, 1956.

[7] Onat, E. T., Schumann, W., and Shield, R. T., *Design of Circular Plates for Minimum Weight*, Brown University, Division of Applied Mathematics, Report DA-2598/3984/20 for Watertown Arsenal, March, 1957.

[8] Onat, E. T., *The Plastic Collapse of Cylindrical Shells under Axially Symmetrical Loading*, Quart. Appl. Math., Vol. 13, pp. 64–72, 1955.

[9] Hodge, P. G., Jr., *Rigid-Plastic Analysis of Symmetrically Loaded Cylindrical Shells*, J. Appl. Mech., Vol. 21, No. 4, pp. 336–342, December, 1954.

The Boundary Layer in Simple Shear Flow Past a Flat Plate

M. B. Glauert*

Department of Mathematics, University of Manchester, Manchester, England

April 8, 1957

THE PROBLEM of the laminar boundary layer on a flat plate in a stream of vorticity ω_0 has been the subject of a recent series of notes by Li.[1, 2, 3] The appropriate boundary-layer equations for steady incompressible flow with no pressure gradient are

$$u(\partial u/\partial x) + v(\partial u/\partial y) = \nu(\partial^2 u/\partial y^2) \tag{1}$$

$$(\partial u/\partial x) + (\partial v/\partial y) = 0 \tag{2}$$

with boundary conditions

$$u = v = 0 \quad \text{at} \quad y = 0 \tag{3}$$

$$u = u_0 + \omega_0 y \quad \text{at} \quad x = 0 \tag{4}$$

where u_0 and ω_0 are constants.

In place of condition (4), Li adopts in his first note[1]

$$u \to u_0 + \omega_0 y \tag{5}$$

as the condition at the outer edge of the boundary layer. On writing

$$\eta = y\sqrt{u_0/\nu x} \quad \xi = \omega_0\sqrt{\nu x/u_0^3} \tag{6}$$

Li obtains a solution in series for the stream function ψ in the form

$$\psi = \sqrt{u_0\nu x}\,\{f_0(\eta) + \xi f_1(\eta) + \ldots\} \tag{7}$$

where

$$u = (\partial\psi/\partial y) \quad v = -(\partial\psi/\partial x) \tag{8}$$

in accordance with Eq. (2). On equating like powers of ξ in Eq. (1),

$$2f_0''' + f_0 f_0'' = 0 \tag{9}$$

$$2f_1''' + f_0 f_1'' - f_0' f_1' + 2f_0'' f_1 = 0 \tag{10}$$

the boundary conditions being

$$f_0 = f_0' = 0 \quad f_1 = f_1' = 0 \quad \text{at} \quad \eta = 0 \tag{11}$$

$$f_0' \to 1 \quad f_1'' \to 1 \quad \text{as} \quad \eta \to \infty \tag{12}$$

The required solution of Eq. (9) is the well-known Blasius function, and Li gives a solution of Eq. (10) obtained by an approximate method.

In a later note[3] Li retracts his previous solution. He points out that, as $\eta \to \infty$, $f_0 \sim \eta - c$, where c is a constant (with the known value 1.7208). It follows that, at the edge of the boundary layer,

$$v \to (1/2)c\sqrt{u_0\nu/x} \tag{13}$$

and hence, in Eq. (1),

$$v(\partial u/\partial y) \to (1/2)\omega_0 c\sqrt{u_0\nu/x} \tag{14}$$

Li deduces that this term must be balanced by a pressure gradient since the other terms of Eq. (1) become zero outside the boundary layer, and on introducing this he obtains a modified Eq. (10) with $-c$ on the right-hand side. He does not carry out a solution of the modified equation.

However, this concept of an induced pressure gradient is a fallacious one. It arises from the use of the boundary condition (5) in place of (4). The correct condition at the outer edge of the boundary layer is

$$u(\partial u/\partial x) + v(\partial u/\partial y) = 0 \tag{15}$$

since neither pressure nor viscous forces are significant, and so u is constant along each streamline. Since the streamlines

* Lecturer in Mathematics.

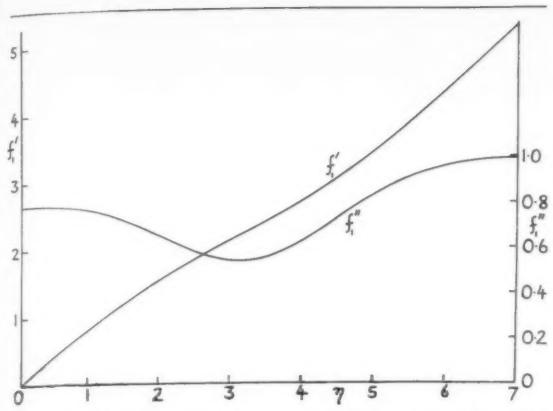

FIG. 1. Variation with distance from the surface (η) of the contributions to the velocity (f_1') and the shearing stress (f_1'') due to stream vorticity.

are displaced by an amount equal to the displacement thickness δ, this implies that, at the edge of the boundary layer,

$$u \to u_0 + \omega_0(y - \delta) \tag{16}$$

In (5), Li requires that u shall be constant at fixed y. This involves an increase of velocity of fluid elements (for $\omega_0 > 0$), and hence an accelerating pressure gradient is called for. There is no mechanism within the boundary layer to induce such a pressure gradient. For all boundary-layer flows (16) is the appropriate type of boundary condition rather than (5), but the difference between the two is apparent only when the external stream has vorticity. In fact, the solution of the boundary layer Eq. (1) under the condition (4) automatically satisfies the revised boundary condition (16). For large η, $f_0 \sim \eta - c$. If $f_1 \sim (1/2)\eta^2 + d\eta + e$ [so that Eq. (12) is satisfied], substitution in Eq. (10) shows that $d = -c$. Hence, from Eq. (7),

$$u = (\partial\psi/\partial y) \to u_0 + \omega_0\left(y - c\sqrt{\nu x/u_0}\right) \tag{17}$$

and thus

$$u(\partial u/\partial x) \to -(1/2)\omega_0 c\sqrt{u_0\nu/x} \tag{18}$$

cancelling with the value of Eq. (14) and so satisfying Eq. (15). This is only as was to be expected. The boundary-layer equations allow for continuity and for the fall to zero of viscous stress with increasing distance from the surface, and so the conditions at the outer edge of the boundary layer must be correctly described. Thus Li's original Eqs. (9)–(12) are indeed the appropriate ones.

The method used by Li[1] to solve Eq. (10) is to replace it by two approximate equations, valid for small and large values of η respectively, and to fix the undetermined constants by matching the solutions at $\eta = 3.0$. For η small, f_0 is replaced by $(1/2)a\eta^2$ (where $a = f_0''(0) = 0.33206$), and for η large, f_0 is replaced by $\eta - c$. These approximations are far too crude for one to expect the solutions to have any range of overlap. In addition, the solution Li gives for small η does not in fact satisfy the appropriate equation.

A far more accurate procedure is to integrate Eq. (10) numerically in a straightforward manner. For η small,

$$f_0 = a(\eta^2/2!) - (1/2)a^2(\eta^5/5!) + (11/4)a^3(\eta^8/8!) + \ldots \tag{19}$$

and hence from Eqs. (10) and (11)

$$f_1 = b[(\eta^2/2!) - (1/2)a(\eta^5/5!) + (23/4)a^2(\eta^8/8!) + \ldots] \tag{20}$$

where b is some constant. With $b = 1$, f_1 and its derivatives were calculated at a set of small values of η, and the solution was then continued by use of Milne's integration formulae,[4]

$$[y_4 - y_0 = (4/3)h(2y_3' - y_2' + 2y_1'), \quad y_2 - y_0 = (1/3)h(y_2' + 4y_1' + y_0')]$$

Using intervals of 0.2 in η and working to four decimal places with a desk calculating machine, the integration was swift and presented no difficulties. It was found that f_1'' approached the limiting value 1.258, showing that the correct value of b is $1/1.258 = 0.795$. The value of b obtained by Li was 0.278, a very serious underestimate.

The variation with η of f_1' and f_1'' is shown in Fig. 1. Since

$$u = u_0\{f_0'(\eta) + \xi f_1'(\eta) + \ldots\} \tag{21}$$

and

$$\tau = \mu(\partial u/\partial y) = \rho u_0^2\sqrt{\nu/u_0 x}\{f_0''(\eta) + \xi f_1''(\eta) + \ldots\} \tag{22}$$

these functions give the contributions to the velocity and shearing stress in the boundary layer, due to the vorticity in the stream. In particular, the skin-friction τ_0 on the plate is given by

$$\begin{aligned}\tau_0 &= \rho u_0^2\sqrt{\nu/u_0 x}\{0.332 + 0.795\xi + \ldots\} \\ &= 0.332\ \rho u_0^2\sqrt{\nu/u_0 x} + 0.795\mu\omega_0 + \ldots\end{aligned} \tag{23}$$

The first term represents the skin-friction due to a uniform stream u_0. Also outside the boundary layer $\tau = \mu\omega_0$. Thus the presence of the boundary layer reduces the effect on the plate of the shear in the external stream.

REFERENCES

[1] Li, T. Y., *Simple Shear Flow Past a Flat Plate in an Incompressible Fluid of Small Viscosity*, Readers' Forum, Journal of the Aeronautical Sciences, Vol. 22, No. 9, pp. 651, 652, September, 1955.

[2] Li, T. Y., *Simple Shear Flow Past a Flat Plate in a Compressible Viscous Fluid*, Readers' Forum, Journal of the Aeronautical Sciences, Vol. 22, No. 10, pp. 724, 725, October, 1955.

[3] Li, T. Y., *Effects of Free-Stream Vorticity on the Behavior of a Viscous Boundary Layer*, Readers' Forum, Journal of the Aeronautical Sciences, Vol. 23, No. 12, pp. 1128, 1129, December, 1956.

[4] Milne, W. E., *Numerical Calculus*, Ch. V; Princeton University Press 1949.

Author's Reply

Ting Yi Li
Department of Aeronautical Engineering, Rensselaer Polytechnic Institute, Troy, N. Y.

May 15, 1957

THE PROBLEM of simple shear flow past a flat plate in an incompressible fluid of small viscosity is the subject matter of Glauert's note above. He has made some interesting observations on the results by the writer published in this JOURNAL. For the sake of reaching a good understanding of the problem, it seems proper to submit the following comments.

The writer is not convinced that the demonstration given in Glauert's note proves the nonexistence of an induced pressure gradient in the present problem. In fact, for large η, if we take

$$f_0 \sim \eta - c$$
$$f_1 \sim (1/2)\eta^2 + d\eta + e$$

Substitution in the following equation

$$2f_1''' + f_0 f_1'' - f_0' f_1' + 2f_0'' f_1 = -c \tag{1}$$

yields $f_1 \sim (1/2)\eta^2 + e$ (i.e., $d = 0$). Hence, for large η,

$$\left.\begin{aligned} &u \to u_\infty = u_0 + \omega_0 y \\ &\partial u/\partial x \to 0 \quad \partial u/\partial y \to \omega_0 \\ &v \to v_\delta = (c/2)\sqrt{(u_0\nu/x)} + \text{higher order term}\end{aligned}\right\} \tag{2}$$

Consequently,

$$u(\partial u/\partial x) + v(\partial u/\partial y) \to \omega_0 v_\delta \simeq (c/2)\omega_0\sqrt{(u_0\nu/x)} \tag{3}$$

Now, in the inviscid free stream the Euler's equation of motion in the x direction (allowing for induced pressure effects) is

$$u(\partial u/\partial x) + v(\partial u/\partial y) = -(1/\rho)(\partial p/\partial x) \tag{4}$$

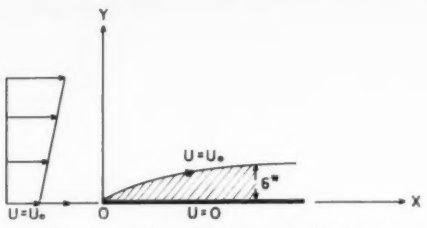

FIG. 1a. δ^* = displacement thickness

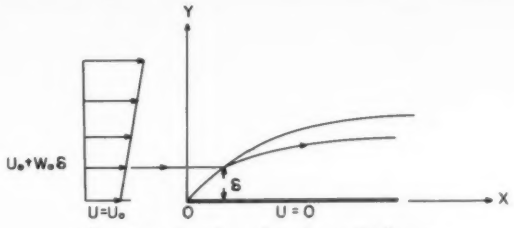

FIG. 1b. δ = boundary-layer thickness.

Comparing Eqs. (3) and (4) we obtain the induced pressure as

$$-(1/\rho)\ (\partial p/\partial x) = v_\delta \omega_0 \tag{5}$$

Therefore, Glauert's type of demonstration is here used to demonstrate the consistency of the induced pressure gradient concept with Eq. (1) above. This seems to show that Glauert's Eq. (15) represents a more restrictive inviscid flow equation than Eq. (4), (it disallows the induced pressure effects). He can obtain the necessary consistency only by adopting his revised boundary condition (16) which reads

$$u \to u_0 + \omega_0(y - \delta^*) \tag{6}$$

for $\eta \to \infty$. The physical interpretation of Eq. (6) can be described as in Fig. 1a. For $x \leq 0$, the streamline corresponding to $u = u_0$ lies on the line $y = 0$. For $x > 0$, this streamline becomes $y = \delta^*$ on which $u = u_0$. This approximate treatment implies that there is no mass flowing into the region $0 < y \leq \delta^*$. In incompressible flow this approximate treatment yields reasonable accuracy, as the writer believes, only when the displacement thickness δ^* is very small—i.e., when the displacement effects are negligible. This physical picture leads to the formulation reported in the writer's first note (Glauert's reference 1). As the displacement effects are not always negligible, an alternative approximation is, as Glauert also recognized, to take u as constant at fixed y (Fig. 1b). This physical picture leads to the formulation reported in the writer's third note (Glauert's reference 3). In support of this latter formulation, one may say that since the viscous effects are confined within the boundary layer, $0 < y \leq \delta$, a streamline from the free stream at $y = \delta$ will maintain its constant velocity until it enters the boundary layer; therefore, the boundary condition (2) should be applied in integrating the boundary-layer equations.

The approximate method used to solve the boundary-layer equations in the first note by the writer was essentially the method used by Kuo.[1] For $\eta \to 0$, the appropriate equation was further simplified by dropping higher order terms in η as was done in Kuo's paper. In this manner, the solution (18) in the writer's first note was obtained. The writer himself was not quite satisfied with this crude method of computations. About a year ago, Mr. R. E. Duffy helped the writer recomputing the solution on a REAC machine. The results were made available to certain groups but were not published so far because, in the writer's opinion, the formulation given in his first note provides only partial answers to the problem. However, the writer is happy to report almost complete agreement between the REAC results and Glauert's data. Mr. Duffy has also computed the velocity profile inside the boundary layer for various values of free stream vorticity, using these REAC results.

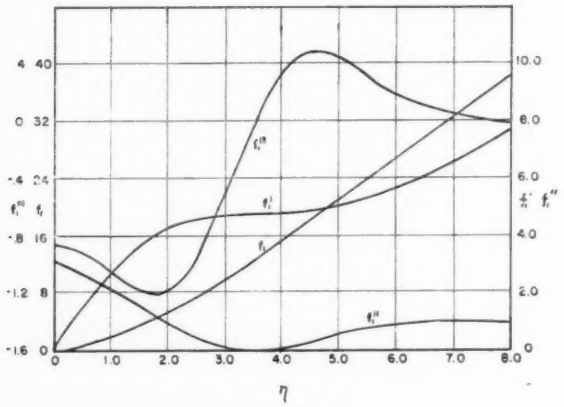

FIG. 2

The nonhomogeneous Eq. (1) has recently been numerically integrated with the help of Mr. W. Lick. The results are shown in Fig. 2. It is noted that here $f_1''(0) = 3.11$ which is considerably higher than Glauert's value. This seems to indicate the importance of the induced pressure term.

Recently, Sakurai[2] investigated the problem of shear flow along a flat plate with uniform suction. Sakurai's Eq. (8) reads, in his notations,

$$\rho[\nu(d^2u/dy^2) - v_0(du/dy)] = \partial p/\partial x = \alpha = -\omega_\infty v_0 \rho$$

In the case of uniform flow past a flat plate with uniform suction, the governing equation is

$$\rho[\nu(d^2u/dy^2) - v_0(du/dy)] = 0 = \partial p/\partial x$$

This example illustrates clearly that the effect of a free-stream vorticity together with v_0 is equivalent to a pressure gradient in the x direction.

REFERENCES

[1] Kuo, Y. H., *On the Flow of an Incompressible Viscous Fluid Past a Flat Plate at Moderate Reynolds Numbers*, J. Math. & Phys., Vol. XXXII, pp. 83–101, October, 1953.

[2] Sakurai, T., *The Shear Flow Along a Flat Plate With Uniform Suction*, Readers' Forum, Journal of the Aeronautical Sciences, Vol. 24, p. 79, January, 1957.

A Series-Expansion Method for Computing Random Gust Responses*

Kenneth A. Foss
Research Engineer, Aeroelastic and Structures Research Laboratory, Massachusetts Institute of Technology, Cambridge, Mass.

July 8, 1957

RIBNER[1] RECENTLY PRESENTED a general unification of the statistical approach to the dynamic response of aircraft in turbulent air. In a follow-up note in the Readers' Forum, Richardson[2] pointed out that, although Ribner's formulation is simple and straightforward, the actual computation of the statistics of a response becomes exceedingly complex and unwieldy when the two-dimensional characteristics of turbulence are considered in conjunction with a lifting-surface aerodynamic theory. A series-expansion method which may alleviate some of the computational difficulties will now be described.

When an airplane is flying through homogeneous turbulence,

* This method was developed under research contract AF 33(616)-3508 sponsored by the Aircraft Laboratory, Wright Air Development Center of the USAF.

the spectral density of the time variation of a stress σ in its flexible structure can be written as

$$\phi_\sigma(\omega) = (2/U) \int_{-\infty}^{\infty} |\Gamma_\sigma(k_1, k_2)|^2 \phi_w(k_1, k_2) dk_2, \quad (\omega = Uk_1) \tag{1}$$

where ϕ_w is a spectral function for the variations of vertical gust velocity w in a horizontal plane; and Γ_σ is a transfer function which can be computed as the steady-state stress response to the two-dimensional sinusoidal upwash pattern

$$w(x, y, t) = e^{i[k_1(Ut-x)+k_2y]} = e^{ik_2y} e^{i\omega[t-(x/U)]} \tag{2}$$

Except for very simple cases, Eq. (1) cannot be integrated in closed form. Furthermore, the asymptotic behavior of the integrand usually resembles that of a damped sinusoid making very difficult any numerical integration technique. However, since practical cases of gust response involve large-scale atmospheric turbulence, the effect of spanwise variations on Eq. (1) can be considered as a small correction to its one-dimensional equivalent,

$$\phi_\sigma(\omega) = |\Gamma_\sigma(k_1, 0)|^2 \phi_w(\omega) \tag{3}$$

where $\phi_w(\omega)$ is the power spectrum of $w(x, 0, t)$ and is related to $\phi_w(k_1, k_2)$ by

$$\phi_w(\omega) = (2/U) \int_{-\infty}^{\infty} \phi_w(k_1, k_2)\, dk_2 \tag{4}$$

This suggests the expansion of $\Gamma_\sigma\ (k_1, k_2)$ into an infinite series about $\Gamma_\sigma\ (k_1, 0)$ which can be accomplished by expanding e^{ik_2y} in Eq. (2) into a series.

The Maclaurin series for this exponential when applied to Eq. (1) would involve integrations of the type,

$$\int_{-\infty}^{\infty} k_2^n \phi_w(k_1, k_2)\, dk_2$$

and the asymptotic behavior of ϕ_w is such that these integrals may not exist for the higher powers of k_2. Thus, in this method e^{ik_2y} will be expanded into a series of functions each of which approaches a finite value as k_2 becomes infinite.

One such set of functions can be obtained from powers of

$$\chi(k_2) = \kappa[1 + (\kappa^2/\lambda^2)]^{-(1/2)} \tag{5}$$

where $\kappa = bk_2/2$, and λ is an arbitrary constant. By substituting the Maclaurin series for

$$\kappa^n = \chi^n[1 - (\chi^2/\lambda^2)]^{-(n/2)}$$

into the Maclaurin series for e^{ik_2y}, the required series expansion of Eq. (2) is obtained in terms of powers of $\chi(k_2)$.

If we now confine our discussion to symmetric responses of the airplane, only the real part of e^{ik_2y} is effective; and Eq. (2) can be expanded into

$$w(x, y, t) = e^{i\omega[t-(x/U)]} \left[1 + \sum_{m=1}^{\infty} \beta_m(y)\, \chi^{2m}(k_2) \right] \tag{6}$$

where

$$\beta_1 = -\eta^2/2!, \quad \beta_2 = [(\eta^4/4!) - (\eta^2/2!\lambda^2)],$$
$$\beta_3 = -[(\eta^6/6!) - (2\eta^4/4!\lambda^2) + (\eta^2/2!\lambda^4)], \ldots \tag{7}$$

and where $\eta = 2y/b$. Since power spectral methods are restricted to linear systems, the transfer function obtained from Eq. (6) can be written as

$$\Gamma_\sigma(k_1, k_2) = \Gamma_\sigma(k_1, 0) + \sum_{m=1}^{\infty} \Gamma_m(\omega) \chi^{2m}(k_2) \tag{8}$$

where each Γ_m is obtained as the response to

$$w_m(x, y, t) = \beta_m(y) e^{i\omega[t-(x/U)]} \tag{9}$$

The generalized forces due to each w_m as well as those due to displacements of the generalized coordinates can be obtained from the linearized unsteady-flow theories used in flutter analyses.

By squaring the absolute magnitude of Eq. (8) one obtains from Eq. (1)

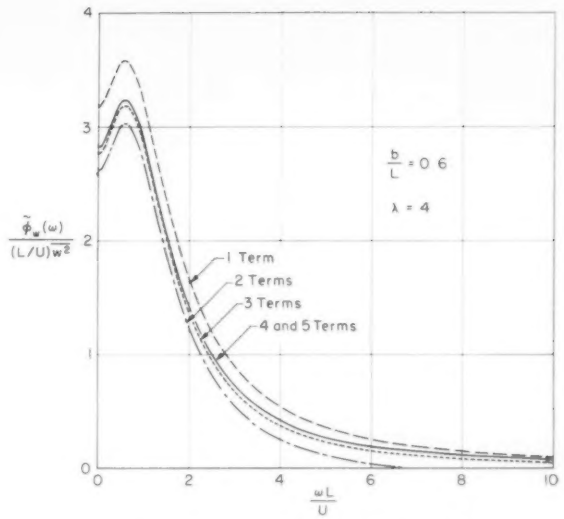

FIG. 1. Series expansion of span-averaged gust spectrum

$$\phi_\sigma(\omega) = |\Gamma_\sigma(k_1, 0)|^2 \phi_w(\omega) + \sum_{m=1}^{\infty} \gamma_m(\omega)\, \psi_m(\omega) \tag{10}$$

where γ_m represents the collecting of terms with like powers of χ, and where

$$\psi_m(\omega) = (2/U) \int_{-\infty}^{\infty} \chi^{2m}(k_2)\, \phi_w(k_1, k_2)\, dk_2 \tag{11}$$

For a particular type of homogeneous turbulence each ψ_m can be evaluated once and for all.

The first term of Eq. (10) is the output spectrum for one-dimensional turbulence, and the remaining terms of the series are a correction which accounts for the spanwise variations of upwash. In large-scale atmospheric turbulence this correction is small and the series should converge rapidly; and the amount of computational work required is roughly the same as that for solving an equivalent one-dimensional problem as many times as the number of terms needed in the series.

To illustrate the convergence of this method, let us consider the simple problem of computing the lift on a rigid uniform wing by strip theory. It has already been shown by Liepmann,[3] Diederich,[4] and Hakkinen and Richardson[5] that the power spectrum of this lift can be written in the form

$$\phi_L(\omega) = |\Gamma_L(k_1, 0)|^2 \tilde{\phi}_w(\omega) \tag{12}$$

where $\tilde{\phi}_w$ is a span-averaged gust spectrum which, for the purpose of the present method, can be defined by

$$\tilde{\phi}_w(\omega) = 2/U \int_{-\infty}^{\infty} \left[(1/b) \int_{-(b/2)}^{b/2} e^{ik_2y}\, dy \right]^2 \phi_w(k_1, k_2)\, dk_2 \tag{13}$$

By making use of the approximate expression for isotropic turbulence given in reference 3, this series-expansion method (with $\lambda = 4$) was applied to Eq. (13); and the results are shown in Fig. 1. For this example, the series has converged for all practical purposes with four terms (the first term is the one-dimensional gust spectrum), when the span to scale-of-turbulence ratio, b/L, equals 0.6. This value of b/L is probably larger than would be experienced in atmospheric turbulence, and other calculations have shown that this example converges with only two terms of the series when b/L is less than 0.2.

REFERENCES

[1] Ribner, H. S., *Spectral Theory of Buffeting and Gust Response: Unification and Extension*, Journal of the Aeronautical Sciences, Vol. 23, No. 12, pp. 1075–1077, 1118, December, 1956

[2] Richardson, A. S., Jr., *On the Prediction of Gust and Buffet Response of Wings and Airfoils*, Readers' Forum, Journal of the Aeronautical Sciences, Vol. 24, No. 5, pp. 385, 386, May, 1957.

[3] Liepmann, H. W., *Extension of the Statistical Approach to Buffeting and Gust Response of Wings of Finite Span*, Journal of the Aeronautical Sciences, Vol. 22, No. 3, pp. 197–200, March, 1955.

[4] Diederich, F. W., *The Dynamic Response of a Large Airplane to Continuous Random Atmospheric Disturbances*, Journal of the Aeronautical Sciences, Vol. 23, No. 10, pp. 917–930, October, 1956.

[5] Hakkinen, R. J., and Richardson, A. S., Jr., *Theoretical and Experimental Investigation of Random Gust Loads, Part I—Aerodynamic Transfer Function of a Simple Wing Configuration in Incompressible Flow*, NACA TN 3878, May, 1957.

Effect of Air Temperature on Vortex Shedding Frequency of Cylinders

William D. Clifford*
Lewis Flight Propulsion Laboratory, NACA, Cleveland, Ohio
July 15, 1957

PREVIOUS INVESTIGATIONS have correlated the Strouhal Number of cylinders as a function of Reynolds Number. The Strouhal Number is $S = fd/U$, where f is the vortex shedding frequency, d is the cylinder diameter, and U is the free-stream velocity. Rayleigh[1] first suggested that the Strouhal Number is a function of the Reynolds Number based on cylinder diameter. Among others, Kovasznay[2] and Roshko[3] have found consistent correlation between Strouhal Number and Reynolds Number in three distinct Reynolds Number ranges: (1) a 40 to 150 Reynolds Number lower range of the classic viscous vortex street region, (2) a 150 to 300 Reynolds Number transition period, and (3) a 300 to 100,000 Reynolds Number upper range where shedding vortices are quickly dissipated.

At the time of this investigation, previous research had not investigated the effect of temperature on Strouhal Number. Stream velocity and cylinder diameter have been common variables, while stream temperature has been held constant at room conditions. It was the purpose of this investigation to determine whether the Reynolds Number completely accounted for the effect of air temperature on Strouhal Number.

Apparatus used in this work consisted of an air supply metered through a pressure regulator and rotameter. The air, heated by an electric heater, then passed through a calming chamber and a convergent nozzle into a 0.875-in. by 1.5-in. long cylindrical duct exhausting into the room. Temperature was varied from room temperature to 300° F. and was measured by a thermocouple located at the exit of the duct. A 0.0625-in. diameter rod was placed 0.125 in. downstream from the nozzle throat. Shedding frequencies were sensed by a hot-wire anemometer at a position 4 diameters downstream of the cylinder, and the signal was relayed through an amplifier into the vertical axis of an oscilloscope. Frequency was determined by connecting an oscillator to the horizontal axis so that the vortex shedding frequency could be determined by the Lissajous figure method. The effect of cylinder blockage on the approach stream velocity was compensated for by the method described in reference 4.

As shown in Fig. 1, complete agreement was not obtained with the data of Roshko and Kovasznay. Consistent variations of the Strouhal-Reynolds Number correlation were observed as the air temperature was varied from room temperature to 300° F. From these observations, Reynolds Number apparently does not completely account for the effect of air temperature on Strouhal Number. The results of this investigation suggest further research into effects of temperature and pressure on Strouhal number.

References

[1] Rayleigh, *Aeolian Tones*, Phil. Mg. and Jour. Sci., Ser. 6, Vol. XXIX, pp. 433–444, April, 1915.

[2] Kovasznay, L. S. G., *Hot-Wire Investigation of the Wake Behind Cylinders at Low Reynolds Numbers*, Proc. Royal Soc. (London), Ser. A, Vol. 198, pp. 174–190, Sept. 7, 1949.

* Co-op Student, University of Detroit.

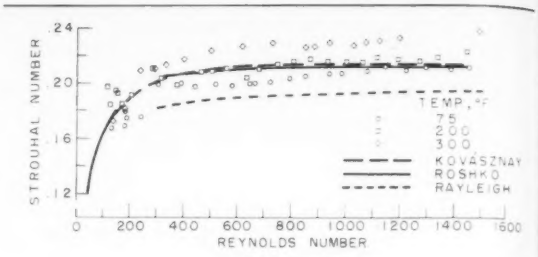

FIG. 1.

[3] Roshko, Anatol, *On the Development of Turbulent Wakes from Vortex Streets*, NACA TN 2913, March, 1953.

[4] Younger, George S., Gabriel, David S., and Mickelsen, William R., *Experimental Study of Isothermal Wake-Flow Characteristics of Various Flame-Holder Shapes*, NACA RM E51K07, January 23, 1952.

Summary of Low-Prandtl-Number Heat-Transfer Results for Forced Convection on a Flat Plate

E. M. Sparrow and J. L. Gregg
Lewis Flight Propulsion Laboratory, NACA, Cleveland, Ohio
July 19, 1957

Introduction

INTEREST in the heat-transfer characteristics of liquid metals has been stimulated by nuclear-reactor applications. The present note is concerned with laminar forced-convection heat transfer over a flat plate for the Prandtl Number range appropriate to liquid metals (0.002–0.03). Exact solutions of the boundary-layer energy equation* have been obtained for two situations: uniform wall temperature and uniform wall heat flux. Space limitations permit us to deal only with heat-transfer results here. Analytical details, plots of velocity and temperature profiles, and tabulations of the new solutions will be given elsewhere.

The previously reported exact solutions of the boundary-layer energy equation have been carried out for Prandtl Numbers greater than 0.6. For the Prandtl Number range of liquid metals, only approximate formulations have been made, the results of which are also presented here.

A sketch of the physical model showing pertinent coordinates and physical quantities is shown in Fig. 1.

Results for Uniform Wall Temperature

The heat-transfer results are reported in terms of the local heat-transfer coefficient, h, and local Nusselt Number, Nu_x. Also involved are the Reynolds Number, Re_x, and the Prandtl Number, Pr. These several quantities have their usual definitions, which are as follows:

$$h \equiv q/(T_w - T_\infty),\ Nu_x \equiv hx/k,\ Re_x \equiv U_\infty x/\nu,\ Pr \equiv c_p\mu/k \quad (1)$$

where q is the local heat flux.

The heat-transfer results based on exact solutions of the boundary-layer equations are shown as the solid curve on Fig. 2 and are tabulated in Table 1.

Fig. 2 contains two other curves depicting the results of approximate formulations. One of these is based on a Kármán-Pohlhausen type approach—i.e., integral formulation plus polynomial approximation for temperature and velocity profiles—

* The phrase "exact solutions of the boundary-layer equations" is used to describe numerically computed similar solutions of the boundary-layer differential equations. This terminology is common in boundary-layer work—e.g., Schlichting.[1]

given in reference 2. From that analysis, the local heat-transfer result for the low Prandtl Number range is

$$Nu_x/(Re_xPr)^{1/2} = 0.529/(1 + 0.82\ Pr^{1/2}) \quad (2)$$

The third curve of Fig. 2 is due to Morgan, Pipkin, and Warner.[3] They obtained a solution of the boundary-layer energy equation utilizing an approximation for the velocity profile. The basis of their analysis is the fact that the viscous boundary layer is much thinner than the thermal boundary layer for very low Prandtl Numbers. So, as a first step, the velocity profile was simply taken as a uniform potential flow, and then an approximate correction was made for the viscous effects. The local heat-transfer results are expressed by

$$Nu_x/(Re_xPr)^{1/2} = 0.564 - 0.547\ Pr^{1/2} \quad (3)$$

As the Prandtl Number decreases, it would be expected that the exact boundary-layer solution should approach more and more closely to Eq. (3), and this is verified by the curves of Fig. 2. The heat-transfer results of both approximate formulations agree very well with the exact solution. The deviations are generally no more than 5 per cent, with Eq. (3) showing even better agreement. As a final observation, it may be noted that the group $Nu_x/(Re_xPr)^{1/2}$ is relatively independent of Prandtl Number in the liquid metal range. In other words, the Nusselt Number is almost a unique function of the Peclet Number ($= Re_xPr$).

Results for Uniform Heat Flux

The parameters defined in Eq. (1) are also used in presenting the results for the uniform-heat-flux case. The solid line of Fig. 3 represents the findings of the exact boundary-layer solutions (see Table 1). The other curves of Fig. 3 depict results based on the approximate formulations which have already been described above. The equations from which these latter curves have been plotted are

$$Nu_x/(Re_xPr)^{1/2} = 0.816/(1 + 1.064\ Pr^{1/2}) \quad (4)$$

for the Kármán-Pohlhausen formulation, and

$$Nu_x/(Re_xPr)^{1/2} = 0.886 - 0.491\ Pr^{1/2} \quad (5)$$

for Morgan's formulation.

Inspection of Fig. 3 shows that the approximate analyses give good results for the uniform-heat-flux case, although the spread among the curves of this figure is slightly greater than on Fig. 2. In particular, the deviation between Morgan's results and the exact solution is both greater and of different sign for the uniform-heat-flux problem than for the uniform-wall-temperature problem. The explanation may partly lie in the fact that the thermal boundary layer is thinner for the uniform-heat-flux case. The Kármán-Pohlhausen method appears to yield results of similar accuracy for the uniform-heat-flux case as for the uniform-wall-temperature case.

From Fig. 3, it is again seen that the Nusselt Number is almost a unique function of the Peclet Number for the liquid metal range.

Fig. 1.

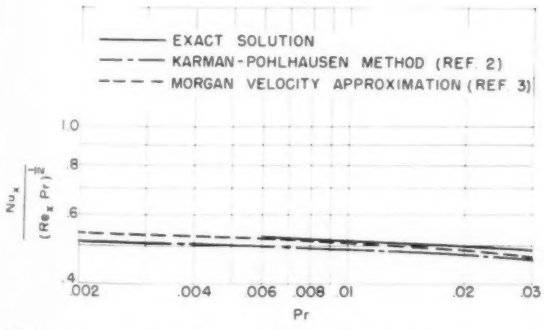

Fig. 2. Local heat-transfer results for uniform-wall-temperature situation ($h_{av} = 2h_{loc}$).

Table 1
Heat-Transfer Results From Exact Solutions

	$Nu_x/(Re_xPr)^{1/2}$	
Pr	Uniform T_w	Uniform q
0.03	0.4873	0.7170
0.01	0.5159	0.7756
0.006	0.5258	0.7969

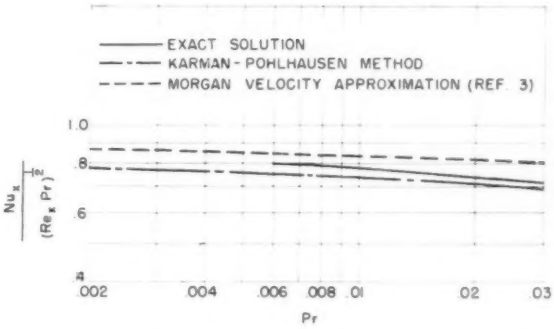

Fig. 3. Local heat-transfer results for uniform-heat-flux situation.

References

[1] Schlichting, Hermann, *Boundary Layer Theory*, Ch. 9; McGraw-Hill Book Co., Inc., N.Y., 1955.

[2] Sparrow, E. M., *Analysis of Laminar Forced-Convection Heat Transfer in Entrance Region of Flat Rectangular Ducts*, NACA TN 3331, 1955.

[3] Morgan, G. W., Pipkin, A. C., and Warner, W. H., *On Heat Transfer in Laminar Boundary Layer Flows of Liquids Having Very Small Prandtl Number*, Tech. Report No. 12, Div. Appl. Math., Brown Univ., March, 1957. (Contract Nonr-562(7).)

An Exact Solution of the Navier-Stokes Equations

W. Chester
Visiting Research Fellow, California Institute of Technology, Pasadena, Calif.
July 18, 1957

The Navier-Stokes equations for a perfect gas with constant thermal conductivity and constant coefficients of viscosity may be written, using the conventional notation, as follows:

$$\nabla\cdot(\rho\mathbf{V}) = 0$$

$$\rho(D\mathbf{V}/Dt) + \nabla p = \mu\nabla^2\mathbf{V} + (\lambda + \mu)\nabla(\nabla\cdot\mathbf{V})$$

$$\rho c_p(DT/Dt) - (Dp/Dt) = \Phi + k\nabla^2 T$$

$$p/p_o = \rho T/\rho_o T_o$$

If we assume that the Cartesian components of the velocity $\mathbf{V} = [u(y), 0, 0]$, that the pressure $p = p(x, t)$, and that the density $\rho = \rho_o$ is constant, then the continuity equation is satisfied, and the momentum and energy equations reduce to

$$\partial p/\partial x = \mu(d^2u/dy^2), \quad [(\partial p/\partial t) + u(\partial p/\partial x)] = (\gamma - 1)\,\mu(du/dy)^2$$

When $\gamma = 1{\cdot}5$, both these equations are satisfied by

$$u = U[(1 - y^2)/a^2]$$

$$T/T_o = p/p_o = 1 - (2U\mu/a^2p_o)(x - Ut)$$

A similar result holds for the circular pipe provided $\gamma = 2$. The last equation is then modified to

$$T/T_o = p/p_o = 1 - (4U\mu/a^2p_o)(x - Ut)$$

The solutions correspond respectively to steady flow with a parabolic velocity profile in an insulated two-dimensional channel of width $2a$ and in an insulated circular pipe of radius a. The velocity along the axis of the channel or pipe is U, and the pressure remains constant for a particle of fluid moving with this velocity. The motion is produced by a linear pressure gradient; the pressure, itself, also increases linearly with time at a fixed point in the channel or pipe, as does the temperature. This could presumably be attained by connecting one end of the channel or pipe to a large reservoir into which heat is being added at a constant rate.

On One-Dimensional Heat Conduction With an Arbitrary Heating Rate

George W. Sutton
Research Engineer, Missile and Ordnance Systems Department, General Electric Company, Philadelphia, Pa.
July 24, 1957

RECENTLY THERE HAS BEEN INTEREST in one-dimensional heat conduction with heat transfer which varies arbitrarily with time at one boundary when the other boundary is insulated (see Fig. 1). This situation may exist, for example, on the skin of a rapidly accelerating aircraft or on a missile re-entering the earth's atmosphere. For this case, the heat conduction equation is

$$T_{XX} - T_\tau = 0 \tag{1}$$

where

$X = x/L$
$\tau = \alpha t/L^2$
t = time
α = thermal diffusivity, $k/\rho C$
T = temperature

The boundary conditions to Eq. (1) are

$$T_X(0, \tau) = 0 \tag{2a}$$

$$T_X(1, \tau) = Lk^{-1}q(t) \quad \text{when } t > 0 \tag{2b}$$

$$T_X(1, \tau) = 0 \quad \text{when } t \leq 0 \tag{2c}$$

where $q(t)$ is an arbitrary heating rate per unit area to the surface.

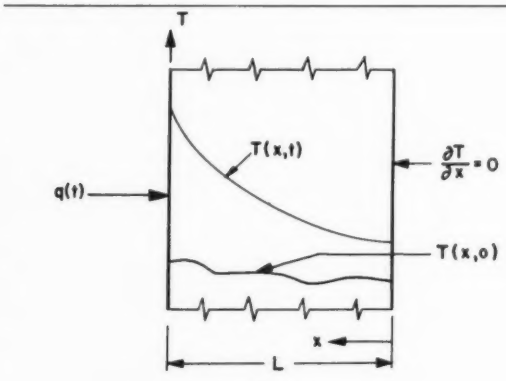

FIG. 1.

If $q(t)$ may be represented by a polynomial—that is,

$$q(t) = \sum_{s=0}^{\infty} A_s t^s \tag{3}$$

then by use of an obvious extension of the method of Laplace transform given in reference 1 the temperature distribution is given by

$$T = Lk^{-1} \sum_{s=0}^{\infty} s!\,(2)^{2s+1} A_s\, \alpha^{-s} L^{2s}\, \tau^{s+1/2} \times$$

$$\sum_{r=2}^{\infty} [i^{2s+1} \operatorname{erfc}(2r + 1 - X\tau^{-1/2}/2) + i^{2s+1} \operatorname{erfc}(2r + 1 + X\tau^{-1/2}/2)] + T_0 \tag{4}$$

where $T(x, 0) = T_0$, a constant. In connection with a study[1] where $s = 1, 2$, design charts of the functions

$$Z_m(X, \tau) = 2^m[(m-1)/2]!\tau^{1/2} \sum_{r=0}^{\infty} i^m \operatorname{erfc}[(2r + 1 - X\tau^{1/2}/2] + i^m \operatorname{erfc}[(2r + 1 + X\tau^{-1/2})/2] \tag{5}$$

where $m \equiv 2s + 1$ were prepared for values of s up to 5; that is, $m = 11$. Thus, if the heating rate may be represented by a polynomial up to the fifth degree, then the temperature distribution becomes very simply:

$$T = Lk^{-1} \sum_{s=0}^{5} A_s l^s Z_{2s+1}[(x/L), (\alpha t/L^2)] + T_0 \tag{6}$$

With the use of the design charts of reference 2, the temperature distribution is easily found. The accuracy of this solution is generally limited to small times where the convergence of the series of Eq. (5) is rapid.

We have, therefore, sought a solution to Eq. (1) which is much simpler to calculate at large times. This solution is given by

$$T(X, \tau) = \sum_{s=0}^{\infty} A_s' \sum_{m=0}^{2(s+1-n)} \sum_{n=0}^{s+1} B_{mn}^{(s)} X_{(s)}^m \tau_{(s)}^n + \int_o^L T(X, 0)\, dX + \sum_{p=1}^{\infty} C_p \cos(p\pi X) e^{-p^2\pi^2\tau} \tag{7}$$

where $A_s' = L^{2s+1}k^{-1}\alpha^{-s}A_s$. Eq. (7) is also an exact solution to the problem.

The coefficients $B_{mn}^{(s)}$ are chosen to satisfy the heat conduction equation and the boundary conditions for the corresponding s term in the heating rate of Eq. (3). The cosine series represents the difference between the initial temperature distribution and the first two terms on the right side of Eq. (7) at $t = 0$. Thus the coefficients C_p are the Fourier cosine coefficients of the function

$$T(X, 0) - \int_0^L T(X, 0)\, dX - \sum_{s=0}^{\infty} A_s' \sum_{m=0}^{2(s+1-n)} B_{mo}^{(s)} X^m \tag{8}$$

The Fourier series decreases rapidly with time so that when $\tau > 0.5$, its contribution is less than 2 per cent to $T(X, \tau)$ and therefore may be neglected. Thus the solution is given simply by a polynomial in X and τ.

The coefficients $B_{mn}^{(s)}$ are simple to obtain. First, Eq. (2a) requires that for any value of n

$$B_{1n}^{(s)} = 0 \tag{9}$$

Next, substitution of Eq. (7) into Eq. (1) yields the following recursion formula for the coefficients:

$$(m + 2)(m + 1)B_{m+2,\, n}^{(s)} = (n + 1)B_{m,\, n+1}^{(s)} \tag{10}$$

Eqs. (9) and (10) show that for all odd values of m

$$B_{mn}^{(s)} = 0 \quad (m \text{ odd}) \tag{11}$$

Substitution of Eq. (7) into Eq. (2b) gives

TABLE I
Values of the Coefficients $B_{mn}^{(s)}$

s	m	n = 0	1	2	3	4	5
0	0	−0.166667	1.000000				
	2	0.500000					
1	0	0.019444	−0.166667	0.500000			
	2	−0.083333	0.500000				
	4	0.041667					
2	0	−0.004101	0.038889	−0.166667	0.333333		
	2	0.019444	−0.166667	0.500000			
	4	−0.013889	0.083333				
	6	0.002778					
3	0	0.001594	−0.142857	0.058333	−0.166667	0.250000	
	2	−0.007143	0.058333	−0.250000	0.500000		
	4	0.004861	−0.041667	0.125000			
	6	−0.001389	0.008333				
	8	0.000175					
4	0	−0.001559	0.010595	−0.126984	0.188889	−0.166667	0.200000
	2	0.005297	−0.126984	0.283333	−0.333333	0.50000	
	4	−0.001058	0.047222	−0.166667	0.166667		
	6	0.001574	−0.011111	0.016667			
	8	−0.001984	0.000595				
	10	0.000007					

$$B_{2,\,s}^{(s)} = 1/2 \tag{12}$$

while for $n \neq s$,

$$\sum_{m=2}^{2(s+1-n)} m\, B_{mn}^{(s)} = 0 \tag{13}$$

By use of the value of $B_{2,\,s}^{(s)}$, and Eqs. (10) and (13), all coefficients may be calculated except $B_{00}^{(s)}$. This coefficient is obtained from the initial condition at $t = 0$; that is

$$\sum_{m=0}^{2(s+1)} \int_0^1 B_{m0}^{(s)}\, X^m dX = 0 \tag{14}$$

for each value of s.

Values of the coefficients $B_{mn}^{(s)}$ which were obtained by the use of this method are tabulated in Table I for values of s up to 4. The coefficients for $s = 2$ given in Table I do not agree with those of Eq. (I-31) in reference 3. However, it is noted that Eq. (I-31) does not satisfy the differential equation.

If the heating rate $q(t)$ cannot conveniently be represented by a polynomial, one may use in exact solution to Eq. (1) with boundary conditions given by Eq. (2), which is

$$T(x, t) = \int_0^t q(t_1) G(x, t - t_1)\, dt_1 + T_0 \tag{15}$$

where the Green's function $G(x, t - t_1)$, which has been obtained by solving Eq. (1) for $q(t) = \delta(t_1)$, is given by:

$$G(x, t - t_1) = (1/\rho CL) \times \left[1 + 2 \sum_{n=1}^{\infty} (-1)^n \cos (n\pi x/L) e^{-(n^2\pi^2\alpha/L^2)(t - t_1)} \right] \tag{16}$$

Thus, the temperature distribution for an arbitrary heating rate may be calculated by simple quadrature of Eq. (15).

REFERENCES

[1] Carslaw, H. S., and Jaeger, J. C., *Conduction of Heat in Solids*, p. 252; Oxford, 1947.

[2] Kaye, J., and Yeh, V. C. M., *Design Charts for Transient Temperature Distribution Resulting from Aerodynamic Heating at Supersonic Speeds*, Journal of the Aeronautical Sciences, Vol. 22, No. 11, pp. 755–762, November, 1955.

[3] Coulbert, C. D., et al., *Temperature Response of Infinite Flat Plates and Slabs to Heat Inputs of Short Duration at One Surface*, UCLA report, April, 1951.

Natural Frequencies of Rectangular Plates With Edges Elastically Restrained Against Rotation

C. V. Joga Rao and C. Lakshmi Kantham

Assistant Professor and Research Student, Respectively, Department of Aeronautical Engineering, Indian Institute of Science, Bangalore, India.

August 2, 1957

PLATES with attachments to heavier members along the edges can be described as having edges elastically restrained against rotation, in many cases uniformly along each edge. At the edges, setting slope $\alpha = \beta M$, when M is the edge bending moment with β always positive, the elastic restraint can be analytically defined with $\beta \to 0$, $\beta \to \infty$ describing respectively, clamped and simply supported edges. In this note natural frequencies of such plates are calculated mainly following the nomenclature of Dana Young.[1]

The differential equation for a uniform vibrating beam of stiffness EI and length l with elastically restrained ends yields the characteristic functions. Taking the origin at the middle and setting $\theta_r = \sqrt[4]{p_r^2 A \rho / EI}\, l$, where $p_r = r^{\text{th}}$ angular frequency A = area of cross section, and ρ = mass density, we have for sym-

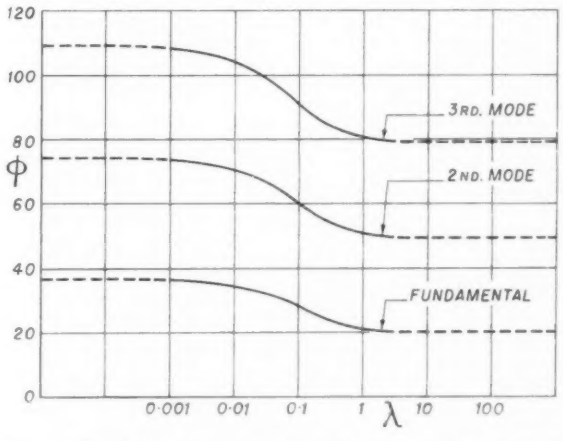

FIG. 1. Variation of frequencies with elastic restraint for a square plate.

metric vibrations

$$X_r = [\cosh(\theta_r x/l)/\cosh(\theta_r/2)] - [\cos(\theta_r x/l)/\cos(\theta_r/2)] \quad (1)$$

with $$\tanh(\theta_r/2) + \tan(\theta_r/2) + 2\beta(EI/l)\theta_r = 0 \quad (2)$$

and for antisymmetric vibrations

$$X_r = [\sinh(\theta_r x/l)/\sinh(\theta_r/2)] - [\sin(\theta_r x/l)/\sin(\theta_r/2)] \quad (3)$$

with

$$\coth(\theta_r/2) - \cot(\theta_r/2) + 2\beta(EI/l)\theta_r = 0 \quad (4)$$

It can be easily verified that, for the two limiting cases $\beta \to 0$, $\beta \to \infty$, Eqs. (2) and (4) together yield the well-known equations $\cos\theta_r \cosh\theta_r = 1$ and $\sin\theta_r = 0$. Putting $\lambda = \beta(EI/l)$, these characteristic functions satisfy the following relationships for symmetric vibrations

$$\left.\begin{aligned}(1/l)\int_{-l/2}^{l/2} X_r X_s\,dx &= 0 \text{ for } r \neq s\\ &= \{\lambda\theta_r[\tanh(\theta_r/2) - \tan(\theta_r/2)] + 2\lambda + 1\} \text{ for } r = s\end{aligned}\right\} \quad (5)$$

$$\left.\begin{aligned}l\int_{-l/2}^{l/2} (dX_r/dx)(dX_s/dx)dx &= -[4\theta_r^2\theta_s^2/(\theta_r^4 - \theta_s^4)]\{\theta_r[\tanh(\theta_r/2) - \tan(\theta_r/2)] - \theta_s[\tanh(\theta_s/2) - \tan(\theta_s/2)]\} \text{ for } r \neq s\\ &= \{(\theta_r^2/2)[\tanh^2(\theta_r/2) + \tan^2(\theta_r/2)] - \theta_r[\tanh(\theta_r/2) - \tan(\theta_r/2)]\} \text{ for } r = s\end{aligned}\right\} \quad (6)$$

$$\left.\begin{aligned}l^3\int_{-l/2}^{l/2} (d^2X_r/dx^2)(d^2X_s/dx^2)dx &= -8\lambda\theta_r^2\theta_s^2 \text{ for } r \neq s\\ &= \theta_r^4\{\lambda\theta_r[\tanh(\theta_r/2) - \tan(\theta_r/2)] - 6\lambda + 1\} \text{ for } r = s\end{aligned}\right\} \quad (7)$$

for antisymmetric vibrations

$$\left.\begin{aligned}(1/l)\int_{-l/2}^{l/2} X_r X_s\,dx &= 0 \text{ for } r \neq s\\ &= \{\lambda\theta_r[\coth(\theta_r/2) + \cot(\theta_r/2)] + 2\lambda + 1\} \text{ for } r = s\end{aligned}\right\} \quad (8)$$

$$\left.\begin{aligned}l\int_{-l/2}^{l/2} (dX_r/dx)(dX_s/dx)dx &= -[4\theta_r^2\theta_p^2/(\theta_r^4 - \theta_s^4)]\{\theta_r[\coth(\theta_r/2) + \cot(\theta_r/2)] - \theta_s[\coth(\theta_s/2) + \cot(\theta_s/2)]\} \text{ for } r \neq s\\ &= \{(\theta_r^2/2)[\coth^2(\theta_r/2) + \cot^2(\theta_r/2)] - \theta_r[\coth(\theta_r/2) + \cot(\theta_r/2)]\} \text{ for } r = s\end{aligned}\right\} \quad (9)$$

$$\left.\begin{aligned}l^3\int_{-l/2}^{l/2} (d^2X_r/dx^2)(d^2X_s/dx^2)dx &= -8\lambda\theta_r^2\theta_s^2 \text{ for } r \neq s\\ &= \theta_r^4\{\lambda\theta_r[\coth(\theta_r/2) + \cot(\theta_r/2)] - 6\lambda + 1\} \text{ for } r = s\end{aligned}\right\} \quad (10)$$

Taking the expression for the deflection of the plate as $w_0 = \sum_m \sum_n A_{mn} X_m(x)\, Y_n(y)$, where $X_m(x)$, $Y_n(y)$ are the characteristic functions of vibrating beams with elastically restrained ends. The strain energy of bending V_p, of the plate is given by[2]

$$V_p = (D/2)\int_{-a/2}^{a/2}\int_{-b/2}^{b/2} [(\partial^2 w_0/\partial x^2) + (\partial^2 w_0/\partial y^2)]^2\,dx dy \quad (11)$$

for the deflection is zero along the boundary; the energy stored in the constraints is given by

$$V_c = (1/2)\oint M\alpha\,ds \quad (12)$$

the contour being the boundary of the plate.

Substituting for w_0 in terms of beam functions,

$$\partial V_p/\partial A_{rs} = (D/a^2)\sum_m \sum_n A_{mn}[(b/a)R_{mr}T_{ns} + (a^3/b^3)R_{ns}T_{mr} + (a/b)(S_{mr}S_{sn} + S_{rn}S_{ns})] \quad (13)$$

where

$$\left.\begin{aligned}R_{mr} &= a^3\int_{-a/2}^{a/2} (d^2X_m/dx^2)(d^2X_r/dx^2)\,dx\\ R_{ns} &= b^3\int_{-b/2}^{b/2} (d^2Y_n/dy^2)(d^2Y_s/dy^2)\,dy\end{aligned}\right\} \quad (14)$$

$$\left.\begin{aligned}T_{mr} &= (1/a)\int_{-a/2}^{a/2} X_m X_r\,dx\\ T_{ns} &= (1/b)\int_{-b/2}^{b/2} Y_n Y_s\,dy\end{aligned}\right\} \quad (15)$$

$$\left.\begin{aligned}S_{mr} &= a\int_{-a/2}^{a/2} X_m (d^2X_r/dx^2)\,dx\\ S_{ns} &= b\int_{-b/2}^{b/2} Y_n (d^2Y_s/dy^2)\,dy\end{aligned}\right\} \quad (16)$$

Hence we write

$$(\partial V_p/\partial A_{rs}) = (D/a^2)\sum_m \sum_n A_{mn} C_{mnrs} \quad (17)$$

Similarly we have

$$\partial V_c/\partial A_{rs} = (8\lambda^2/\beta)(b/a^2)\sum_m \sum_n A_{mn}[\theta_m^2\theta_r^2 T_{ns} + (a^2/b^2)\theta_n^2\theta_s^2 T_{mr}] = (\lambda^2/\beta)(b/a^2)\sum_m \sum_n A_{mn} B_{mnrs} \quad (18)$$

and from consideration of kinetic energy

$$\partial T/\partial A_{rs} = ab\rho hp^2 \sum_m \sum_n A_{mn} T_{mr} T_{ns} = ab\rho hp^2 \sum_m \sum_n A_{mn} T_{mnrs} \quad (19)$$

where h is the thickness of the plate.

From principle of minimization, we have for a square plate

$$\sum_m \sum_n A_{mn}[C_{mnrs} + \lambda(1 - \nu^2)B_{mnrs} - \phi^2 T_{mnrs}] = 0 \quad (20)$$

where $\phi^2 = a^4\rho hp^2/D$, D being the flexural rigidity of the plate. The system of simultaneous equations (20) has been solved for ϕ for various values of λ for a square plate to obtain the lowest three frequencies. The convergence has been found to be rapid. The results are presented in Fig. 1.

The results agree satisfactorily with the experimental values for the fundamental frequency obtained by Hoppmann and Greenspon.[3] This procedure can be modified to evaluate frequencies of rectangular plates with one value of elastic restraint factor along two parallel edges and with another value along the other two parallel edges. This is of interest in evaluation of natural frequencies of rectangular wing panels.

References

[1] Young, Dana, *Vibration of Rectangular Plates by the Ritz Method*, J. Appl. Mech., Vol. 17, pp. 448–453, December, 1950.

[2] Wang, C. T., *Applied Elasticity*, pp. 286, 287; McGraw-Hill Book Co., Inc., N.Y., 1953.

[3] Hoppmann, W. H., II, and Greenspon, J., *An Experimental Device for Obtaining Elastic Rotational Constraint on Boundary of a Plate*, Proc. of the Second U.S. Nat. Congress of Applied Mechanics, pp. 187–191, 1954.